
Recent Developments in the Dynamics of Advanced Rotor Systems

Wayne Johnson

FOR REFERENCE

NOT TO BE TAKEN FROM THIS ROOM

March 1985

LIBRARY COPY

APR 29 1985

LANGLEY RESEARCH CENTER
LIBRARY, NASA
HAMPTON, VIRGINIA

NASA

National Aeronautics and
Space Administration



NF01044

Recent Developments in the Dynamics of Advanced Rotor Systems

Wayne Johnson, NASA Ames Research Center, Moffett Field, California

NASA

National Aeronautics and
Space Administration

Ames Research Center
Moffett Field, California 94035

N85-24320 #

RECENT DEVELOPMENTS IN THE DYNAMICS
OF ADVANCED ROTOR SYSTEMS

Wayne Johnson
NASA Ames Research Center
Moffett Field, California 94035, USA

SUMMARY

The problems that have been encountered in the dynamics of advanced rotor systems are described. The methods for analyzing these problems are discussed, as are past solutions of the problems. To begin, the basic dynamic problems of rotors are discussed: aeroelastic stability, rotor and airframe loads, and aircraft vibration. Next, advanced topics that are the subject of current research are described: vibration control, dynamic inflow, finite element analyses, and composite materials. Finally, the dynamics of various rotorcraft configurations are considered: hingeless rotors, bearingless rotors, rotors with circulation control, coupled rotor/engine dynamics, articulated rotors, and tilting proprotor aircraft.

NOMENCLATURE

C_T	rotor thrust coefficient
EI	blade bending stiffness
f	ratio of blade torsional stiffness to pitch link stiffness
K_P	pitch/flap coupling; positive for flap up, pitch down
K_P^β	pitch/lag coupling; positive for lag back, pitch down
K_β^ζ	flap hinge spring
K_ζ	lag hinge spring
K_θ	pitch hinge spring
r	rotor blade radial station
R	structural flap/lag coupling ($R = 0$ for no coupling, $R = 1$ for complete coupling); or blade radius
V	helicopter forward velocity
β	blade flap degree of freedom
β_d	blade droop angle
β_p	hub precone angle
ζ	blade lag degree of freedom
ζ_s	blade sweep angle
θ	blade pitch angle

θ_f	flexbeam pitch angle
θ_h	hub flap/lag flexure pitch angle
μ	advance ratio (forward velocity divided by rotor tip speed)
ν_β	rotating natural flap frequency, per rev
ν_ζ	rotating natural lag frequency, per rev
σ	damping (real part of eigenvalue, negative for stability); or rotor solidity (ratio of blade area to disk area)
Ω	rotor rotational speed
ω_ϕ	blade pitch frequency, per rev

1. INTRODUCTION

Good dynamic characteristics are a prerequisite for the success of any rotorcraft. Without an adequate aeroelastic stability margin, acceptable rotor and airframe loads, and low aircraft vibration, the machine cannot fulfill its mission, regardless of its performance capabilities. Indeed, the dynamic characteristics often define the operating limits of a rotorcraft. Perhaps more than any other discipline involved in helicopter engineering, the dynamics are very configuration-dependent. In this lecture, the dynamics problems that have been encountered in the development of advanced rotor systems are discussed. The methods of analyzing these problems, as well as past solutions, are reviewed. First, the basic dynamic problems of rotors are discussed; next, advanced topics that are the subject of current research; and finally, the dynamics of various rotorcraft configurations.

In the recent surveys of rotary wing dynamics (Refs. 1-6), the emphasis was on the theory of hingeless rotor stability. Loewy (Ref. 1) provided a discussion of dynamics problems in general. Hohenemser's (Ref. 2) subject was flight dynamics, but he included stability phenomena that involved the fundamental blade modes (hence not vibration); he covered experimental results as well. Friedmann (Ref. 3) gave a good chronological discussion. Friedmann (Ref. 4) dealt with the aerodynamics analysis in particular. Ormiston (Ref. 5) covered bearingless as well as hingeless rotors, and experimental as well as theoretical results. Lowey (Ref. 6) discussed helicopter vibration.

2. BASIC DYNAMIC PROBLEMS

To begin, the basic dynamic problems of rotors will be discussed: aeroelastic stability, rotor and airframe loads, and aircraft vibration. The emphasis will be on describing the primary characteristics of these problems, and the general capability to analyze them.

2.1 Stability

A summary of the basic results from rotary wing stability analysis is appropriate before considering recent developments. Johnson (Ref. 7) provides a complete derivation of these results, as well as references to the original literature.

2.1.1 Flap-Lag Stability

Rotor blade flap-lag stability has received much attention because the lag mode damping is low without a mechanical damper, and because the couplings between flap and lag motion are often complicated in new configurations. With no pitch/lag coupling and a flap frequency of 1/rev, the aerodynamic and Coriolis flap moments due to lag velocity nearly cancel, so the flap equation is decoupled from the lag motion. It follows that the flap-lag motion is stable for an articulated rotor: a rotor with small lag frequency, flap frequency near 1/rev, small pitch/lag and pitch/flap couplings, in hover or low advance ratio. Moreover, the articulated rotor will have a mechanical lag damper (for ground resonance stability). This same canceling of the flap moments due to lag velocity occurs if the flap frequency is above 1/rev with ideal precone, for then the flap spring is not contributing to the coning moment and the coning angle is the same as for a flap frequency of exactly 1/rev. The aerodynamic and Coriolis forces are generally proportional to the rotor thrust, so the lag moments due to flapping are small at low collective. It follows that any flap-lag instability will be a high collective phenomenon.

For a hingeless rotor with no pitch/flap or pitch/lag coupling, or flap/lag structural coupling, it is found that the critical condition for flap-lag stability is zero precone and flap frequency = lag frequency = 1.15/rev. Such a rotor blade is stable with ideal precone and for a flap frequency less than 1/rev or greater than 1.41/rev. The effect of pitch/flap coupling is primarily to introduce the effective flap frequency, including the aerodynamic spring due to pitch/flap coupling, in place of the structural/centrifugal flap frequency in this analysis (note that a flap frequency less than 1/rev then is possible, with negative pitch/flap coupling). The lag mode structural or mechanical damping required for stability increases with the rotor thrust. However, the blade viscous drag damping alone is sufficient to provide stability up to roughly a $C_T/\sigma = 0.10$ for the critical condition defined above. So, in general, any reasonable level of structural damping is sufficient to stabilize a hingeless rotor. In forward flight (at advance ratios of around 0.4), an instability is possible even for an articulated rotor, but, again, the instability is mild, and a moderate amount of lag damping is still sufficient to stabilize the motion.

A flap-lag instability is also possible at high collective pitch due to stall. The loss of flap damping because of the reduced lift-curve slope allows the instability. This phenomenon can only occur in hover, since in forward flight stall is encountered only on part of the rotor disk.

2.1.2 Pitch/Lag, Pitch/Flap, and Flap/Lag Coupling

Flap-lag stability becomes a problem largely because of pitch/lag coupling. For articulated or soft-inplane hingeless rotors (lag frequency less than 1/rev), positive pitch/lag coupling (lag back, pitch down) is destabilizing. For a stiff-inplane hingeless rotor (lag frequency above 1/rev), positive pitch/lag coupling is destabilizing with full flap/lag structural coupling, while negative pitch/lag coupling is destabilizing with no flap/lag coupling (pure inplane and pure out-of-plane modes). With an articulated rotor, the pitch/flap and pitch/lag couplings are determined by the geometry of the root hinges and control system. With a hingeless rotor, in addition to such kinematic couplings, there are effective couplings due to the nonlinear bending and torsion loads on the blade. Structural coupling of the flap and lag motion is produced by pitch of the structural principal axes of the rotor blade. Even a small amount of flap motion in the lag mode as a result of such coupling is very stabilizing because of the high aerodynamic damping associated with out-of-plane motion.

Elementary, but useful, expressions for the effective pitch/lag and pitch/flap couplings can be obtained considering a flap-lag-torsion spring model of a hingeless rotor. A complete derivation is given in Ref. 7. Elastic flap deflection introduces a component of the trim lag moment about the pitch spring; elastic lag deflection introduces a component of the trim flap moment about the pitch spring. For pitch springs inboard and outboard of the droop (representing control system stiffness and blade elastic torsion, respectively), the total nose-up moments are:

$$K_t \phi_t = \beta_e M_\zeta - \zeta_e M_\beta$$

$$K_c \phi_c = (\beta_e - \beta_d) M_\zeta - (\zeta_e + \zeta_s) M_\beta$$

The pitch angles, precone, droop and sweep, elastic flap and lag deflection, and flap and lag moments are defined in Fig. 1. The total pitch deflection is then:

$$\theta = \phi_t + \phi_c = \left(\frac{1}{K_c} + \frac{1}{K_t} \right) (\beta_e M_\zeta - \zeta_e M_\beta) + \frac{1}{K_c} (-\beta_d M_\zeta - \zeta_s M_\beta)$$

$$= \frac{1}{K_\theta} (K_\zeta - K_\beta) \beta_e \zeta_e + \frac{1}{K_c} (-K_\zeta \beta_d \zeta_e - K_\beta \zeta_s \beta_e)$$

where the K's are the spring constants, and $K_\theta^{-1} = K_c^{-1} + K_t^{-1}$. Hence, because of the blade pitch flexibility, bending of the blade produces a pitch deflection. With no droop or sweep, the pitch moment is:

$$M_\theta = K_\theta \theta = I \Omega^2 (1 + v_\zeta^2 - v_\beta^2) \beta_e \zeta_e$$

where the flap and lag springs have been written in terms of the rotating natural frequencies (per rev; I is the blade moment of inertia and Ω is the rotor rotational speed). The effective pitch/lag coupling (positive for lag back, pitch down) is:

$$\begin{aligned}
K_{P_{\zeta}} &= -\frac{\partial \theta}{\partial \zeta_e} = -\frac{K_{\zeta} - K_{\beta}}{K_{\theta}} \beta_e + \frac{K_{\zeta}}{K_c} \beta_d \\
&= -\frac{K_{\zeta} - K_{\beta}}{K_{\theta}} \frac{\beta_i - \beta_p + \beta_d}{v_{\beta}^2} + \frac{K_{\zeta}}{K_c} \beta_d
\end{aligned}$$

where v_{β} is the flap frequency (per rev), and the ideal precone in hover (the coning angle for a flap frequency of exactly 1/rev; see Ref. 7) is:

$$\beta_i = \frac{\gamma}{8} \frac{6C_T}{\sigma a}$$

(γ = Lock number, a = two-dimensional lift curve slope).

With a matched stiffness design (equal flap and lag hinge springs), or ideal precone so the elastic flap deflection is zero, the first term in the equation for the pitch/lag coupling is absent and the coupling is solely due to droop producing a moment about the control system spring. In general, the first term is important also. In particular, at low pitch the precone will be larger than ideal, hence the elastic flap deflection β_e will be negative, and from above the pitch/lag coupling will be positive. It follows there can be an instability at low collective for a soft-inplane rotor with precone, because of the effective pitch/lag coupling introduced by the blade pitch flexibility. Alternatively, using a precone value less than the ideal precone, or increasing the blade pitch stiffness, will be favorable for stability. The damping and inertia of the torsion motion are much less important. It is found that a quasistatic torsion model is adequate, except for low torsion stiffness; but a model without the torsion motion entirely is not adequate except for very high torsion stiffness.

Similarly the effective pitch/flap coupling (positive for flap up, pitch down; $K_{P_{\beta}} = \tan \delta_3$) is:

$$\begin{aligned}
K_{P_{\beta}} &= -\frac{\partial \theta}{\partial \beta_e} = -\frac{K_{\zeta} - K_{\beta}}{K_{\theta}} \zeta_e + \frac{K_{\beta}}{K_c} \zeta_s \\
&= -\frac{K_{\zeta} - K_{\beta}}{K_{\theta}} \frac{\gamma C_Q / \sigma a}{v_{\zeta}^2} + \frac{K_{\beta}}{K_c} \zeta_s
\end{aligned}$$

(v_{ζ} = lag frequency, per rev; C_Q = torque coefficient). Note that with neither droop nor sweep, the pitch/lag or pitch/flap coupling per radian of elastic blade deflection is:

$$K_p \text{ per rad} = - \frac{I\Omega^2}{K_\theta} (1 + v_\zeta^2 - v_\beta^2)$$

A similar result can be derived for the torsion moment at an arbitrary radial station on the blade (Ref. 7). Considering the out-of-plane forces with a moment arm due to inplane deflection, and the inplane forces with a moment arm due to out-of-plane deflection, gives a torsion moment:

$$\Delta T = M_x x'' - M_z z'' = (EI_\beta - EI_\zeta) x'' z''$$

where M_x and M_z are the section flap and lag bending moments; EI_β and EI_ζ are the flap and lag bending stiffnesses; z'' and x'' are the out-of-plane and inplane curvatures. Hence there is a nonlinear load coupling bending and torsion, proportional to the difference between the bending stiffnesses. This coupling is zero for a matched stiffness design. Normally the chordwise stiffness is much greater than the flapwise stiffness, but nearly equal stiffnesses can be obtained at the root of a soft-inplane rotor blade.

2.1.3 Ground and Air Resonance

When the aircraft body motion is added to the problem, the stability phenomena that are often of most importance are ground resonance and air resonance. Ground resonance is a dynamic instability involving the coupling of the blade lag motion with the inplane motion of the rotor hub (see Ref. 7 for a complete discussion and analysis). This instability is characterized by a resonance of the frequency of the rotor lag motion (specifically the regressing lag mode in the nonrotating frame) and a natural frequency of the structure supporting the rotor (Fig. 2). Since the lag frequency depends on the rotor rotational speed, such resonances define critical speed ranges for the rotor. An instability is possible at a resonance if the rotating lag frequency is below 1/rev, as it is for articulated and soft inplane hingeless rotors. With articulated rotors, the critical mode is usually an oscillation of the helicopter on the landing gear when in contact with the ground. The classical ground resonance analysis considers four degrees of freedom: longitudinal and lateral inplane motion of the rotor hub, and the progressing and regressing lag modes. The actual vibration modes of the rotor support, such as the motion of the helicopter on its landing gear, will probably involve tilt of the shaft as well, but it is the inplane hub motion that dominates the ground resonance phenomenon, particularly for articulated rotors. Also for articulated rotors, the damping of the rotor and support comes almost entirely from mechanical dampers and structural damping, so the aerodynamic forces are neglected. The coupling of the body and the rotor lag motion is determined by the first moment of inertia of the blade. For small rotor mass compared to body mode generalized mass (which is usually the case), the Deutsch criterion (Ref. 7) provides a good estimate of the damping required for stability:

$$\frac{C_x}{\omega_x^2} C_\zeta > \frac{N}{4} \frac{1 - v_\zeta}{v_\zeta} S_\zeta^2$$

at a rotor speed of $\Omega = \omega_x / (1 - v_\zeta)$. Here C_x and C_ζ are the dimensional body mode and rotor lag damping coefficients; ω_x is the frequency (rad/sec) of the body mode; N is the number of blades; v_ζ is the per-rev natural frequency of the lag motion; and S_ζ is the first moment of inertia of the blade (product of the blade mass and the radial center of gravity location). The factor $(1 - v_\zeta)/v_\zeta$ determines the severity of the instability. For an articulated rotor this factor is large, and a mechanical lag damper is needed. For a soft-inplane hingeless rotor this factor is small, so the blade structural damping may be sufficient for stability. For a stiff-inplane hingeless rotor this factor is negative, so there is no ground resonance problem.

A similar stability phenomenon exists in flight, particularly with a hingeless rotor, and then it is called air resonance. The blade flap motion and the rotor aerodynamics must be included in an analysis of air resonance, since the flap stiffness and aerodynamics determine the frequency and damping of the body modes in flight. The critical stability case still occurs at a resonance with the regressing lag mode (Fig. 2). For air resonance, there are no springs on the body motion, as exist in the ground resonance problem. To the rotor degrees-of-freedom the analysis adds the aircraft rigid body motions, hence the eigenvalues associated with the flight dynamics. Singly, the pitch or roll motion would each add a real, damped eigenvalue; together they add an oscillatory mode (if the pitch and roll inertias are not too different). The pitch, roll, longitudinal, and lateral motions together add two real, damped roots and two unstable or low-damped oscillatory modes (in hover). When the frequencies of these modes are low, they are not part of the air resonance problem. Rather, air resonance involves the regressing flap mode, which includes considerable body motion, particularly with a hingeless rotor. When the frequencies of the body modes are high and the frequency of the regressing flap mode low, the above distinctions are less useful. The coupled flap-lag motion has reduced stability at high collective, hence air resonance stability tends to decrease as collective pitch increases. Articulated rotors have mechanical lag dampers and relatively little body motion in the regressing flap mode. Thus air resonance is primarily a problem for soft-inplane hingeless or bearingless rotors.

2.2 Stability--Recent Developments

2.2.1 Hingeless Rotors

Ormiston and Hodges (Ref. 8) developed a theory for flap-lag stability, based on a rotor blade model consisting of rigid blades with hinge springs. They identified the stabilizing influence of the proper choice of pitch/lag coupling, and the use of structural flap/lag coupling. Their analysis provided a description of the basic high collective flap-lag instability, including a definition of the critical case of flap frequency and lag frequency equal to 1.15. Figures 3 to 5 show the flap-lag stability boundaries as a function of flap and lag frequencies, collective

pitch, structural flap/lag coupling ($R = 0$ for no coupling, $R = 1$ for complete coupling), and pitch/lag coupling.

Lytwyn, Miao, and Woitsch (Ref. 9) developed an analysis of hingeless rotor air and ground resonance, using the rigid blade and hinge spring model. The analysis was applied to the BO-105 helicopter.

Burkam and Miao (Ref. 10) conducted a wind tunnel test of a model hingeless rotor with body pitch and roll motion (intended to model BO-105 air resonance; flap frequency 1.12/rev and lag frequency 0.62/rev, pitch bearing inboard of bending flexibility). They used the theory of Ref. 9 to identify favorable couplings, including the favorable pitch/lag coupling with under-precone. The original pitch links were stiff enough so that no instabilities were encountered in the test; the pitch link stiffness was significantly reduced in order to obtain measurable stability boundaries. The flap damping contributed to the body mode damping with this hingeless rotor. A high collective boundary was identified as air resonance, produced by the increase in roll mode frequency with collective increase. The analysis had shown that increased control system stiffness would stabilize this phenomenon, by reducing the effective couplings. A mild, low collective instability involved primarily the lag motion (although locking out the body increased the damping ratio by about 0.005). Figure 6 compares the predicted and measured stability boundaries. Figures 7-9 show the measured boundaries as a function of hub precone, inplane damping, and blade sweep.

Reichert and Huber (Ref. 11) analyzed the BO-105 helicopter with a rigid blade and hinge spring rotor model. A pitch-flap-lag-torsion hinge sequence was used for the flight dynamics calculations. A pitch-flap-lag rotor model with body roll and pitch motion was used for loads and stability calculations. The mechanism for pitch/flap and pitch/lag coupling in a hingeless rotor with an inboard feather bearing was discussed.

Huber (Ref. 12) analyzed the BO-105 helicopter using the method of Ref. 11, extended to five body degrees of freedom (no yaw motion or tail rotor model). The analysis was applicable to both hover and forward flight. Two-dimensional airfoil tables (including stall and compressibility effects) were used. The dynamic behavior was determined from a numerical integration in time for various control or external inputs. The pitch moment component of the flap moment when the blade lags, and the lag moment when the blade flaps, was discussed. Although the torsion moment at an arbitrary radial station was considered, the flap and lag moments were largest at the root and most of the torsion flexibility was in the control system. Hence, it was mainly the rigid pitch motion that was of concern. The influence of sweep, droop, control system stiffness, and thrust on the effective coupling was significant because of their influence on the elastic flap deflection (Fig. 10). Low precone was desired for increased lag stability through favorable pitch/lag coupling. The analysis showed a high-thrust instability due to stall. The reduction in lift-curve slope produced a loss of flap damping, which allowed a flap-lag instability (Fig. 11). This phenomenon was predicted to occur at about 2.2 g load factor in hover, hence was not within the operating envelope of the helicopter.

Miao and Huber (Ref. 13) conducted a wind tunnel test of a model soft-inplane hingeless rotor with body pitch and roll freedom. The theory of Ref. 12 was used, analyzing the predicted time histories to obtain frequencies and damping, just as for the experimental data. The analysis predicted the damping in hover well (Figs. 12 and 13).

Hansford and Simons (Ref. 14) developed an analysis for application to the Lynx hingeless rotor. They discussed the torsion moment due to the product of the flap and lag moments, noting that zero coupling was possible only with matched stiffness outboard of the feathering hinge or all the bending flexibility inboard of the feathering hinge (the latter is difficult to achieve except with hinges). Most of the torsion flexibility was in the control system, so they only considered the pitch moment at the blade root.

2.2.2 Rigid Blade Models

Ormiston (Ref. 15) examined combinations of pitch/lag coupling and structural flap/lag coupling to stabilize soft-inplane hingeless rotors, using the theory of Ref. 8. Flap/lag coupling was introduced by means of pitch of the structural principal axes relative to the aerodynamic pitch. Pitch/lag and flap/lag coupling were predicted to be very stabilizing (Fig. 14).

Kaza and Kvaternik (Ref. 16) analyzed hingeless rotor flap-lag stability, considering the influence of hinge sequence in the rigid blade with springs model. A lag hinge inboard, flap hinge outboard sequence was used in Ref. 8. For the flap-then-lag sequence, additional aerodynamic forces are introduced, equivalent to a pitch/lag coupling equal to the blade coning angle (Fig. 15). They also considered the influence of forward flight.

Ormiston and Bousman (Ref. 17) conducted a test of the flap-lag stability of a hingeless model rotor in hover. The blades used hinges and flexures. The experiment was designed to check the predictions of Ref. 8: the minimum stability with equal flap and lag frequencies (without flap/lag coupling); and the significant stability increase with structural flap/lag coupling. Figure 16 shows the capability of the theory. In addition, a stall-induced flap/lag instability was found at high thrust, attributed to the reduction of the flap damping because of the reduced lift-curve slope in the stall regime (Fig. 17).

Bousman, Sharpe, and Ormiston (Ref. 18) conducted a hover test of a model soft-inplane hingeless rotor, in order to verify the theory of Ref. 8. A rigid blade with flap and lag hinge flexures was used. Pitch/lag coupling was introduced by skewing the lag flexure, while flap/lag coupling was introduced by pitching the principal axes of the flexure relative to the hub plane (the blade collective pitch was changed outboard of the flexures). The significant stability improvement with pitch/lag or flap/lag coupling (and even more in combination) was verified by the experiment (Fig. 18). Generally, the predictions were good, except that the damping measured at low collective with both pitch/lag and flap/lag coupling present was higher than predicted (Fig. 19). It was speculated that the discrepancy might be due to unsteady wake effects.

2.2.3 Elastic Blade Models

Hodges and Ormiston (Ref. 19) analyzed the elastic flap-lag-torsion motion of a uniform cantilever blade in hover, using the theory of Hodges and Dowell (Ref. 20). An axial-inplane-vertical-torsion deflection sequence was used; the torsion variable definition neglected a second order kinematic term however (except in the aerodynamic angle of attack). Later work showed that the number of modes used was probably not sufficient. Full flap/lag structural coupling was used in all cases. The effective pitch/lag and pitch/flap coupling due to torsion was discussed. The influence of the torsion degree-of-freedom was quasistatic above a torsion frequency of 4/rev, and negligible above a frequency of 10 to 15/rev. An instability was identified at low collective with moderate torsion stiffness and precone, produced by the effective pitch/lag coupling (positive, hence destabilizing for both soft and stiff inplane rotors with full flap/lag structural coupling).

Friedmann and Tong (Ref. 21) considered the elastic flap-lag stability of a hingeless rotor, neglecting structural flap/lag coupling. The motion was analyzed using an asymptotic expansion based on the method of multiple time scales (including an expansion for small advance ratio). For hover they obtained ellipse-like instability boundaries on the lag frequency-flap frequency plane (similar to Fig. 3, which is for a rigid blade). The asymptotic expansion method identified the instabilities as limit cycles, unstable on the top-right quadrant of the ellipse, and stable elsewhere.

Friedmann (Refs. 22 and 23) developed an analysis of hovering rotor blade flap-lag stability, including the rigid pitch degree of freedom (inboard of the bending flexibility). He neglected structural flap/lag coupling. The destabilizing influence of precone with low pitch frequency was shown (Ref. 22). The conclusions about the influence of droop were incorrect, because of a missing term in the equations.

Hodges and Ormiston (Ref. 24) extended the theoretical work of Ref. 19. They used six free vibration modes of the rotating blades, and considered zero or partial structural coupling (by setting the structural principal axes to a fraction of the aerodynamic pitch angle). Figure 20 shows the flap-lag stability boundaries for the elastic blade (compare to Fig. 4 for a rigid blade). Figures 21-23 show flap-lag-torsion stability boundaries as a function of lag and torsion frequencies, collective pitch, structural flap/lag coupling, and precone.

Friedmann and Straub (Ref. 25) developed a finite-element formulation for the analysis of elastic flap-lag stability in hover. They observed some influence of the second lag bending mode on the stability boundaries for flap/lag coupling around $R = 0.6$ (Fig. 24).

Hodges and Ormiston (Ref. 26) extended the analysis of Refs. 19 and 24 to include pitch-link flexibility and blade droop. The influence of the distribution of pitch flexibility between the pitch link and the blade elastic torsion was considered, including the role in the effective pitch/lag coupling. Figures 25 and 26 show the influence of $f =$ ratio of torsional stiffness to pitch link stiffness ($f = 0$ for a torsionally rigid blade, $f = \infty$ for a rigid control system). There

was little effect of the distribution when the precone and droop were both zero; and with all the flexibility in the blade torsion ($f = \infty$), precone and droop are equivalent. In general the effect of the distribution and the effect of droop are significant.

Friedmann (Ref. 27) developed a theory for flap-lag stability in hover, including both pitch link flexibility and elastic torsion. An axial-inplane-vertical-torsion deflection model was used, including structural flap/lag coupling. The analysis differed from Refs. 24 and 26 primarily in the representation of torsion deflection. The influence of the distribution of pitch flexibility between the pitch link and the blade elastic torsion was considered (Fig. 27). The effect of using the nonlinear equations for the static (trim) deflection was examined. The low collective instability due to precone was relatively weak, since 0.25% to 0.75% structural damping was sufficient to eliminate it (Fig. 28). Structural damping had little influence on the high collective boundary.

Kaza and Kvaternik (Ref. 28) derived the nonlinear equations for the dynamics of an elastic blade in forward flight. They considered both axial-inplane-vertical-torsion and axial-vertical-inplane-torsion deflection sequences in developing the equations.

Johnson (Ref. 29) developed an analysis of helicopter performance, loads, and stability (CAMRAD, for Comprehensive Analytical Model of Rotorcraft Aerodynamics and Dynamics). Warmbrodt and Peterson (Ref. 30) conducted a hover test of a full-scale hingeless rotor (BO-105). The lag damping measurements were compared with calculations obtained from the analysis of Ref. 29. It was essential to include in the analysis the blade pitch and torsion modes (because of their role in determining the effective pitch/lag coupling) and the dynamic inflow model for unsteady aerodynamics (Fig. 29). Good correlation was obtained for the influence of thrust (Fig. 30). A minimum of the measured damping around 400 rpm was not predicted however; the discrepancy could be caused by interaction with the wind-tunnel support (the regressing lag mode was in resonance with the longitudinal balance mode at 400 rpm), but including the body modes in the analysis did not change the predicted damping.

2.2.4 Forward Flight

Miao and Huber (Ref. 13) conducted a wind-tunnel test of a model soft-inplane hingeless rotor with body pitch and roll freedom. The tests showed a favorable effect of reduced precone in forward flight (Fig. 31), just as in hover. The rotor stability increased with forward speed (Fig. 32).

Peters (Ref. 31) analyzed the influence of forward flight on flap-lag stability, using the rigid blade with hinge spring model of Ref. 8. The effects of precone, pitch/flap coupling, and pitch/lag coupling were generally the same at moderate advance ratio as at hover. Figures 33-35 show the influence of advance ratio on flap-lag stability (see Figs. 3-5 for hover). For a particular combination of flap and lag frequencies, the stability was significantly changed above about $\mu = 0.4$. The influence of the periodic coefficients on the stability was not great, however, until much higher speeds (Fig. 36).

Friedmann and Silverthorn (Ref. 32) analyzed flap-lag stability of an elastic blade at high advance ratio. They included structural flap/lag coupling and reverse flow, and linearized the equations about the equilibrium position in hover. Friedmann and Shamie (Ref. 33) continued the analysis of elastic flap-lag stability in forward flight. They linearized the equations about the time-varying blade response of forward flight, which produced much different results than the linearization about hover (Ref. 32). The rotor was trimmed to specified thrust and propulsive force, and zero hub moment (propulsive trim); or trimmed to zero hub moment for fixed collective and shaft angle (moment trim). The stability solution was somewhat sensitive to the trim method, particularly for soft-inplane rotors. Only the blade flap motion was considered in the trim solution.

Friedmann and Kottapalli (Ref. 34) analyzed hingeless rotor flap-lag-torsion stability in forward flight. Reverse flow was included in the aerodynamics, but not stall. Forward flight introduced more variables in the rotor trim solution, and the trim blade deflections were time varying (periodic functions of the rotor azimuth). Moreover, the linearized equations for stability calculations had periodic coefficients. They trimmed the rotor thrust and propulsive force, with zero pitch and roll moments about the helicopter center of gravity, using only the blade flap motion (Fig. 37). For a stiff-inplane rotor, an instability was encountered at an advance ratio of about 0.4, just after the flap mode entered the 1/rev region due to the influence of the periodic coefficients (see Ref. 7). When this case was trimmed to zero hub moment, with fixed collective and shaft angles, it was stable, implying both that the instability is relatively weak (the analysis neglected structural damping) and that the stability solution is sensitive to the trim in forward flight (a reflection of the nonlinearity).

Reddy and Warmbrodt (Ref. 35) analyzed the flap-lag-torsion stability of an elastic blade in forward flight, including multi-blade coordinates and dynamic inflow. The equations were symbolically generated and coded by the computer, beginning with the formulation of Ref. 28 and the ordering scheme of Ref. 24. For the case of propulsive trim with a stiff-inplane rotor, using only the flap motion in the trim solution (as in Fig. 37) gave lower predicted stability than a full flap-lag-torsion trim solution (Fig. 38). Elastic flap/lag coupling (R) and the blade torsion motion significantly influenced the stability for a stiff-inplane rotor (Fig. 38). For a soft-inplane rotor, the stability was increased slightly using a full flap-lag-torsion trim solution, using flap/lag coupling ($R = 1$), or including the blade torsion motion; the character of the stability solution was not changed however. The effect of periodic coefficients was evident in the split roots around an advance ratio of 0.4 in Fig. 38. The periodic coefficients were not a major factor in the instability however; a constant coefficient approximation predicted the instability speed very well.

2.2.5 Bearingless Rotors

Bielawa (Ref. 36) developed an aeroelastic analysis (G400) for bearingless rotors, considering an elastic blade and redundant load paths at the root. A time-history solution gave steady state loads, and transients (for stability), in both

hover and forward flight. A linearized analysis gave eigenvalues (for stability) in hover.

Bielawa, Cheney, and Novak (Ref. 37) conducted small-scale wind tunnel tests of a stiff-inplane composite bearingless rotor (CBR). The rotor used a flat flexbeam of carbon-epoxy, and a torque rod behind the flexbeam. A cantilever torque rod configuration (unconstrained at the root) showed significant pitch washout and pitch/flap coupling. With the torque rod pinned at each end, the rotor was stable and the measured performance and loads were similar to those of a hingeless rotor. A bearingless rotor was designed using an external torque tube, with a snubber at the root to minimize the couplings. Stability was calculated for soft-inplane and stiff-inplane configurations using the analysis of Ref. 36. The predictions showed a high-collective flap-lag instability, as for hingeless rotors with no pitch/lag coupling.

Hodges (Ref. 38) developed an analysis of bearingless rotor air resonance in hover (FLAIR, for Flexbeam Air Resonance). He considered rigid blades, attached to the hub by a single flexible beam or strap, with four rigid body degrees of freedom for the fuselage (excluding vertical and yaw motion, which are not coupled with the air-resonance modes for hover). Leading-edge or trailing-edge pitch-arm geometry was allowed, or both (a pitch control with snubber configuration). An iterative structural analysis obtained the trim flexbeam deflection, then numerical perturbations of the flexbeam stiffness gave the linear equations for a stability analysis.

Hodges (Ref. 39) compared results from the theory of Ref. 38 (for a single flexure with a rigid pitch arm and rigid blade) and from wind-tunnel measurements on a model bearingless rotor (with twin C-beams and a torque rod). Figure 39 shows the influence of precone and droop (such that the total $\beta_p - \beta_d = 2.5^\circ$) and flexbeam prepitch (with the corresponding flexbeam to blade angle set so that the net blade built-in pitch was 7.95°). The data showed that negative droop (producing negative pitch/lag coupling) was preferred to positive precone. There was a small, but favorable, effect of flexbeam pitch angle on air resonance stability because of the increased structural coupling.

Lytwyn (Ref. 40) developed an analysis of bearingless rotor stability. A modal representation of the blades was used, and Floquet theory was used in forward flight. Figures 40 and 41 compare calculated and measured stability for the bearingless main rotor (BMR) on a whirl stand and in flight. Warmbrodt, McCloud, Sheffler, and Staley (Ref. 41) conducted a full-scale wind-tunnel test of the BMR. Hover and forward flight stability measurements were compared with the predictions of Ref. 40 (Fig. 42).

Dawson (Ref. 42) conducted a hover test of model bearingless rotor inplane mode stability (with no body motion). The experiment was designed to verify the predictions of Ref. 38. The rotor had a single flexbeam with an external torque tube. The configurations tested were mainly at zero precone, with the pitch link arm at the leading edge, the trailing edge, or both. With both leading and trailing edge pitch link arms, the blade was stiffer in torsion and there was no pitch/flap coupling. With only the leading edge or trailing edge arm, one position tested was

near the equivalent flap hinge radial station. The influence of pitch/flap coupling was examined by varying the radial location of the pitch arm. The rotor was stiff-inplane at low rotational speed and soft-inplane at high speed. Figures 43 and 44 show the influence of pitch link location and precone/droop; the calculations were obtained from the analysis of Ref. 38 (FLAIR). Figure 43 also shows predictions for one case based on the analysis of Ref. 36 (G400). A pitch-flap flutter instability was encountered in some cases; for example, it occurred in one configuration (trailing edge pitch link, positive pitch/flap coupling, precone) near zero collective and high rotational speed at a resonance of the first torsion and second flap bending mode frequencies. The theory did not predict such instabilities because it lacked higher blade bending modes and unsteady aerodynamics. In general, the experimental results were more complicated than anticipated, with frequent encounters of high blade loads at moderate collective, and pitch-flap flutter.

Bousman and Dawson (Ref. 43) elaborated on the flutter results from hover tests of two- and three-bladed bearingless rotors (Ref. 42). Three types of flutter were identified, all involving little blade lag motion. The first type involved the second flap mode and first torsion mode, and was considered a classical flap-pitch flutter since it occurred around 2.5/rev and at all collective pitch angles. The second type was a single degree-of-freedom flutter of the first torsion mode, occurring above 3/rev and at low collective. The third type was a single degree-of-freedom flutter of the regressing flap mode (for the three-bladed rotor only), occurring slightly above 1/rev and at low collective. Since the purpose of the test was to measure those dynamic characteristics involving the lag motion, a systematic examination of the influence of operating condition and blade parameters on the flutter instabilities was not conducted. Type 1 flutter occurred only with a leading edge pitch link. Type 2 flutter occurred only with an inboard, trailing edge pitch link (positive pitch/flap coupling). Type 3 flutter occurred only with the three-bladed rotor, with an outboard, trailing edge or inboard, leading edge pitch link (negative pitch/flap coupling). The blade configuration with both leading and trailing edge pitch links had a high-torsion frequency, so never encountered flutter. The occurrence of a single degree-of-freedom instability at low collective suggested a wake-excited flutter. The type 3 instability indeed occurred very near 1/rev, and in the correct mode for wake-reinforcement of the unsteady aerodynamic forces. The type 2 flutter, however, was not observed in a mode that would be expected to be associated with wake reinforcement.

Sivaneri and Chopra (Ref. 44) applied a finite element analysis to the calculation of bearingless rotor flap-lag-torsion stability in hover. Significant differences were found between a solution modeling correctly a multiple load-path blade root, and a solution for an equivalent single beam (Figs. 45 and 46). The differences were traced to the nonlinear stiffness elements coupling the flap-lag-torsion motion. In particular, when the pitch of the twin beams at the blade root varied with collective, the flap and lag stiffness and the flap/lag coupling varied. The equivalent properties of the single-beam model could not be defined to reproduce this behavior, hence could not match the the correct blade frequencies at all collective pitch values.

Chopra (Ref. 45) used a finite element analysis to calculate stability for the bearingless rotor model of Ref. 42. The results are shown for one case in Fig. 43. The analysis used seven elements (three on the blade and two each on the flexbeam and the torque tube), plus a spring representing the pitch link.

2.2.6 Ground and Air Resonance

Ormiston (Ref. 46) developed an analysis of ground and air resonance, using the rigid blade with hinge spring model. It was found that pitch/lag and flap/lag coupling did not affect ground resonance at zero thrust, but could stabilize ground resonance at high thrust. These couplings were also predicted to stabilize air resonance, hence could be alternatives to lag-mode structural damping.

Bousman (Ref. 47) conducted a hover test of air resonance stability using a model hingeless rotor (a ground-based test, but the body frequencies were appropriate for air resonance rather than ground resonance). The rotor of Ref. 18 was used, with rigid blades and flap/lag flexures. The rotors were soft-inplane at the resonances with the body pitch and roll modes. Two cases were considered, one matched stiffness and one with the flap flexure much softer than the lag flexure. The test was intended to check the predictions of Ref. 46 that pitch/lag and flap/lag coupling could stabilize air resonance. It was found that these couplings did increase the damping, but were not sufficient to stabilize the case with a soft flap flexure (Fig. 47). The instability was less severe for the matched stiffness configuration, so pitch/lag coupling was indeed able to provide stability. The theory of Ref. 38 was used to analyze this configuration. Generally, the body mode damping was under-predicted by the theory; it was speculated that this discrepancy was due to unsteady aerodynamics. The theory tended to be less accurate at high collectives. The measured damping increased with collective (except at an air resonance instability), while the theory did not (particularly at the higher rotor speeds).

Yeager, Hamouda, and Mantay (Ref. 48) conducted a wind tunnel test of a model soft-inplane hingeless rotor, with body pitch and roll motion. The measurements showed the favorable influence of precone or negative droop on the stability. Calculations using the method of Ref. 29 gave good correlation with the experimental data, for both hover and forward flight (Figs. 48 and 49).

Hooper (Ref. 49) used the analysis of Ref. 38 to examine the influence of blade-design parameters on the air resonance and ground resonance stability of a bearingless rotor. The configuration considered involved a single-beam flexure, and a rigid torque tube with a single shear restraint (pitch link) on the flexbeam axis (for zero coupling). Air resonance instability was predicted for high rotor speed and high collective, at the resonance with the regressing flap mode. Hub and blade sweep, hub and blade prepitch, and hub precone did not change the stability significantly. Blade negative droop or vertical offset of the torque tube shear restraint above the flexbeam were stabilizing. Both parameter changes produced negative pitch/lag coupling, which stabilized the blade flap-lag motion sufficiently that the air resonance instability occurred only in a narrow rotor speed range at resonance (which occurred at a fairly low rotor speed as well). The ground resonance instabilities, at resonances with the body pitch and roll modes, were more severe and

less sensitive to collective than the air resonance instability. Negative droop or vertical offset of the shear restraint stabilized the pitch mode resonance (at low rotor speed) but destabilized the roll mode resonance (at high rotor speed). At low collective even the pitch mode was destabilized slightly by these parameters. It was concluded that it would be necessary to design the helicopter to avoid the roll mode, or use damping augmentation.

2.3 Loads

Regarding the prediction of rotor and airframe structural loads, it is not possible to identify a single assumption, a single limitation, or a single discipline that dominates the problem. For a good prediction of loads it is necessary to do everything right, all of the time. With current technology it is possible to do some of the things right, some of the time. Most of the recent development of rotor dynamics theory has concerned the stability problem. The loads analysis requires the full nonlinear solution, not just the linearized equations, and demands much more attention to the aerodynamics.

Piziali (Ref. 50) made the observation that there had been significant progress in the development of rotor aeroelastic computer simulations, but that the progress had been primarily in expanding the scope of the predictive capability. During the previous decade, the improvement in correlation between measurements and predictions had not been significant. Piziali was speaking at the 1973 AGARD conference on rotor loads, and referring to progress since the initial work with nonuniform inflow calculations in the early 1960s. The statement is equally valid now; recent advances have been in scope, not accuracy. It is possible to make loads predictions for the new rotor concepts that are of sufficient accuracy to support engineering design and development. Yet the level of accuracy for these predictions is about the same as the capability for today's conventional rotors when they were new; and the correlation of measured and predicted loads on conventional rotors has not improved significantly either. Piziali also made the comment that the technology level did not then limit the structural representation, but it did limit the aerodynamic representation; the participants at the conference did not agree. Reichert agreed that the limiting factor in the aerodynamics is obtaining a fundamental model of the phenomena, and he added that the limiting factor in the dynamics is the complexity of the code. Carlson and Kerr emphasized the multidisciplinary nature of the loads problem. Yen and Weller (Ref. 51) remarked that a good prediction of loads requires an accurate representation of the structure, state-of-the-art aerodynamics, plus the user's knowledge and experience with the analysis. So there is still some art as well as science in the task.

The AGARD conference of 1973 (Refs. 52-58) provided a good summary of rotor loads predictive capability. Generally the computer codes used then are still the primary design tools of the industry. Figures 50-55 illustrate the predictive capability for articulated, teetering, and hingeless rotors. More recent efforts (Refs. 51 and 59-62) have produced similar results (Figs. 56-60).

Sopher, Studwell, Cassarino, and Kottapalli (Ref. 63) compared predicted and measured loads for a wind tunnel test of an articulated model rotor (representative

of the UH-60). Calculated edgewise bending loads were higher than measured (Fig. 61), due to a high 5/rev predicted load. The predicted edgewise first elastic bending mode was at 5/rev, so there was a significant increase when body motion was included in the analysis. The calculated torsion loads were low, because of underprediction of the 1/rev to 4/rev harmonics. The sensitivity of the loads to prescribed higher harmonic control changes was significantly underpredicted (but the measured edgewise loads showed a significant 6/rev component, so the control in the rotating frame might not have been pure 3/rev).

It is more difficult to predict blade torsion and pitch link loads than to predict bending loads. The torsion forces (aerodynamic, inertial, and structural) are higher order than the forces responsible for bending loads, and blade stall is particularly significant for torsion loads. Staley (Ref. 59) calculated hingeless rotor loads using a computer code originally developed for teetering and articulated rotors (Fig. 59). This theory significantly underpredicted oscillatory pitch link loads above 60 knots, because the measured loads were predominantly 1/rev while the calculated loads were 3/rev. Sheffler (Ref. 60) was able to predict blade bending loads well even at high thrust and high speed (Fig. 60). The prediction of the torsion moment at high thrust was poor even at moderate speed however (Fig. 62), because stall was encountered too early in the theory and thereafter the calculated load did not increase much with thrust.

Yen and Weller (Ref. 51) calculated loads on an articulated rotor, both with standard blades and with tabbed blades (Fig. 57). Their results illustrate well the limits of current load prediction capability. The calculated mean and oscillatory pitch link loads agreed well with test (Fig. 63). Yet examination of the corresponding time histories (Fig. 64) reveals that the fundamental phenomena involved were not being modeled correctly: the tab changed the measured time history dramatically, while the predictions for the two blades had very similar character.

2.4 Vibration

Rotor-induced vibration prediction adds an increased importance of the airframe structural dynamics to the many disciplines already required for loads prediction. Reichert (Ref. 64) discussed various means for vibration control on helicopters: pendulum or bifilar absorbers on the blades or hub; rotor isolation, anti-resonance isolators, or absorbers on the airframe; and higher harmonic control. There has been a clear trend of reduced helicopter vibration in newer designs--after vibration treatment has been included (Fig. 65). Reichert made the point that analysis of vibration is not adequate, and identified the need to model the airframe as well as the rotor.

Cronkrite (Ref. 65) compared NASTRAN predictions and shake test results for AH-1G airframe structural dynamics. A model intended to be valid up to about 30 Hz (above 5/rev) was developed. The structural damping was particularly difficult to quantify for the analysis; here 2% critical damping was assumed. In the frequency response above 20 Hz, the tests showed more damping than predicted (Figs. 66 and 67).

Stoppel and Degener (Ref. 66) compared NASTRAN predictions and shake test results for BO-105 airframe structural dynamics. A large order model was needed for accuracy. A frequency error of about 5% was achieved for the lowest modes, and 10% for the higher modes (Fig. 68). It was noted that the large concentrated masses typical of helicopter structures result in many modes at relatively low frequency (specifically, below 8/rev or about 56 Hz for the BO-105).

Gabel, Reed, Ricks, and Kesack (Ref. 67) developed a NASTRAN finite element model of a CH-47D airframe, emphasizing the prediction of structural vibration. They documented the planning and development of the NASTRAN model, the predictions, the shake test, and the correlation of the measured and predicted response. The correlation below about 20 Hz was considered good by the standards of the industry (Fig. 69), particularly the forced vibration at 3/rev and 6/rev. The predictions at high frequency were not considered good. The calculations were based on 2.5% structural damping for all modes. Correct modeling of the damping would improve the prediction of peak amplitudes (for example, in the lateral response shown in Fig. 69). To improve the correlation of mode shape and frequency, it would be necessary to increase the detail of the structural modeling (including the test fixture), and of the mass distribution. Figure 70 illustrates the achievable improvement.

Sopher, Studwell, Cassarino, and Kottapalli (Ref. 63) compared predicted and measured vibration for a wind tunnel test of an articulated model rotor (representative of the UH-60). Two representations of the rotor support structure were considered: a three-mode model, consisting of the modes nearest 4/rev (between 3.4 and 5.2/rev), and a nine-mode model, consisting of all body modes from 1.9 to 6.5/rev. The trends of the vibration with forward speed and higher harmonic control were predicted satisfactorily, but the absolute levels were not correct (Fig. 71). The predicted absolute levels of vibration were sensitive to the body modal characteristics. The vibration change due to a prescribed higher harmonic control input was underpredicted, although the results were improved using the nine-mode body model (Fig. 72). Comparison was also made between the experimentally determined optimum vibration using higher harmonic control and the theoretically determined optimum (not using the measured values of the control inputs).

Gabel and Reichert (Ref. 68) examined the use of pendulum absorbers to reduce the vibration level on the BO-105 helicopter in transition, between 20 and 40 knots (Figs. 73 and 74). Flap and lag pendulum absorbers for 3/rev vibration were used. A blade tuning weight, to get the third flap mode below 5/rev, was also used; the tuning weight was not effective alone however. The final configuration of pendulum absorbers and tuning weights was 1.25% of the gross weight.

3. ADVANCED TOPICS IN DYNAMICS

Next, advanced topics that are the subject of current research will be considered: vibration control, dynamic inflow, finite element analyses, and composite materials.

3.1 Vibration Control

Passive control of helicopter vibration, such as discussed above, has the disadvantages of significant weight penalty and lack of flexibility. There are numerous concepts for active control of vibration, for example, Ham (Ref. 69), Kretz (Ref. 70), Gupta and DuVal (Ref. 71), and Jacob and Lehmann (Ref. 72). The present discussion will concentrate on the concept that has been carried to flight tests--the self-tuning regulator. This approach is based on the use of blade pitch motion at harmonics of the rotor speed above 2/rev in the rotating frame, and hence is referred to as multicyclic or higher-harmonic control. Among the early work was a test reported by McCloud and Kretz (Ref. 73) and Kretz, Aubrun, and Larche (Ref. 74), of multicyclic control on a full-scale jet-flap rotor in a wind tunnel. Johnson (Ref. 75) gives a full derivation and comparison of the various self-tuning regulators for multicyclic control of helicopter vibration. Only the version of the regulator that has been flight tested will be discussed here.

A self-tuning regulator is a control system combining recursive parameter estimation with linear feedback. As developed for multicyclic control of helicopter vibration and loads, this regulator is characterized by (1) a linear, quasi-static, frequency-domain model of the helicopter response to control; (2) identification of the helicopter model by a Kalman filter; and (3) a quadratic performance function controller. Figure 75 outlines the control task: minimize airframe vibration (and perhaps loads or even power) using blade pitch control (defined in the rotating or nonrotating frame).

The requirement for an adaptive control system, in which the parameters describing the helicopter model are identified on line, follows from the inability of current analytical tools to predict vibration characteristics with sufficient accuracy; and from sufficient sensitivity of the vibration characteristics to changes in aircraft configuration and flight condition that a prescribed-parameter control system would be ineffective or at least inefficient.

It is assumed that the helicopter can be represented by a linear, quasi-static frequency-domain model relating the output vector z (consisting of harmonics of the vibration) to the input vector θ (consisting of harmonics of blade pitch control) at time $t_n = n \Delta t$:

$$z_n = z_0 + T\theta_n$$

The sampling interval Δt must be long enough for transients to die out and the harmonics to be measured. The assumption of linear response to control is supported by the experimental observation that only a small multicyclic control amplitude (of the order of 0.5 to 1.5 deg) is required for vibration alleviation. There is theoretical and experimental evidence both supporting and contradicting the assumption of linearity. There are observed phenomena that may be attributable to nonlinearity, and there are arguments that an iterative linear model is appropriate even for a nonlinear system.

The uncontrolled vibration level z_0 and the control matrix T are not known; the state-of-the-art of vibration prediction is not sufficient to allow their calculation to the required accuracy. Hence, an adaptive control system is required, in which these parameters are to be identified during the control process. Grouping the unknown parameters into a single matrix and introducing measurement noise gives:

$$z_n = [T z_0](\theta_n^T \ 1)^T + v_n$$

The measurement noise v_n is assumed to have zero mean, variance r_n , and Gaussian probability distribution. The lack of knowledge of the system parameters will be expressed by modeling them as a random process:

$$[T z_0]_{n+1} = [T z_0]_n + U_n$$

where U_n is a random variable with zero mean, variance Q_n , and Gaussian probability distribution. This equation implies that the parameters vary and that the order of the change in one time-step can be estimated, but no information is available about the specific dynamics governing the variation of the parameters. Then the minimum error-variance estimate of the parameters is obtained from a Kalman filter:

$$[\hat{T} \ \hat{z}_0]_n = [\hat{T} \ \hat{z}_0]_{n-1} + (z_n - \hat{z}_{on-1} - \hat{T}_{n-1} \theta_n) k_n^T$$

The Kalman gains are obtained from:

$$k_n = P_n (\theta_n^T \ 1)^T / r_n$$

$$P_n^{-1} = (P_{n-1} + Q_{n-1})^{-1} + (\theta_n^T \ 1)^T (\theta_n^T \ 1) / r_n$$

where P_n is the variance of the error in the estimate, after the measurement. (See Ref. 75 for further details; the estimation of parameters is in fact done by rows.)

The control algorithm is based on the minimization of a quadratic performance index:

$$J = z_n^T W_z z_n + \theta_n^T W_\theta \theta_n + \Delta\theta_n^T W_{\Delta\theta} \Delta\theta_n$$

where $\Delta\theta_n = \theta_n - \theta_{n-1}$. Typically, the weighting matrices are diagonal, so J is a weighted sum of the mean squares of the vibration, loads, and control. The matrices W_θ and $W_{\Delta\theta}$ constrain the amplitude and the rate of change of the control, respectively. The control law is obtained by substituting for z_n , setting the derivative of J with respect to control to zero, and solving for θ_n :

$$\theta_n = Cz_0 + DW_{\Delta\theta} \theta_{n-1}$$

where

$$C = -DT^T W_z$$

$$D = (T^T W_z T + W_\theta + W_{\Delta\theta})^{-1}$$

This is referred to as an open-loop control law in Ref. 75, since it is based on the uncontrolled vibration level z_0 . In the adaptive system, z_0 is in fact identified from the current vibration measurement z_n . An alternative form of the control law is:

$$\Delta\theta_n = Cz_{n-1} - DW_{\theta} \theta_{n-1}$$

which involves the direct feedback of the measured vibration, whether the system parameters are identified or not (referred to as a closed-loop control law; see Ref. 75 for further details).

Limiting the control amplitude by use of the weighting matrix W_θ has the effect of reducing system effectiveness at all conditions. It is preferable that the control authority be sufficient to allow full use of the active alleviation system. Implementation of external constraints on rate of change of control leads to poor dynamic response; such limits should be an integral part of the control law. Limiting the rate of change of the control by use of the weighting matrix $W_{\Delta\theta}$ is very beneficial: the dynamic response of the system is unacceptable without it and good with it, yet a control rate limit does not change the final optimum solution.

The above derivation of the control law assumed that the parameters are known; the result was a deterministic controller. With unknown estimated parameters, the certainty-equivalence principle may be applied: the deterministic control solution is simply used with the estimated parameter values. Alternatively, the possibility of errors in the parameter estimates can be acknowledged by minimizing the expected value of the performance index:

$$J = E(z_n^T W_z z_n) + \theta_n^T W_\theta \theta_n + \Delta\theta_n^T W_{\Delta\theta} \Delta\theta_n$$

which produces a cautious controller. The result is equivalent to introducing a weighting matrix on the control amplitude or rate, proportional to the parameter error-variance (which is calculated in the course of the Kalman filter identification procedure; the a priori estimate error, $M_n = P_{n-1} + Q_{n-1}$, is used). With the closed-loop form of the control law, caution introduces an effective limit on the control rate ($W_{\Delta\theta}$). With the open-loop form of the control law, caution introduces an effective limit on the control amplitude (W_θ). Reference 75 provides complete details. Hence the cautious controller provides a means to automatically introduce control limits to compensate for uncertainty in the parameter estimates. That the controller development process need not be concerned with picking the weighting matrix is an advantage; that the designer no longer has the option of selecting the weighting matrix is a disadvantage. Use of a rate limit ($W_{\Delta\theta}$) is probably always

desirable, but is not provided by the caution with the open-loop form of the control law. There is an additional problem (that may be of more theoretical than practical concern). The number of parameters to be identified will be much greater than the number of measurements, implying an identifiability problem: there may not be enough information in the measurements to identify all the parameters individually. Simulations show that the feedback control system generally is well behaved, which may be explained by the view that it is necessary to accurately identify the control values required for minimum vibration (about the same in number as the number of measurements), not the individual values of all the parameters. The identifiability problem can, however, be reflected in large values of the parameter error-variance in the Kalman filter, which would introduce large control limits with the cautious controller.

The two options for identification (off-line or adaptive) and the two options for control (feedback of z_0 or z_n ; i.e., open loop or closed loop) implies four configurations for the self-tuning regulator (Ref. 75). The configuration of interest here is the adaptive open-loop regulator (Fig. 76), consisting of on-line identification of the parameters and calculation of the gain matrix, with control based on the identified value of the uncontrolled vibration level z_0 . This system has been investigated analytically, and in both wind tunnel and flight tests. The configuration tested was the cautious controller, without explicit limits on control amplitude or rate (W_θ or $W_{\Delta\theta}$).

Hammond (Ref. 76) tested a four-bladed, model articulated rotor in a wind tunnel, with the adaptive open-loop regulator. The cautious controller form was required for smooth operation during changing test conditions. Vibration alleviation capability was assessed in terms of the vibratory hub moments and vertical shear (Fig. 77). A 70%-90% reduction of the 4/rev vertical force was achieved, and a 30%-70% reduction of the 4/rev pitch moment; the 4/rev roll moment was reduced only slightly. The higher harmonic control produced some decrease in blade flapwise bending loads; and an increase in edgewise bending, torsion, and pitch link loads (Fig. 78).

Molusis, Hammond, and Cline (Ref. 77) extended the work of Ref. 76 by using feedback of acceleration rather than hub load measurements. The regulator was tested in steady-state operating conditions; with varying wind-tunnel speed; and with collective pitch variations. Generally, the conditions for minimum vibration levels did not correspond to those for minimum oscillatory hub loads; it was essential to sense the vibration directly. The cautious controller showed smooth operation and good tracking ability. The vertical and longitudinal vibrations were reduced significantly, but the lateral acceleration was increased at low speed (Fig. 79). The influence of the regulator on blade loads was similar to that in Ref. 76.

Wood, Powers, Cline, and Hammond (Ref. 78) reported results from flight tests of this regulator on an OH-6A helicopter. Again, the adaptive, open-loop regulator with caution was used. The 4/rev vertical and lateral vibration were reduced significantly (Fig. 80), but the longitudinal vibration increased at high speed. The

pitch link loads were increased by the presence of higher harmonic control, and there was some increase in blade bending loads (Fig. 81).

Gupta, Wood, Logan, and Cline (Ref. 79) conducted further higher harmonic control flight tests with the OH-6A. The controller software was changed from fixed point to floating point for better accuracy. The system and measurement noise variances in the Kalman filter were adjusted in flight to optimize the identification. The result of these changes was a significant improvement in the performance of the regulator (Fig. 80). The control system reduced the cockpit vibration on all three axes simultaneously.

3.2 Dynamic Inflow

Despite the long-established importance of unsteady aerodynamic forces in aeroelastic phenomena, an entirely satisfactory model for rotary wing unsteady aerodynamics is still not available. A model for the noncirculatory loads can be readily obtained from two-dimensional unsteady airfoil theory, but the results from either two-dimensional or fixed-wing three-dimensional wing theory for the circulatory loads are not applicable since the wake models are not correct for rotary wings. The development of a general theory for rotor unsteady airloads is difficult because of the complex geometry of the rotor wake, even in hover. Moreover, in forward flight a time-invariant model of the system is not possible because of the periodically varying aerodynamic environment of the blades. Consequently, attention has recently been focused on the development of relatively simple models for the unsteady aerodynamics. These models take the form of differential equations for parameters defining the wake-induced velocity distribution over the rotor disk, hence are referred to as dynamic inflow models. Johnson (Refs. 7 and 80) and Gaonkar and Peters (Ref. 81) provided a derivation and discussion of dynamic inflow.

Typically, the wake induced velocity perturbation is represented by a linear variation over the rotor disk:

$$\delta\lambda = \lambda_u + \lambda_x r \cos \psi + \lambda_y r \sin \psi$$

where r and ψ are the polar coordinates of the rotor disk, so λ_u defines a uniform variation of the induced velocity, while λ_x and λ_y define longitudinal and lateral variations, respectively. The induced velocity variables are related to the net aerodynamic loads on the rotor (thrust C_T , pitch moment C_{M_y} , and roll moment C_{M_x}) by a first order differential equation:

$$\tau \dot{\lambda} + \lambda = (\partial\lambda/\partial L)L$$

where

$$\lambda = (\lambda_u \quad \lambda_x \quad \lambda_y)^T$$

$$L = (C_T \quad -C_{M_y} \quad C_{M_x})^T$$

This is a low-order, global model of the rotor unsteady aerodynamics. The model can only represent low-frequency effects. Note that with no flap-hinge offset, an articulated rotor cannot sustain a hub moment. Hence, the linear components of the dynamic inflow model are primarily important for hingeless rotors.

The derivative matrix $\partial\lambda/\partial L$ can be obtained from differential momentum theory (see Peters (Ref. 82) and Johnson (Ref. 7)) or from unsteady actuator disk theory (see Miller (Ref. 83), Pitt and Peters (Ref. 84), and Johnson (Ref. 7)). Rotor response and stability measurements, as well as parameter identification work, generally support the values so obtained for hover. The inflow dynamics model is not as well verified for forward flight as for hover, but the model of Pitt and Peters (Ref. 84) is proving to be very effective (see Ref. 81).

Typically, the time lag is written $\tau = \kappa(\partial\lambda/\partial L)$, where κ is a diagonal, constant matrix. The values for the constants in κ are obtained by considering the apparent mass of an impermeable disk subject to linear or angular motion (see Peters (Ref. 82) and Pitt and Peters (Ref. 84)). These estimates are supported by experimental data and parameter identification, at least to within a factor of two (Ref. 80). Without the time lag ($\tau = 0$), a quasi-static inflow model is obtained, the effects of which are expressed by a lift deficiency function (Refs. 7 and 80). For rotor dynamics problems in which the dominant aerodynamic forces are the lift perturbations due to angle-of-attack changes, the magnitude of the aerodynamic influence is described by the blade Lock number (which contains the section lift curve slope). Hence, in such cases, the effects of the quasi-static inflow model can be largely represented by the use of an effective Lock number that is the product of the actual Lock number and the lift deficiency function (see Curtiss and Shupe (Ref. 85)). A quasi-static inflow dynamics model has long been used in handling qualities analyses. The need for the time lag appears to depend on the specific problem involved. The influence of the time lag is often enough to be measurable, but the quasi-static model may still give qualitatively correct results.

In applications of the dynamic inflow model, the model has been found to be important more often than not, which is a reflection of the importance of unsteady aerodynamics to rotor aeroelastic problems. Dynamic inflow is a practical way to add unsteady aerodynamics to rotor stability calculations, because it is a finite state model (ordinary differential equations). The simplicity of the model, as well as its fundamental limitations, follow from the assumptions of low frequency and an actuator disk representation.

Peters and Gaonkar (Ref. 86) calculated the influence of dynamic inflow (using the model of Ref. 82) on the flap-lag stability in forward flight. The rigid blade with springs model of a hingeless rotor was used, with no pitch/lag or flap/lag coupling. The influence of unsteady aerodynamics was significant, particularly for the regressing lag mode (Fig. 82).

Johnson (Ref. 80) calculated the influence of dynamic inflow on hingeless rotor ground resonance, comparing with the experimental data of Ref. 47 (discussed above). It was shown that the unsteady aerodynamics were essential for a correct calculation

of the body mode damping (Fig. 83). For the matched stiffness configuration, the test identified a low frequency mode that did not correspond to any expected structural mode of the system (Fig. 84; the body pitch and roll modes and the regressing lag mode were accounted for, and the regressing flap mode was known to have too much damping to be observed in this experiment). The calculations associated this mode with the dynamic inflow variables (of course highly coupled with the flap and body motion; Fig. 85), and also predicted that the mode should be measurable for the matched stiffness configuration but not for the other configuration tested (which had a reduced flap flexure stiffness, hence reduced hub moment capability). Thus the existence of this mode in the experimental data, and its successful prediction, confirmed the global, low-frequency character of the unsteady aerodynamics of the rotor--confirmed (for this problem) the fundamental assumptions of the dynamic inflow model.

Warmbrodt and Peterson (Ref. 30) measured the lag damping of a BO-105 rotor in hover. Calculations of the blade stability (using the analysis of Ref. 29) showed the necessity for the dynamic inflow model in this case (Fig. 86). They also noted that it should be possible to directly measure the unsteady aerodynamic influence, since it is predicted to be present in the regressive (low frequency) lag mode but absent in the progressive (high frequency) lag mode.

3.3 Finite Elements

The use of finite element techniques for structural dynamic modeling promises to bring long-needed flexibility to rotorcraft analyses. Such flexibility is particularly desired in the modeling of the rotor hub and blade root, where most of the design innovation appears in new configurations. The survey of Friedmann (Ref. 4) included a review of finite element methods. The use of a finite element method for the free vibration modes of a rotor blade is not uncommon. What still requires development is a full application of finite element discretization to the nonlinear, coupled aerodynamics/dynamics/structural problem of calculating rotor response. A major limitation of rotor analyses based on finite element methods is the very long computing times required. In most applications of finite elements to rotor problems it has been necessary to introduce free vibration modes at some stage, in order to reduce the number of degrees of freedom to a manageable level.

Yasue (Ref. 87) developed a finite element analysis for the flap-lag-torsion response of a rotor to vertical gusts in forward flight. The degrees of freedom for each element were: displacement and slope of the inplane, vertical, and torsion deflection, at each end of the element. The deflection was represented then by third order polynomials within the element. Rigid pitch motion of the blade was introduced at the blade root. The trim solution was obtained from the linear equations for the bending motion only, using a Galerkin technique (not finite elements). Then the gust response was calculated from linearized equations for the free vibration modes, which were obtained from the finite element representation.

Friedmann and Straub (Ref. 25) developed a finite element formulation for the elastic flap-lag stability of a rotor in hover. The spatial dependence of the linearized partial differential equations of motion was discretized using a local

Galerkin method of weighted residuals. The degrees-of-freedom for an element were the displacement and slope of the vertical and inplane deflections, at each end of the element (Fig. 87, without torsion). Cubic interpolation polynomials were used for the displacement within an element. Free vibration modes were calculated from the finite element model, and then the nonlinear finite element equations were transformed to modal equations. Finally the nonlinear modal equations were solved for the static equilibrium deflection, and the linearized equations were solved for the stability. The solution was converged with four or five elements used to model a uniform blade; six to eight elements were required when torsion motion was included.

Sivaneri and Chopra (Ref. 88) developed a finite element analysis for the flap-lag-torsion dynamics of a hovering rotor. They obtained the steady state deflection by solving the finite element equations directly (in previous work, the finite element method was used to calculate the free vibration modes, which were then used to solve for the trim blade deflection). The beam equations of Ref. 20 were used. The blade motion was represented by first radial, then inplane, then vertical, and finally pitch deflection (u , v , w , and θ). The pitch θ was comprised of the collective and built-in twist contributions, plus the geometric torsion deflection ϕ :

$$\hat{\phi} = \phi - \int_0^x v''w' dx$$

where ϕ is the elastic torsion degree of freedom, and x is the blade radial coordinate. The variable $\hat{\phi}$, rather than the torsion degree of freedom ϕ , was used in the finite element model because the inter-element coupling is defined in terms of the geometric displacement and rotation at nodes. The analysis was restricted to single load path designs. It followed that the centrifugal force was known a priori along each element; the equation of axial force equilibrium could be directly integrated for u ; and so the axial displacement u could be eliminated from the equations. Hence the degrees of freedom for each element were: the inplane and vertical displacement and slope (v , v' , w , w'), and the geometric twist displacement ($\hat{\phi}$), at each end of the beam (Fig. 87). The displacement within the beam was interpolated using Hermite polynomials: third order for v and w deflections (corresponding to a linear variation of bending moment), and first order for $\hat{\phi}$ (corresponding to a constant torsion moment). Examples were executed for hover, using 10 elements to represent the blade. The trim problem required solution of a nonlinear algebraic equation, with a banded spring matrix. The equations were linearized about the trim solution to calculate stability. The damping matrix was not banded even for a single load path, because of the Coriolis forces (entering an element equation through the axial displacement). The linearized equations were first solved for the free vibration modes, and then these modes were used as degrees of freedom in the stability analysis.

Silvaneri and Chopra (Ref. 44) extended the analysis of Ref. 88 to the case of a rotor blade with multiple load paths at the root--a bearingless rotor. With multiple load paths, the distribution of the centrifugal force among them was not

known a priori. So it was no longer possible to eliminate the axial displacement variable and equations from the analysis; moreover, it became necessary to iterate on the calculation of the centrifugal force in the solution procedure. Here the degrees of freedom for each element were: axial displacement (u), inplane and vertical displacement and slope (v, v', w, w'), and the geometric twist displacement ($\hat{\phi}$) at each end; axial displacement (u) at two interior nodes, equally spaced along the element length; and the geometric twist displacement ($\hat{\phi}$) at the element midpoint (Fig. 87). The displacement within the beam was interpolated using Hermite polynomials: third order for v and w deflections and second order for $\hat{\phi}$ (corresponding to a linear variation of bending and torsion moments), and third order for the axial displacement u (corresponding to a quadratic variation of the tension force). The interior node for $\hat{\phi}$ was introduced so the torsion moment variation would be linear, consistent with the bending moment variation. The two interior nodes for u were introduced so the tension variation would be quadratic, consistent with the centrifugal force for uniform mass distribution. The multiple beams at the root and the single beam of the outboard blade were joined at a rigid clevis. The solution procedure followed that of Ref. 88. The mass and stiffness matrices were not banded with a multiple load path at the root. Examples were executed using six to ten elements to represent a bearingless rotor (Figs. 45 and 46).

Rutkowski (Ref. 89) developed a finite element analysis for the rotor flap bending and airframe vertical motion. The equations for the coupled rotor and fuselage motion were linear in this case; hence the trim solution did not influence the stability. The stability was calculated using the free vibration modes (for the entire system, rotor and body), which were obtained from the finite element analysis. A single load path was assumed for the rotor blades; the element equations were therefore similar to those of Ref. 88.

Lefrancq and Masure (Ref. 90) developed a finite element analysis that was used to calculate the frequency and damping of the Triflex tail rotor. The analysis was used to examine the influence of the weight and stiffness of the sleeve.

Borri, Lanz, and Mantegazza (Ref. 91) and Borri, Lanz, Mantegazza, Orlandi, and Russo (Ref. 92) developed a rotor analysis using the finite element representation for azimuthal variations as well as spacial displacements (STHR, for Stability and Trim Analysis of Helicopter Rotor). The analysis used a finite element or component representation of an isolated rotor blade, including the control system and blade root geometry. The blade response was calculated, and the method was intended to calculate stability as well. By using a finite element representation for the time variation, the dynamics problem was reduced to a nonlinear static problem, to which the conventional techniques of static finite element structural analysis could be applied (for assembly, solution, and data management). It was noted that the computation time became very large when many space-time elements were used.

Giavotto, Borri, Russo, and Ceriotti (Ref. 93) continued the development of the analysis of Refs. 91 and 92. The dynamics problem was formulated as nonlinear algebraic equations. The trim solution was obtained from the constraint that the motion be the same at the beginning and at the end of one rotor revolution. Perturbations of all variables at the beginning and end of one revolution then gave the

state transition matrix for a Floquet stability analysis. This state transition matrix was identical to the converged derivative matrix that was already required in the Newton-Raphson solution for the trim response.

Hodges (Ref. 94) developed a finite element computer code (GRASP, for General Rotorcraft Aeroelastic Stability Program) for the stability of a coupled rotor body in hover or vertical flight. Beam and rigid body elements were considered. No small angle assumptions were made in defining the orientations of the elements, and multiple load-path structures could be analyzed. The variable order, nonlinear, slender beam element was assumed to undergo small strains, but the rotations due to deformation could be large. The nonlinear algebraic equations were solved for the static deflection, and then the linearized equations were assembled and solved for the stability.

3.4 Composites

The use of composite materials for rotor blades and hubs and in helicopter airframes is increasingly common. Composite materials are replacing metals because of better fatigue and strength characteristics for a given stiffness, and better damage tolerance and failure characteristics. For a given bending stiffness (EI), cross section size (z_{max}), and load (M), the maximum stress in a beam is proportional to the modulus: $\sigma_{max} = Mz_{max}/I = (Mz_{max}/EI)E$. Hence, for rotor blade materials a high strength to modulus ratio is desired. Composite materials such as fiberglass and graphite have σ/E values several times that of steel or aluminum. (The lower modulus (E) of composites implies a larger area moment I for a given stiffness. For cases where a large I is unacceptable, titanium may be a good compromise, with σ/E and E values between composites and steel.) Composites can offer advantages in fatigue characteristics and failure modes as well. The use of composite materials also allows additional design flexibility, bringing the opportunity to tailor detailed structural properties as well as overall structural couplings of rotor blades. This additional flexibility will not be fully utilized until the rotor analyses can handle all the unique characteristics of composite materials.

Composite materials are generally orthotropic: the material properties are symmetric with respect to three planes, when one of the coordinates is aligned with the fiber direction. For an orthotropic material, Hooke's law relating the stress tensor to the strain tensor takes the form:

Worndle (Ref. 96) developed an analysis for the section properties of a composite blade (such as stiffnesses and shear center). The fiber-reinforced material was assumed to be orthotropic, with one axis aligned with the blade span axis, but the other two axes not corresponding to the section axis system. Hence, beam theory was used for a monoclinic material, with the plane of symmetry normal to the span axis. A finite element method was used to solve for the required warping function.

Hong and Chopra (Ref. 97) calculated the flap-lag-torsion stability of a composite rotor blade in hover. The finite element methods of Ref. 88 were used. The equations for a rotating beam were derived following Ref. 20. The composite material introduced the possibility of stiffness terms coupling bending/torsion and tension/torsion. The rotor spar was represented by a box beam, each side consisting of several laminates of composite material, each laminate at a specified ply angle. The section was monoclinic. For horizontal laminates the plane of symmetry was horizontal (the $x-y$ plane; with the x -coordinate spanwise, y inplane, and z vertical). For vertical laminates the plane of symmetry was vertical (the $x-z$ plane). Hence, the shear stress, σ_{xy} or σ_{xz} for the horizontal or vertical laminates, respectively, were coupled to the normal strain ϵ_{xx} by the parameter Q_{16} . Transforming the orthotropic material properties at ply angle Λ to the section coordinate system gave Q_{16} for each laminate. Q_{16} would be zero for isotropic materials, or with ply angles of $\Lambda = 0$ or 90° . A nonzero value of Q_{16} introduced linear and nonlinear terms into the equations for beam deflection, extension, and torsion, producing bending/torsion and extension/torsion coupling. For a symmetric orientation of the plies on the sides of the spar, the ply angle introduced a pitch/lag type of coupling, that had a significant effect on the lag damping (Fig. 88). For a symmetric orientation of the plies on the top and bottom of the spar, the ply angle introduced a pitch/flap type of coupling, that had a significant effect on the flap mode frequency. For an antisymmetric orientation of the plies, the ply angle introduced an extension/torsion coupling; this was a nonlinear effect, but had a significant influence on the stability (Fig. 89).

4. DYNAMICS OF ROTORCRAFT CONFIGURATIONS

Finally, the dynamics of various rotorcraft configurations are considered: hingeless rotors, bearingless rotors, rotors utilizing circulation control, coupled rotor/engine dynamics, articulated rotors, and tilting proprotor aircraft. The emphasis is on describing the design approaches, problems encountered during development, and solutions to those problems.

4.1 Hingeless Rotors

The hingeless rotor replaces the flap and lag hinges of the articulated rotor with bending flexibility at the blade root. The pitch bearing is retained. The hingeless rotor offers the advantages of mechanical simplicity and increased hub moment capability. The latter has a favorable influence on handling qualities, by increasing the damping and control power of the rotor. These advantages are accompanied by new stability phenomena, and some adverse effects of the increased hub

moments, including higher vibration and gust response, and increased angle-of-attack instability. The dynamics analyses required to support the design of a hingeless rotor are more complicated, since structural modes replace the fundamental rigid body modes of the articulated blade.

Ormiston (Ref. 5) and Strehlow and Enenkl (Ref. 98) summarized the design considerations for hingeless rotors. The frequencies of the fundamental flap and lag modes are the first design choices. A flap frequency of 1.10 to 1.15/rev was typical of the first successful hingeless rotors. The current trend is to require lower flap frequencies, for reduced vibration and gust response and to minimize adverse handling qualities effects at high speed. The goal is a flap frequency in the range 1.06 to 1.08/rev (an articulated rotor would have a frequency less than about 1.04/rev). This range is difficult to achieve with a hingeless rotor, although the use of small hubs made from composite materials helps. A soft-inplane rotor (lag frequency below 1/rev) will be susceptible to air and ground resonance instabilities, and hence may require a lag damper. A lag frequency above 0.6/rev is desired for air and ground resonance stability, and the frequency must be below about 0.8/rev for acceptable loads. A matched stiffness design would require a lag frequency of about 0.5/rev. A stiff-inplane rotor (lag frequency above 1/rev) has no ground or air resonance problems, but will have higher loads, and the flap-lag-torsion stability phenomena generally display a greater complexity and sensitivity. Acceptable loads and strength have been achieved by the use of advanced materials, and most often by the selection of the soft-inplane configuration for main rotors. Acceptable stability can be achieved by designing the rotor for minimum coupling of the blade modes (such as by using nearly a matched stiffness design); or by designing the rotor specifically for favorable values of pitch/lag and flap/lag coupling over the operating range.

4.1.1 AH-56A

Carlson and Kerr (Ref. 58) described the design of the AH-56A helicopter: a four-bladed, hingeless, gyro-controlled rotor. The rotor was stiff-inplane, with a lag frequency of about 1.3/rev. The control gyro utilized feather-moment feedback with a swept-forward blade to improve the aircraft dynamics. The dynamic characteristics were analyzed using the REXOR code, which produced a time history solution. The rotor was represented by two flapwise and one inplane bending modes, the control system flexibility, and quasi-static torsion motion; the body and gyro motion included pitch, roll, vertical, and rotational speed degrees of freedom. Figure 90 compares the measured and calculated stability.

Anderson (Ref. 99) described a reactionless flap-lag instability that was encountered in AH-56A flight tests at low speed (20 to 30 knots) and high lift, producing chordwise loads sufficient to buckle the blade trailing edge (Fig. 91). The blade droop contribution to the effective pitch/lag coupling was identified. The stability problem was cured by increasing the blade droop (producing negative pitch/lag coupling, which is stabilizing for a stiff-inplane rotor with full flap/lag structural coupling).

Anderson and Johnston (Ref. 100) described a phenomenon (called a hop mode) encountered on the AH-56A, involving coupling of the regressive lag mode, the body roll mode, and the rotor coning mode. There was a coupling and coalescence of the coning mode frequency with the roll and lag modes as aircraft forward speed increased. An instability occurred at about 200 knots (Fig. 92). The cure involved reducing the kinematic pitch/flap coupling and increasing the control system stiffness, so that the frequencies of these modes would not vary with forward speed; the instability boundary was thereby increased to about 270 knots.

4.1.2 BO-105

Huber (Ref. 12) described the BO-105 helicopter: a soft-inplane, hingeless rotor. The rotor had a stiff titanium hub, incorporating the pitch bearings, and fiberglass blades. Fiberglass was used to achieve low stiffness and good fatigue life. All the blade bending occurred outboard of the pitch bearings. The fundamental design approach was to use the strong couplings inherent in such a rotor to provide good dynamic characteristics and stability (Fig. 93). The rotor had no lag damper. The rotor had no droop or sweep, 2.5° precone, a flap frequency of 1.12/rev, lag frequency of 0.67/rev, and pitch frequency of 3.6/rev. Hence, the effective pitch/lag and pitch/flap couplings were about 0.1 per degree of elastic blade deflection (Fig. 10). The analysis of Ref. 11 was used to support the design.

Reichert (Ref. 57) and Reichert and Weiland (Ref. 101) discussed the BO-105 rotor loads. The maximum oscillatory bending moments normally occurred at the blade midspan on an articulated rotor, but occurred at the blade root on a hingeless rotor. The hingeless rotor peak loads (at the root) were much higher than the articulated rotor peak loads; but on the outboard portion of the blade the loads were lower than on an articulated rotor. The 1/rev blade motion dominated the flap and lag bending moments. Because the blade loads were dominated by the 1/rev motion of the fundamental flap and lag modes, good correlation between predicted and measured loads was obtained (using the analysis of Ref. 11; see Fig. 55). The aeroelastic couplings were important for the loads as well as for stability; hence, the blade pitch motion must be included in the analysis. For helicopter vibration, the higher harmonics and additional modes were important, so a better analysis than that of Ref. 11 would be required for good predictions.

Reichert and Weiland (Ref. 101) discussed the BO-105 helicopter ground and air resonance characteristics. The relatively high lag frequency and lag damping were sufficient to preclude any stability problem, without a mechanical lag damper.

Kloppel, Kampa, and Isselhorst (Ref. 102) presented measurements of the lag damping of the BO-105 rotor in hover on a whirl tower. Warmbrodt and Peterson (Ref. 30) measured the damping of the full-scale rotor on a wind tunnel test stand. Figure 94 compares the measurements with the calculations using the analysis of Ref. 29.

Strehlow and Enenkl (Ref. 98) identified the source of the BO-105 blade lag damping as primarily mechanical losses in the blade root attachment fitting. Consequently, the equivalent viscous damping was a nonlinear function of the blade lag

bending moment (Fig. 95). Kloppel, Kampa, and Isselhorst (Ref. 102) showed the influence of the nonlinear structural damping on the calculated forward flight stability (Fig. 96; the lower theoretical curve corresponds to Fig. 95, while the upper curve is for a slightly different variation of structural damping with lag moment).

4.1.3 Lynx

Balmford (Ref. 103) described the development of a research hingeless rotor on a Scout helicopter. The intent was to match articulated rotor behavior, by minimizing the structural flap/lag/torsion coupling and minimizing the feather moments due to flap and lag motion. Hence, the hub configuration consisted of an inboard flap flexure, then a feathering bearing (so there would be no feather moment due to flapping), then a matched stiffness lag flexure outboard. The rotor had a high control system and blade torsion stiffness. The compromise between 1/rev blade loads and ground/air resonance stability led to a lag frequency of 0.64/rev. A ground resonance instability was encountered in tests at maximum overspeed rotor rpm, due to lower body frequency and lower lag damping than anticipated. Therefore, lag dampers were installed. Air resonance (analyzed for hover only) and vibration were no problem. Rotor bending loads were calculated using a normal mode method, and good correlation with flight test results was achieved (Fig. 54). Control loads were no problem.

Hansford and Simons (Ref. 14) described the design of the Lynx hingeless rotor. A hingeless hub was desired for simplicity, but dynamic characteristics not too far from those of an articulated rotor were preferred. Rather than use the blade couplings to control the rotor dynamics, and deal with the adverse effects of the couplings and sensitivity to flight condition, the couplings were minimized throughout the flight envelope. A rotor designed with an inboard feather bearing, a flap frequency of 1.09/rev, lag frequency of 0.58/rev, and pitch frequency of 5/rev would have an effective pitch/lag and pitch/flap coupling of 0.4 per degree of elastic deflection. For a flap frequency in the range 1.09 to 1.14/rev, zero coupling would require a lag frequency of 0.43 to 0.55/rev--too low for available materials, and too low for good ground resonance stability. Thus the design approach for the Lynx concentrated on matching the blade flap and lag stiffness where the product of the bending moments was highest at the root (Fig. 97). This was accomplished by using a circular, flexible element outboard of the pitch bearing. A fully matched stiffness design would require that this flexible element be too long, and the lag frequency would be too low. Hence, a flap flexure was introduced between the hub and the pitch bearing, to reduce the effective coupling associated with out-of-plane deflection relative to the feathering axis (this design also allowed independent selection of the flap and lag frequencies). Finally, for better ground resonance stability, the lag frequency was increased to 0.64/rev and a lag damper was used. The resulting design had only a small effective pitch/lag and pitch/flap coupling: 0.015 per degree of elastic deflection.

Berrington (Ref. 104) discussed the Lynx rotor design and dynamic characteristics. There was no problem with ground or air resonance. The vibration was

initially high, but was reduced to 0.05 to 0.10 g by manipulation of the airframe structural modes.

4.1.4 ABC

Burgess (Ref. 105) describes the Advancing Blade Concept (ABC) helicopter: a stiff-inplane hingeless rotor. The hub moment capability of a hingeless rotor was used in the concept to allow the rotor to fly with a net rolling moment in forward flight, alleviating the retreating-blade stall limit. To balance the rolling moment, a coaxial-rotor configuration was used, and adequate blade clearance between the two rotors in forward flight required high stiffness. The ABC rotor flap frequency was about 1.5/rev and the lag frequency about 1.4/rev. Blade loads for design of the rotor were calculated using a normal mode analysis. Flutter analysis for the rotor design was performed using a frozen coefficient method, considering only flap and torsion modes.

Young and Simon (Ref. 106) discussed ABC helicopter dynamics. The high stiffness required for tip clearance resulted in good stress margins in the blade, but also produced high bending loads through the feather bearing at the blade root, with a significant impact on fatigue life. In flight tests the shaft stresses exceeded endurance in descent, because of the hub moment needed to balance the horizontal tail moment; this problem was corrected by introducing coupling of the elevator to the collective stick. Blade inplane stability was no problem. The coaxial rotors were phased such that the 3/rev symmetric vibratory forces (vertical force, longitudinal force, and pitch moment) tended to cancel. The vibration due to 3/rev lateral force and roll moment was high, however. The vibration was significantly reduced by an absorber (Fig. 98).

Abbe, Blackwell, and Jenney (Ref. 107) discussed ABC rotor stability. As a result of the high stiffness and coaxial configuration, the lag mode was almost pure inplane motion, involving little coupling with the flap, torsion, control, or airframe motion. The measured damping showed little variation with airspeed (Fig. 99), but the upper rotor damping did decrease for high rates of descent at 80 to 100 knots. A normal mode analysis with time integration was used to calculate the stability.

Linden and Ruddell (Ref. 108) and Ruddell et al. (Ref. 109) discussed the ABC helicopter vibration characteristics. With the coaxial configuration, the vibration depended on the rotor phasing: for a blade crossover at 90° azimuth, the symmetric hub forces (vertical force, longitudinal force, pitch moment) tended to cancel; for a blade crossover at 0° azimuth, the antisymmetric hub forces (lateral force, roll moment, yaw moment) tended to cancel. The dominant excitation of the airframe came from the pitch or roll moment, because of the high flap stiffness. The flight tests were first conducted with a 90° crossover; excessive cockpit vibration was encountered, and the maximum speed achieved was 204 knots. Then the flight tests were conducted with a 0° crossover, and the vibration was significantly reduced (Fig. 100). The vibration level was still high, but no vibration treatment had been installed yet. It was established that the vibration level of the ABC tended to be lower than that of a conventional helicopter at the same speed (comparing both

without vibration treatment); but the ABC vibration was higher than that of a conventional helicopter at their respective maximum speeds. The maximum speed achieved in the flight tests was 263 knots (diving), limited by upper rotor shaft endurance loads. A possible correction for this loads limit would involve using the elevator to reduce the hub moment required from the rotor.

4.1.5 BK-117

Huber and Masue (Ref. 110) described the design of the BK-117 helicopter: a soft-inplane hingeless rotor. The design philosophy and the resulting rotor configuration were the same as for the BO-105 rotor: a stiff titanium hub with pitch bearings, and fiberglass blades. The flap frequency was 1.10/rev and lag frequency 0.65/rev (compared to 1.12 and 0.67 for the BO-105). As a result of the BO-105 analytical work (Ref. 11), the blade center of gravity was placed at 23.5% chord (compared to 25% chord for the BO-105) in order to introduce blade center-of-gravity/aerodynamic-center coupling favorable for handling qualities. The blade had 2.5° precone and no droop (same as BO-105), and 1.0° aft sweep (the BO-105 had no sweep). Whirl tower tests showed stability somewhat better than the BO-105 (Fig. 101; the analytical results correlated best for the BO-105, undoubtedly reflecting the long use of the analysis for that rotor). Flight tests showed that the loads and air/ground resonance stability were no problem (Fig. 102). The vibration level was still moderately high after just tuning the blade frequencies (Fig. 103). A NASTRAN analysis and shake test identified fuselage modes near 4/rev; local stiffening of the structure showed a decrease in local vibration but only a minor change in cabin vibration. Flap pendulum absorbers on the blades (originally demonstrated for the BO-105) significantly reduced vibration in transition. A multiaxis antiresonance isolation system, involving four vertical mechanical isolators and one lateral hydraulic isolator, was very effective in reducing the vibration at all speeds, even during transients.

Strehlow and Enenkl (Ref. 98) discussed the BK-117 design philosophy and development. The rotor precone resulted in upward elastic flap deflection of about 0.9° in hover, hence pitch/lag coupling of -0.2, which was favorable for flap-lag stability. The BK-117 used blade tuning weights to control 3/rev and 5/rev rotor loads and 4/rev hub moments, hence to minimize vibration. Ground resonance stability was not a problem. The aircraft had a stiff landing gear, so the body pitch mode had the lowest frequency and the roll mode resonance was above normal rotor operating speed.

4.2 Bearingless Rotors

In the quest for design simplicity, the next logical step from the hingeless rotor is the bearingless rotor, in which structural flexibility rather than hinges and bearings is used to provide blade pitch as well as flap-lag motion. Such a hub configuration becomes practical largely through the use of composite materials. Simplicity is a goal because of the favorable implications for rotor system weight, cost, and reliability. The elimination of the feather bearing, however, introduces even more complicated dynamic phenomena than for the hingeless rotor. Bousman,

Ormiston, and Mirick (Ref. 111) and Strehlow and Enenkl (Ref. 98) discussed design considerations for bearingless rotors. As for hingeless rotors, it is desired to have a low flap frequency in order to minimize gust response, vibration, and adverse handling qualities effects. Bousman gives a flap frequency goal of about 1.03 to 1.05/rev; Strehlow defines the goal as 1.06 to 1.08/rev. These values can be achieved by introducing a structural flap flexure into the design, which is possible with composite materials. Bearingless rotor designs for main rotors are soft-inplane, for manageable blade loads. Generally some lag damping source beyond structural damping is desired to improve aeromechanical stability. Most bearingless tail rotor designs are stiff-inplane. Many designs are being developed and tested. Perhaps the most common configuration now is a flexbeam with an inboard flap flexure, an external torque tube, and a snubber/damper at the root of the torque tube.

4.2.1 XH-51A

Donham, Cardinale, and Sachs (Ref. 112) described the development of a soft-inplane bearingless rotor for the XH-51A helicopter. The rotor used steel flexures at the root, with polar symmetry for a matched stiffness configuration; the lag frequency was 0.65/rev. The low inplane stiffness was necessary to achieve the desired torsion flexibility. Pitch control was by means of a steel torque rod forward of the flexbeam, mounted with flexible couplings to eliminate bending loads. The XH-51A rotor was gyro-controlled, although a smaller gyro was needed compared to the stiff-inplane hingeless rotor. The matched stiffness eliminated feather moments due to flap or lag deflection, which would be undesirable feedback signals to the gyro; a smaller and simpler control system was thereby possible. The rotor system was 11% lighter than the stiff-inplane hingeless rotor. In flight tests (Fig. 104) the aircraft showed marginal air resonance stability: an instability at about 86% normal rotor speed, which was considered an insufficient margin for autorotation (design operating range was 89% to 106% rpm). The rotor was tested with negative pitch/flap and pitch/lag coupling; analysis suggested that positive pitch/flap coupling would stabilize the air resonance. Ground resonance stability was acceptable (critical rotor speeds were above 106% rpm) on a smooth, prepared surface with complete contact of the skids and the ground. Partial skid contact, on a rough or soft surface, could have resulted in an unstable condition.

4.2.2 BMR

Staley, Gabel, and MacDonald (Ref. 113) described the development of the Bearingless Main Rotor (BMR). The soft-inplane rotor used twin fiberglass flexbeams, extending to 25% radius, and a graphite torque rod between the beams, cantilevered at the outboard end and pinned at the root. The rotor was tested on a BO-105 aircraft, and the fundamental frequencies were chosen to match those of the BO-105 hingeless rotor: flap frequency 1.12/rev and lag frequency 0.69/rev. The flexbeams used 12.5° prepitch to introduce structural flap/lag coupling, and 2.5° negative droop to improve stability. The rotor design was developed using a hover stability analysis (based on the rigid blade and hinge spring model with prescribed couplings), and small scale wind tunnel tests. Flight tests showed that lag damping and air resonance were no problem (Figs. 105 and 106). Vibration characteristics

were similar to those of the BO-105. The BMR air/ground resonance damping was generally lower than that for the BO-105; the structural damping was about 1% for the BMR compared to 3% for the BO-105 (Fig. 107). Ground resonance tests with the original landing gear configuration showed an instability at low collective, at 102% rpm on concrete and 95% rpm on turf (the body frequencies are lower on turf; Figs. 108 and 109). When the landing gear skid was stiffened, the ground resonance stability on concrete was acceptable. Neutral stability was then encountered on turf at low collective and 97.5% rpm. For these flight tests it was possible to simply avoid that operating condition; for a new helicopter a soft landing gear design would be used to eliminate the problem. The analysis was not able to predict all of the ground resonance problems; it assumed complete contact of the landing gear with the ground, and did not allow for variations of landing gear characteristics with rotor thrust.

Dixon (Ref. 114) described the development of the BMR design. The design started with an I-beam of Kevlar for the flexbeam (for low stress, low torsion moment due to twist, and ease of fabrication); and a leading edge torque rod. A torque sleeve was rejected because it would be necessary to develop an elastomeric bearing for the inboard attachment, and because no fairing was desired during the flight research (to allow inspection and instrumentation maintenance). Concern about lack of fatigue data and the compressive strength of the Kevlar led to the use of S-glass for the flexbeam; the stress was lower with the S-glass, but the torsion moment needed to twist the blade was higher. The outboard connection was simplified by splitting the I-beam into two C-beams, and placing the torque rod between the C-beams, at the center of twist. This design introduced the difficulty that a dual beam is not a classical problem in structural and dynamics analyses. Graphite for the torque rod provided the simplest and lightest design. Separate beams for each blade, rather than a through-hub design, was chosen to allow research variations in flexbeam configuration. Negative droop of 2.5° relative to the torsion flexure was used for stability. The wind tunnel model tests showed that 12.5° of beam pretwist improved the stability, although it complicated the hub design. Limits in the analytical tools for stability prediction included the use of an equivalent hinge model, inadequate model of the landing gear, and no forward flight. The analysis of Ref. 40 was developed in response to these limitations. Limits for loads predictions included the lack of a true multi-load path model.

Warmbrodt, McCloud, Sheffler, and Staley (Ref. 41) conducted a full-scale wind tunnel test of the BMR rotor. The measured damping compared well with flight test results (Fig. 110), indicating the absence of coupling with body motions at normal rotor speed. Sheffler, Warmbrodt, and Staley (Ref. 115) considered lag damping augmentation in the full-scale wind tunnel test of the BMR (Ref. 41). An elastomeric damping material was bonded to the top and bottom surfaces of the C-beams, and constrained by an outer layer of graphite reinforced epoxy laminate. The lag damping of the rotor increased by 1.5% critical (about 50% higher); the lag frequency was increased by about 0.04/rev.

Warmbrodt and Peterson (Ref. 30) compared the hover stability measured in full-scale tests of the BMR and the BO-105 rotors. At design rotational speed and

thrust, the BMR was more stable. The BMR stability was lower than that of the BO-105 at low thrust, and significantly lower at 82% rotor speed.

McHugh, Staley, and Sheffler (Ref. 116) conducted model wind-tunnel tests to develop a bearingless rotor with low flap frequency. The goal was a flap frequency of about 1.04/rev (compared to 1.12/rev for the BMR). Two designs were considered: a dual beam configuration, like the BMR, with a flap frequency of 1.03 to 1.05/rev (for zero to design thrust, respectively); and a single flexstrap configuration (torque rod below the strap), with a flap frequency of 1.03 to 1.04/rev. Air resonance instabilities were encountered below 100% rpm (Figs. 111 and 112). Adding constrained layers of elastomeric damping material significantly increased the damping (Fig. 112); reducing the lag frequency lowered the rotor speed of the instability. The same stability boundary and damping levels as the BMR were achieved for the dual beam configuration with a lag frequency reduced to 0.58/rev; and for the single flexstrap configuration with a lag frequency of 0.62/rev and the added damping material (Fig. 113).

4.2.3 Triflex

Cassier (Ref. 117) described the development of the Triflex main rotor: a three-bladed, soft-inplane bearingless rotor, tested on a Gazelle helicopter. The Triflex had a single beam at each blade root with pitch, flap, and lag flexibility; and a rigid pitch horn at the outboard end of the flexure. Each flexure was constructed of unidirectional glass-fiber and epoxy-resin rovings embedded in an elastomeric matrix. The elastomeric matrix maintained the spacing between the rovings during bending, and provided damping. The rotor had a flap frequency of 1.06/rev, lag frequency of 0.72/rev, 2.5° precone, and pitch/flap coupling of 0.5 for stability. Whirl tests showed no stability problems, but the lag response was high during start and stop at low collective. The lag damping was about 1%, which was less than predicted. Flight tests showed a weak tendency for a ground resonance instability (with a resonance slightly above normal rotor speed) because of the low lag damping. The problem was cured by installation of a hydraulic damper on the landing gear. There was no air resonance stability problem, but a resonance of the regressing lag mode with the engine lateral mode at about 110% rpm resulted in increased vibration, particularly at high speed. The problem was cured by locking out the flexible longitudinal mount of the main gear box. Generally the vibration (normally a concern with the Gazelle helicopter because of a fuselage mode near 3/rev) was increased with the Triflex rotor. Maximum forward speed was achieved after installation of bifilar pendulums. The control system loads were higher than for an articulated rotor. The flight envelope was therefore limited somewhat by control loads, since the normal Gazelle control actuators were used.

In further development of the Triflex rotor, Aerospatiale increased the number of blades to four, in order to reduce the vibration with the Gazelle fuselage. The four-bladed hub was also easier to fabricate. The elastomer provided more lag damping than for the three-bladed hub, but a more conservative flight test approach required the installation of a lag damper to insure ground resonance stability. It is anticipated that the use of a new elastomeric matrix will eliminate the need for

a lag damper. Flight tests showed no pitch-up tendency of the aircraft, acceptable vibration (without absorbers), and no stability problems. Primary development of the Triflex hub configuration was completed. Some design changes would be desirable, particularly to improve fatigue life: a new elastomer, stronger control actuators, and stiffer pitch arms.

4.2.4 Model 680

Metzger (Ref. 118) described the Model 680: a soft-inplane bearingless main rotor. The rotor was developed with the goals of reducing the number of parts by 50% and the weight by 15%, increasing the fatigue life, and achieving low vibration with minimum weight penalty. The four-bladed hub had flexbeams with a flap flexure inboard and a torsion section outboard. For simplicity, the initial design had a pitch horn attached to the blade at the end of the flexbeam (20% radius), with no shear restraint or lag damper. To eliminate the large moments at the blade interface produced by control input and a significant pitch control washout, the design was changed to a torque tube with shear restraint. In model tests of configurations without dampers, the stability margin was not acceptable. Hence, elastomeric lag dampers were added at the shear restraints. The flexbeam and torque tube were made from fiberglass-epoxy. The torque tube was stiffness designed, so graphite-epoxy would be lighter. The rotor and pylon were designed for low vibration: the rotor dynamics were tailored to reduce 4/rev vibration; a linkage-focused pylon with longitudinal and lateral restraint springs was used; and vertical isolation was achieved using "Liquid Inertial Vibration Eliminators" between the transmission and pylon. The rotor was flight tested on a Model 222 helicopter. Shake tests showed 3% rotor damping would be needed for ground resonance stability; at least 3.5% was available from the lag dampers alone. Ground and air resonance were no problem, and the loads measured in flight indicated a fatigue life of at least 10,000 hr for the hub. The 4/rev vibration was below 0.1 g from hover to 170 knots. The vertical isolators were not needed at high speed, but were responsible for eliminating a transition vibration peak of 0.3 g at 30 knots.

Weller (Ref. 119) conducted hover and wind tunnel tests of a model of the 680 rotor: a soft-inplane bearingless rotor. The rotor support included body pitch and roll motion. The basic design philosophy required a soft flapping stiffness and the use of elastomeric damping for lag stability. The through-hub flexbeams had a flap flexure inboard, then a torsionally soft cruciform section outboard. The external cuff or torque tube was shear-restrained at the inboard end, to minimize the couplings and flexure loads due to pitch link shear forces. An elastomer was used at the cuff restraint to augment the inplane structural damping. The damper-restraint was oriented 11° nose down, so that with the trailing edge pitch link a negative pitch/lag coupling (stabilizing) was produced for collective angles above 11°. The rotor had a flap frequency of 1.04/rev, lag frequency of 0.69/rev, and 2.75° of precone. Hover stability (eigenvalues) was calculated using a modal analysis (the modes included the effects of the redundant load path) and dynamic inflow. Forward flight stability was calculated from time histories, using the C81 program. The model rotor tests showed an instability at the body roll resonance (at 0.675/rev), but full scale flight tests showed significantly higher damping, with no

ground resonance problem. The model was gimballed at a point corresponding to the aircraft center of gravity (for air resonance simulation), while for the aircraft on the ground the rotation point was below the landing gear. The lower roll moment of inertia in the former case was sufficient to introduce the instability. Most of the parameters investigated experimentally showed little effect on the stability of this rotor; the built-in lag damper provided sufficient stability. The influence of droop and sweep were predicted well for the isolated rotor case (Fig. 114). While droop and sweep produced measurable damping changes for the isolated rotor, their influence was negligible for the coupled rotor/body case (the hover analysis still predicted an unfavorable influence of sweep, however). Forward flight increased the damping at the body roll mode resonance (70% rotor speed), but had little influence at the pitch mode resonance (Fig. 115). The analyses were accurate for the baseline configuration. Trends with some parameters (precone, damping, body motion) were predicted well, while others (sweep, control system stiffness) were not. The forward flight predictions were generally less accurate than the hover predictions.

4.2.5 Experimental Main Rotors

Seitz and Singer (Ref. 120) and Kloppel, Kampa, and Isselhorst (Ref. 102) described an experimental bearingless main rotor. The analysis used to design the rotor was a rigid blade and hinge spring model. A key parameter was the blade-to-beam droop. With low flap stiffness, the flap and lag bending take place inboard of the blade pitch change. Hence, the effective pitch/lag coupling depends primarily on the droop

$$K_{P_{\zeta}} = K_{\zeta} \beta_d / K_c$$

so negative droop will provide the desired (stabilizing) negative pitch/lag coupling. The experimental main rotor used BO-105 blades and hub. A T-beam was used (for small control force to twist the blade, and low stress) with a midchord torque rod. A damper, consisting of an elastomeric layer bonded to the flexbeam and covered by a stiff carbon fiber beam, provided an increase in lag structural damping of about 0.5% critical (50% higher; see Ref. 98). The rotor had a flap frequency of 1.10/rev and lag frequency of 0.68/rev (compared to 1.12 and 0.67 for the BO-105 hingeless rotor), -2° of droop and 1° of precone. Whirl tests showed that the rotor had less damping than the BO-105, even with the lag damper (Fig. 116). Ground resonance calculations indicated that stiffening of the BO-105 gear would be required to move the body pitch mode resonance from 104% rpm to 108% rpm. Air resonance calculations showed no problem, although the stability would be less than that of the BO-105. The reduced flap stiffness helped by lowering the roll mode frequency; however, a design with higher damping level would be preferred.

Seitz and Singer (Ref. 120) described two bearingless main rotor designs. The first design used a single flexbeam and torque tube configuration. The flexbeam had a cruciform section for torsion, with a flat flexure at the root for low flap frequency (1.07/rev). The elliptical, outer torque tube was constrained in shear by a snubber at the root (raising the lag frequency to 0.70/rev). The second design used a double flexbeam and mid torque rod configuration. The flexbeams had a T-section

for torsion, and a flat flexure at the root (flap frequency 1.07/rev). Twin beam behavior was observed in the second lag mode in particular. Composite materials were essential to achieve the required tailoring of flexbeam properties.

4.2.6 ITR

Bousman, Ormiston, and Mirick (Ref. 111) discussed the bearingless hub design trends evident in the results of the U.S. Army/NASA Integrated Technology Rotor (ITR) program. The hub design goals included: hub drag $D/q = 0.15\%$ rotor disk area (performance); weight = 2.5% gross weight (performance and cost); parts count = 50 (cost and maintenance); hub moment stiffness = 1.03/rev flap frequency (vibration, gust response, handling qualities); hub tilt capability without fatigue = 5° , fatigue life = 10,000 hr, mean time between removal = 3000 hr (reliability and maintainability); provision for lag dampers; torsion stiffness such that swashplate actuator loads = current levels; and low production costs. Each of these goals could be achieved separately, but it was difficult to obtain all of them at once. It was decided to relax the flap frequency goal to 1.05/rev and the hub tilt goal to 4° for the next phase. The low flap frequency goal led to some consideration of gimballed or flap-hinge designs (with lag and pitch flexbeams), but most of the configurations examined were bearingless, and all were soft-inplane designs. The flexbeam design considerations were strength and fatigue life, with the low hub moment stiffness. The flexbeam could have a cross section varying along its length (with a flap flexure inboard and torsion section outboard), or not (which would be simpler to make and would avoid structural problems at the section transitions). Single, twin, and quadruple beam configurations were examined; a laminated beam was also considered, for lower flap stiffness. Sometimes a shoe was required to control the flap bending curvature (on low stiffness designs). Many cross sections were possible for the torsion section of the flexbeam. The pitch control design considerations were weight, drag, and aeroelastic couplings. All the designs considered in these investigations included a shear restraint to react the control load at the root, so the control introduced was a pure torque. Without such a shear restraint, control input would produce a flap deflection also, hence more pitch link travel would be required; and the effective pitch/flap and pitch/lag couplings would be more complicated. The pitch control options included having the torque structure separate from the flexbeam or enclosing it; having the torque structure carry bending loads or not; and perhaps using an elastomeric damper in the shear restraint (which required that the torque structure be stiff in chord bending, or offset chordwise). Probably 1% to 3% damping could be obtained from structural damping, which would likely not be sufficient for aeromechanical and aeroelastic stability. The use of elastomeric dampers could give 3% to 6% damping, which would be acceptable. The dampers could be combined with the shear restraint, or could be a constrained layer of elastomeric material on the flexbeam. Analytical tools could not yet provide the detailed guidance needed for selecting aeroelastic couplings, but negative droop for negative pitch/lag coupling and beam prepitch for flap/lag structural coupling were desirable. Regarding materials, composites were essential for the required strength and the ability to achieve the separation of bending and torsion stiffnesses. Graphite tended to give a lighter, more compact, lower flap-

stiffness design (from good stiffness to weight ratio); while fiberglass had better fracture toughness and failure modes for reliability and maintainability.

4.3 Bearingless Rotors--Tail Rotors

Bearingless tail rotor designs have been developed with the same goals as for main rotors: simplicity, with the resulting reduced weight and cost; improved maintainability; and improved survivability. There are two major differences compared to main rotors: the loads penalty is less severe, so most tail rotor designs are stiff-inplane; and several bearingless tail rotor designs are either ready for or in production.

Maloney and Porterfield (Ref. 121) developed an experimental bearingless tail rotor for the UH-1H helicopter. The blades had dual, fiberglass flexbeams; extensions of the airfoil formed a torque tube, with a shear reaction bearing at the root. The rotor was designed as a teetering hub with 35° of pitch/flap coupling (standard UH-1 configuration). A flap-lag instability was encountered in whirl tests because the lag frequency (about 1.3/rev) was lower than expected. Locking out the teeter motion eliminated the instability, but the increased hub moment limited the envelope. Analyses were not particularly helpful for this problem.

Fenaughty and Noehren (Ref. 122) described the development of the bearingless tail rotor for the UH-60 helicopter. Extensions of the blade spars formed through-hub flexbeams of uniaxial graphite/epoxy. With graphite rather than fiberglass, a smaller cross section could be used, hence a lower weight and lower torsion stiffness were possible. Extensions of the blade skin formed an external torque tube of fiberglass. Originally the torque tube was restrained inboard by the control system only, which allowed pitch/bending coupling. A snubber was added to negate the coupling and eliminate lost motion. The flap frequency (about 1.25/rev) and lag frequency (1.6 to 1.7/rev) were kept separate for flap-lag stability. Offset of the zero lift axis (aerodynamic pitch) above the flexbeam structural axis kept the lag frequency above 1.6/rev over the entire collective range. Flight tests showed that flap-lag stability was no problem. It was estimated that the bearingless design reduced the weight by 30% and the number of parts by 25%.

Shaw and Edwards (Ref. 123) developed a bearingless tail rotor for the YUH-61A helicopter. They were particularly concerned about survivability, so chose to achieve stability through flap/lag coupling rather than by frequency separation. The through-hub flexbeam was a thin, wide strap of fiberglass. Fiberglass was chosen over boron or graphite for its survivability characteristics: less brittle and slower propagation of severe damage. The strap was wide for survivability and thin for low hub moments. The rotor was thus stiff-inplane, and with 65° of pitch/flap coupling the flap and lag frequency separation was small. A rigid pitch horn was used for collective control (no shear restraint). In wind tunnel tests, the rotor initially encountered flap-lag instabilities in cyclic and reactionless modes (which had slightly different lag frequencies; Fig. 117), and a stall excited flap-lag-torsion oscillation at the second flap/first torsion mode frequency (Fig. 118). The theoretical tools available included a modal frequency analysis, and a rigid blade and hinge spring stability analysis; these tools provided guidance but were

not sufficient for predicting absolute levels of stability. The wind tunnel tests established several parameters with favorable influence on stability: sweep, which introduced flap/lag and aerodynamic coupling; tip weights, which changed the frequencies; and a blunter leading edge contour, which eliminated leading edge stall.

Huber, Frommlet, and Buchs (Ref. 124) described the development of a bearingless tail rotor for the BO-105 and BK-117 helicopters. Soft-inplane designs were considered to minimize oscillatory inplane loads, reduce weight, and reduce control loads. The helicopter airframe modes were such that ground and air resonance would be no problem (no airframe modes were within the 6 to 14 Hz range of the tail rotor regressing lag mode). Two rotors were designed. The first was a three-bladed rotor. The fiberglass flexbeam consisted of twin C-beams, converging at the blade, where they formed the blade spar. A rigid pitch arm (metal or composite) with no shear restraint would be used. The rotor would have a flap frequency of 1.03/rev, 45° of pitch/flap coupling, and a lag frequency of 0.65/rev. The second was a four-bladed rotor. The single element, through-hub, fiberglass flexbeam had a flat flexure inboard for low flap stiffness, and a cruciform torsion section outboard. Damping elements consisted of four viscoelastic sheets on chordwise arms of the flexbeam, bridged by carbon-fiber plates. A rigid pitch arm (composite) with no shear restraint would be used. The rotor would have a flap frequency of 1.04/rev, 45° of pitch/flap coupling, and a lag frequency of 0.69/rev. Counter-weights at the blade root would minimize control forces. These rotors were analyzed using the rigid blade and hinge spring model developed for the BO-105 rotor. Calculations indicated no problems with air or ground resonance: at least 1.5% inplane structural damping was needed, but 3.5% should be possible using the damping elements. These designs achieved a 20% weight reduction, and a 20% production cost reduction was predicted.

Blachere and D'Ambra (Ref. 125) described a Triflex tail rotor design. The rotor used a single arm flexbeam and a rigid pitch control sleeve, constrained at the root by a bearing. The flexbeam consisted of a bundle of roving threads (R-glass and epoxy resin) embedded in an elastomeric matrix for damping. The rotor had a flap frequency of 1.06 to 1.10/rev and a lag frequency above 0.5/rev.

Banerjee, Johnston, and Messinger (Ref. 126) described the development of an experimental bearingless tail rotor for the AH-64 helicopter. The through-hub, flat flexbeam formed an extension of the blade spar. The flexbeam was attached to the hub by elastomeric shear pads, such that the cyclic lag frequency was stiff-inplane (about 1.3/rev) for stability and low 1/rev loads; and the reactionless lag frequency was soft-inplane (about 0.7/rev) for low 2/rev loads and for damping from the elastomers. An external torque tube was used, with an elastomeric shear restraint on the inboard end. The flap frequency was about 1.2/rev. Negative pitch/lag coupling and 35° of pitch/flap coupling were obtained through pitch horn and pitch link geometry. Wind tunnel tests showed no stability problems over the operating range of the tail rotor.

4.4 Rotors with Circulation Control

In a rotor utilizing circulation control, a thin jet of air is blown from a spanwise slot along a rounded trailing edge. The jet remains attached over the curved surface due to the Coanda effect. Such blowing delays separation by energizing the boundary layer, and controls circulation by shifting the stagnation point. Hence with such a rotor, lift is controlled by the blowing as well as by the geometric pitch of the blade.

The lift coefficient is now a function of both angle of attack α and blowing coefficient $C_\mu = (\text{jet momentum})/\rho(1/2)V^2c$ (here ρ is the air density, V the airfoil section velocity, and c the chord). Then the perturbation lift force due to blade motion is:

$$\begin{aligned}\delta L &= \delta[(1/2)\rho V^2 c c_\ell] \\ &= (1/2)\rho V^2 c [c_{\ell_\alpha} \delta\alpha + c_{\ell_\mu} \delta C_\mu + c_\ell 2\delta V/V] \\ &= (1/2)\rho V^2 c [c_{\ell_\alpha} \delta\alpha + 2(c_\ell - C_\mu c_{\ell_\mu})\delta V/V]\end{aligned}$$

where $\delta C_\mu = -2C_\mu \delta V/V$ follows assuming that the jet momentum is constant during the motion. Normally an increase in the velocity (δV) implies a larger lift because of both the increased dynamic pressure and the decreased induced angle of attack. With a circulation control airfoil, the velocity increase in addition decreases the blowing coefficient, thereby decreasing the lift. A moderate amount of blowing will reduce the net lift perturbation due to inplane velocity perturbation; a large amount of blowing will change the sign of the lift perturbation. Trailing edge blowing may be expected therefore to alter the dynamic characteristics of the rotor. A moderate level of blowing will reduce the aerodynamic flap/lag coupling, and a large amount will change the sign. Hence there will be a tendency for flap-lag motion to be stabilized at low values of C_μ , while new instability regions (at low thrust with either high or low lag frequency) appear for high C_μ .

Chopra and Johnson (Ref. 127) analyzed the hover stability of rotors utilizing circulation control. The rigid blade with hinge spring model was used for flap-lag and flap-lag-torsion stability calculations. The general character of the dynamics was like that of conventional rotors. Instabilities were possible, but were mild and a low level of structural damping or flap/lag structural coupling would eliminate them (Fig. 119). An exception was the flap-lag instability of a soft-inplane rotor at high C_μ ; structural damping or flap/lag coupling was not sufficient for stability. Pitch/lag coupling had a large effect on the stability, pitch/flap coupling less effect. A quasistatic torsion model was satisfactory for the pitch frequencies typical of rotors using circulation control. It was noted, however, that the aerodynamic pitch damping was low for the pitch axis at the mid-chord (a possible design choice with such rotors), so adequate torsion structural damping was important. Calculations for configurations representative of the Kaman Circulation

Control Rotor (Fig. 120; flap frequency 1.1/rev, lag frequency 1.4/rev, no flap/lag coupling, large pitch/lag coupling) and the Lockheed X-Wing (Fig. 121; flap frequency 1.8/rev, lag frequency 3.6/rev, full flap/lag coupling, moderate structural damping) showed no stability problems. Both rotors were tested in the wind tunnel at full scale, with no indications of instabilities.

Chopra (Ref. 45) used a finite element analysis to calculate the hover stability of a bearingless rotor with circulation control. A configuration with both leading-edge and trailing-edge pitch links on an external torque tube was considered. The structural damping and the damping at the torque tube shear restraint were neglected. There was a significant influence of the blowing level on the predicted stability (Fig. 122). High blowing coefficient (hence, low collective for a given thrust) was destabilizing at low and moderate thrust. The instability was not particularly severe, so it should be possible to design the torque tube shear restraint with sufficient damping to stabilize the motion.

4.5 Rotor/Engine Dynamics

Much of the U.S.A. industry experience with rotor/engine dynamics problems has been reported in efforts sponsored by the U.S. Army (Refs. 128-132). The problems and solutions have been categorized by Warmbrodt and Hull (Ref. 133). There are numerous cases of excessive rotor-induced vibration of the propulsion system; the usual correction involves modifying the structure (such as the engine mount) or weight to move the natural frequency away from the forcing frequency. A second type of problem is excessive vibration (forced or self-excited) because of engine/drive-train/rotor resonances; this has been corrected by modifying the rotor dynamic characteristics. A third type of problem is engine/drive-train torque oscillations, often involving a high gain fuel control system; this problem may require modifications to the drive-train flexibility, the fuel controller, or the blade lag dampers. A fourth type of problem is excessive main rotor overspeed or droop during maneuvers, which is corrected by revising the engine/fuel control system.

It is a characteristic of the analytical tools available for these problems that either the propulsion system model lacks the detail of the rotor model, or conversely. The problems are multidisciplinary, but the analyses are not. High gain control systems are making it important to have good dynamic models of the propulsion system, but such models are usually either not available or not coupled with the good rotor models. The engine vibration problems usually involve complicated structural dynamics, that cannot be predicted well even with a finite element model of the airframe.

Fredrickson, Rumford, and Stephenson (Ref. 134) described a rotor speed governor problem that occurred on the CH-47C helicopter. In flight tests of a growth version of the rotor and engine, a 4.1 Hz oscillation in the engine shaft torque and rotor speed was encountered. The phenomenon was present in hover and on the ground, but not in forward flight. The oscillations were 8% to 10% of the maximum steady torque and fuel flow; the lag damper force oscillated below the preload value. The effect could be duplicated analytically only by stiffening the lag damper. The mode involved consisted of the rotor-lag motion opposed by the transmission and engine

turbine. This mode was predicted to be at 3.1 Hz rather than the observed 4.1 Hz, a difference attributed to the lag damper. By improving the math model of the lag damper, it was possible to calculate the oscillation well. The problem could be corrected by softening the lag damper, but that led to unacceptable ground resonance characteristics. Reduced fuel-control gain also worked, but was marginal in cold air. The final solution was to both reduce the gain and increase the time constant in the fuel control, such that the gain at 4 Hz was reduced by a factor of three (Fig. 123). The engine response to power demands by the pilot was not perceptibly degraded.

Fredrickson (Ref. 135) described a rotor/drive system 4/rev torsional resonance that occurred in the Model 347 tandem helicopter. High 4/rev blade chord bending moments were encountered in transition and in high speed at high gross weight. The mode involved consisted of the collective lag motions of the two rotors opposing each other through the shaft. A blade chord frequency at 5.3/rev produced a coupled blade and drive system frequency at 4/rev. The problem was corrected by raising the chord frequency above 6/rev, and hence, the coupled system frequency to 4.3/rev, by use of boron fiber doublers bonded to the blade trailing edge and boron skins applied to several blade boxes (the simplest solution, if not necessarily the best).

Twomey and Ham (Ref. 130) described two problems encountered on the CH-53E helicopter. The first problem was an oscillation of the rotor and drive system in the third torsional mode. In flight tests, 3.6/rev cockpit vibration occurred in specific flight conditions, with a time to double amplitude of 10 to 12 sec. The mode involved consisted of collective edgewise bending and the drive system torsion. The rotor blade motion was a combination of rigid and first elastic bending, such that there was little motion at the lag damper. An analysis including the fuel controller and the blade edgewise motion did not indicate an instability. It was speculated that the instability arose from coupling in forward flight of the 3.6/rev collective edgewise mode with a 2.6/rev cyclic flapwise mode. The cure involved reducing the blade edgewise stiffness (lowering the natural frequency to 3.45/rev to decouple it from the flapwise mode, and to increase the modal motion at the lag damper). For the flight tests the blade was softened by removing graphite strips that had been added to the trailing edge to improve the stress levels; the blades were redesigned for production. The second problem was a feedback oscillation of the rotor and drive system first torsional mode. In flight tests, a low frequency (2 Hz) oscillation of the aircraft occurred in forward flight. The mode involved consisted of the collective rotor lag motion, opposing the drive train and engine torsion, and the fuel controller. The background 1/rev motion in forward flight decreased the effectiveness of the lag dampers. A bench test was conducted to determine the equivalent viscous damping of the lag damper with a background of 1/rev and higher harmonic motion. Flight-test data on the harmonics of the lag motion then allowed a specification of the equivalent damping available as a function of flight speed and rotor speed. A good prediction of the stability was achieved when the reduction of the lag damping in forward flight had thereby been accounted for. The cure involved increasing the power turbine governor time constant from 0.165 to 0.7 sec, thus reducing the fuel controller gain by a factor of

15 at 2 Hz. This modification had little influence on the engine power response to pilot commands.

Thibert and Maquin (Ref. 136) discussed a transmission oscillation that occurred during development of a larger fan-in-fin tail rotor for the SA-365-N1 helicopter. A substantial torque oscillation at 4.4 to 5.8 Hz was observed in high-speed flight with slip, upon a sudden increase of the tail rotor pitch. Analysis (a combination of linearized eigenvalue and nonlinear time history calculations) showed coupled main rotor and tail rotor modes at 4.6 and 4.9 Hz, involving little engine response; the 4.6 Hz mode was lower damped. Analysis and flight test showed that increased lag damping and increased governor time constant had little influence on the phenomenon. The analysis suggested that stiffening the tail rotor transmission by 33% would increase the frequency of the mode and so also increase its damping (by increasing the coupling with the 4.9 Hz mode, which then became less damped). The correction, confirmed by flight tests, involved replacing a duralumin central tail transmission shaft with a steel shaft. For the production aircraft it was possible to simply thicken the shaft (a lighter weight solution).

4.6 Articulated Rotors

It should not be assumed that articulated rotors are without interesting dynamic phenomena. Many problems encountered in the development of more conventional design concepts simply are not reported. A couple of examples will serve as notice against complacency.

Silverthorn (Ref. 137) described an advancing whirl mode instability encountered on an articulated main rotor. The phenomenon involved the rotor cyclic motions (rigid flap, lag, and pitch, with little bending), flexibility of the rotor support structure, and cyclic pitch/mast-bending coupling during pitch and roll motion of the hub relative to the fuselage. A 14 to 15 Hz (about 3/rev) instability was predicted to occur at 104% normal rotor speed (Fig. 124). The rotor was predicted to be stable without the influence of aerodynamics or the pitch/mast-bending coupling. In whirl tests the instability was encountered at 119% rpm, still below the required stability margin of 120% rpm. Better correlation with theory was achieved using measured structural damping and eliminating a three-dimensional aerodynamic-center shift at the blade tips. The analysis suggested that a forward shift of the blade center-of-gravity would help, but that implied a blade redesign and weight increase. The cure adopted involved increasing the support structure stiffness, so the stability boundary was well above 126% rpm in both whirl and flight tests. Adding swept tips (hence moving the aerodynamic center aft relative to the center-of-gravity) also stabilized the motion.

Neff (Ref. 138) described an instability encountered in an experimental articulated rotor on the OH-6A helicopter, involving the first elastic chord, the second elastic flap, and the first reactionless torsion blade modes. Shortly after entry to autorotation and establishment of stabilized descent, the main rotor blades abruptly went out of track and a severe vibration was felt in the controls and the airframe. The pilot applied power before the static load limits were exceeded. The blade loads data indicated a 4.63/rev mode with -0.6% damping. Analysis had

initially predicted stability, with a first chord frequency at 4.4/rev. A fixed root was introduced for the chord bending boundary condition (with a four-stage friction lag damper, the blade was probably fully restrained at the mean position of autorotation), and effective pitch/lag and flap/lag coupling due to the mean out-of-plane bending was added (the flap bending at the tip significantly increased in autorotation). The analysis still predicted stability, but the first chord frequency was at 4.75/rev. Finally, the reactionless control system stiffness rather than the cyclic stiffness was used (an increase by a factor of seven, from 13,600 to 100,000 in.-lb/rad). Then the mode was predicted to be unstable, at 4.66/rev and -0.65% damping (Fig. 125). The theory suggested that an aft shift of the tip weight (with the net blade center-of-gravity still forward of the aerodynamic-center) would stabilize the motion, which was confirmed by flight tests. Subsequently, a similar problem was predicted to occur in a growth version of the production rotor. An aft shift of the tip center-of-gravity was introduced, and there were no stability problems in the flight tests.

4.6 Tilting Proprotor Aircraft

Investigations of the dynamics of tilting proprotor aircraft have generally focused on the whirl-flutter stability. Whirl flutter is a coupled motion of the proprotor and the airframe (typically the wing elastic modes) that becomes unstable at high forward speed. The rigid body and elastic motion of the blades makes tiltrotor whirl flutter a different, and more complicated, phenomenon than the whirl flutter of a propeller-driven airplane. Johnson (Ref. 139) assessed the present capability to predict tilting proprotor dynamics. Considerable work has been done and confidence gained on predicting whirl flutter stability. New designs will require the ability to analyze new hub configurations, and likely will require a better treatment of high-speed aerodynamic effects on the rotors. Most tiltrotor designs, including the gimballed rotor of the XV-15, have dynamic characteristics similar to those of hingeless rotors, notably the importance of pitch/lag and flap/lag coupling. In addition, the tiltrotor must operate over large ranges of rotor speed and collective pitch. Rotor loads remain important, since they can define the upper limit of the conversion corridor. Oscillatory loads on the airframe, particularly the nacelle and wing, can be a problem (normally cured by good structural design or structural modification, rather than by accurate prediction). Basically the tilt rotor configuration eliminates most concerns with fuselage vibration. Even in helicopter mode, the wing dynamics provide some vibration absorption, and the rotors can be tilted forward to minimize the wake-induced vibration at low speed.

Generally, the aerodynamic analysis is simpler for the proprotor (high inflow, axial flight) than for the helicopter rotor (low inflow, edgewise flight). Axial flight implies a symmetric aerodynamic environment, hence constant-coefficient equations of motion. In high inflow, both the inplane and the out-of-plane blade motion produce a first order change in the blade angle of attack, hence through the lift-curve slope a first order change in lift, which has both inplane and out-of-plane components. So the lift-curve slope terms dominate the aerodynamic forces (Ref. 140), which depend then mainly on the Lock number and the ratio of flight

speed to tip speed. In contrast, for the rotor with low inflow, inplane motion produces lift and drag perturbations due to the dynamic pressure change, and tilts the mean lift and drag forces; so the inplane forces or forces due to the inplane motion are small, and depend on the blade trim loading (see Ref. 7). Lift changes due to angle-of-attack perturbations, normally responsible for the high aerodynamic damping of the rotor flap motion, in the proprotor also produce a high aerodynamic damping of the blade inplane motion. Another result of high inflow is the large collective pitch and built-in twist required; and operating in both helicopter and airplane modes requires a large range of collective pitch.

For the gimbaled, stiff-inplane proprotor design, blade pitch motion has a significant influence on whirl flutter (Fig. 126), through the introduction of effective pitch/lag coupling (Refs. 141 and 142). The blade precone is normally selected for hover, so in propeller configuration the precone is too large. There will be a downward elastic coning deflection of the blade. With no droop and small thrust, the effective pitch/lag coupling is negative and proportional to the precone. Negative pitch/lag coupling has a destabilizing influence on the whirl flutter. Figure 127 shows the stabilizing influence of reduced precone or increased control system stiffness, through the reduction in magnitude of pitch/lag coupling. Blade droop has a similar effect, while not increasing hover coning loads as does reduced precone (since droop becomes aft blade sweep at the low collective pitch angles of hover). The blade inplane motion has an effect on whirl flutter stability levels also (Fig. 126), particularly at resonances of the regressing lag mode with a wing mode (Ref. 140). With a soft-inplane rotor, air resonance is possible at low-flight speeds, particularly involving the wing vertical-bending mode (Fig. 128). At operating flight speeds, the air resonance is stabilized by the aerodynamic lag damping in high inflow and the wing aerodynamic damping.

With increasing Mach number, the blade lift-curve slope first increases, which increases the aerodynamic forces involved in whirl flutter, and so has an unfavorable influence on the stability (Fig. 129). After lift divergence (at a Mach number of around 0.7 to 0.8), the lift-curve slope decreases. If the blade section Mach number is above the lift divergence Mach number over a large fraction of the blade tip, the reduction in aerodynamic forces will significantly increase the stability. This phenomenon becomes particularly important as the speed of sound decreases at higher altitude (Ref. 142).

The rotor rotational-speed degree-of-freedom has a major influence on the whirl flutter stability (Refs. 140 and 143). Vertical bending of the wing is accompanied by a roll motion of the rotor shaft. If the rotor rotational speed is fixed relative to the pylon, this roll motion will be transmitted to the rotor, and the high aerodynamic damping of the rotor will greatly stabilize the wing mode (Fig. 130). If the rotor is windmilling, the rotational degree of freedom will be free relative to the pylon, and this source of damping will be absent. Typically, the engine inertia, engine damping, and rotor-speed governor offer little restraint of the rotational-speed degree of freedom in the symmetric motions of a tilting proprotor aircraft. The difference between powered and windmilling stability (Fig. 130) is primarily due to the difference in trimmed blade deflection. In the antisymmetric

motions, however, the interconnect shaft constrains the rotor speed, introducing a differential speed mode with a natural frequency of the same order as the wing modes.

Tilting proprotor stability can be analyzed using a rigid blade and hinge spring model for the rotor. As for hingeless and bearingless helicopter rotors, the key to success with such theories is in the correct specification of the effective pitch/lag, pitch/flap, and flap/lag couplings. Elastic flap-lag-torsion rotor models have also been developed for tilting proprotors (Refs. 29 and 141). To the models developed for helicopter rotors, it is necessary to add high inflow aerodynamics, and the structural dynamics of blades with large collective and large twist. The calculations shown in Figs. 126-130 were produced using the analysis of Ref. 29.

Johnson (Ref. 144) presented a comparison of predicted and measured whirl flutter damping. Figure 131 shows the wing beam bending mode stability for a rotor windmilling on a cantilever wing in a wind tunnel. The calculations were also produced using the analysis of Ref. 29. The rotor was a small-scale model of an early gimballed hub design for the Bell/Boeing JVX aircraft.

Bilger, Marr, and Zahedi (Ref. 145) described the dynamic characteristics of the XV-15 Tilt Rotor Research Aircraft. Whirl flutter stability and blade loads were no problem in the aircraft flight tests. Initially the pylon loads (in the conversion spindle and downstop) were high (Fig. 132). A pylon lateral mode was excited at 2/rev; the source of the excitation was the second cyclic rotor mode loads at 1/rev and 3/rev, acting through the gimbal. The correction involved reducing the downstop stiffness by a factor of 4.4, in order to move the load peak (at resonance with the pylon lateral mode) below the rotor speed of interest. Initially the loads in the engine coupling gearbox were high as well (Fig. 133). The 2/rev excitation forces were reduced by optimizing the lateral and longitudinal cyclic pitch in airplane configuration to maintain zero flapping at high speed. The reduction in downstop stiffness also reduced the 2/rev engine loads. These problems were both associated with the design of the gimbal, and the complicated load paths in the pylon.

5. CONCLUDING REMARKS

5.1 Basic Dynamic Problems

Stability concerns for advanced rotorcraft have centered on flap-lag stability and air/ground resonance. The pitch/lag coupling and structural flap/lag coupling have a major influence on the stability. The effective coupling is a result of the rotor blade nonlinear dynamics, and depends on the detailed hub parameters.

Simple analytical models of hingeless rotors have been derived for research purposes and to support aircraft development. There has been experimental verification of these models, and they have provided much understanding of the basic dynamic phenomena. There have been strong research programs to develop elastic blade

analyses for hingeless rotors. There has been limited experimental verification of the models, and they are starting to be used to support aircraft development. For bearingless rotors, simple theoretical models are less useful, because the dynamics of the actual configurations are so complex. As usual, designers of new rotors are ahead of the analyzers.

Rotor loads is the forced response problem, requiring the full nonlinear solution rather than just the linearized equations, and much more attention to aerodynamics. Generally there have been advances in the scope of loads prediction capability, but not in the accuracy. The prediction of mean and oscillatory loads is acceptable for design purposes, but detailed examination of correlations shows that the phenomena are still not completely understood.

Rotor-induced vibration adds the airframe structural dynamics to the problem. The attention in aircraft development is on vibration reduction, either passive or active, rather than on vibration prediction.

5.2 Advanced Topics in Dynamics

In higher harmonic-control research, the promise of the self-tuning regulator concept is beginning to be realized. The dynamic inflow models are a productive start for routine use of unsteady aerodynamics in rotor dynamics. Finite elements bring needed flexibility to rotor analyses, but the large number of degrees of freedom introduces major difficulties with complexity and computation time. The analyses being developed for composite rotors are necessary to realize the potential design flexibility of the materials.

5.3 Dynamics of Rotorcraft Configurations

There are soft-inplane hingeless main rotors in production. Lower flap frequencies are desired, to reduce the vibration and gust response and to minimize adverse handling qualities effects. Vibration more often than stability has been a problem in hingeless rotor development.

Experimental bearingless rotors have been developed, in further pursuit of design simplicity. The main rotor designs are soft-inplane, while the tail rotor designs are mostly stiff-inplane. Perhaps the most common configuration involves a flexbeam with an inboard flap flexure (for low flap frequency), plus an external torque tube with a snubber/damper at the root (for control of the pitch/bending coupling and augmentation of the structural damping). Stability has been a major concern, particularly air/ground resonance.

In rotors using circulation control, the trailing-edge blowing directly influences the lag dynamics, but the rotors tend to be very stiff. Coupled engine/rotor dynamic problems include local vibrations, and fuel controller dynamics with recent high-gain designs. Often the interdisciplinary nature of these engine/rotor problems is not fully reflected in the analyses. With articulated rotors, multimode dynamics can still provide surprises.

Concerns regarding tilting proprotor aircraft dynamics have focused on whirl flutter, which requires the addition of high inflow aerodynamics and high-pitch/high-twist structural dynamics to the analyses. The dynamic phenomena of hingeless rotors are generally a factor as well.

New rotorcraft configurations have generally been developed with the support of simple theories (or none); tests have been essential. Advanced analyses are only now beginning to help aircraft development. The designers remain one step ahead of the analyzers. A more flexible theoretical approach is needed, separating the helicopter and rotor configuration from the mathematical modeling. In tests of innovative designs, the real hardware may be expected to continue to provide interesting new dynamic problems.

REFERENCES

1. Loewy, R. G., "A Review of Rotary-Wing V/STOL Dynamic and Aeroelastic Problems." J. Am. Helicop. Soc., vol. 14, no. 3, July 1969.
2. Hohenemser, K. H., "Hingeless Rotorcraft Flight Dynamics." AGARD AG-197, 1974.
3. Friedmann, P., "Recent Developments in Rotary-Wing Aeroelasticity." J. Aircraft, vol. 14, no. 11, Nov. 1977.
4. Friedmann, P., "Formulation and Solution of Rotary-Wing Aeroelastic Stability and Response Problems." Vertica, vol. 7, no. 2, 1983.
5. Ormiston, R. A., "Investigations of Hingeless Rotor Stability." Vertica, vol. 7, no. 2, 1983.
6. Loewy, R. G., "Helicopter Vibrations: A Technological Perspective." J. Am. Helicop. Soc., vol. 29, no. 4, Oct. 1984.
7. Johnson, W., Helicopter Theory. Princeton University Press, Princeton, New Jersey, 1980.
8. Ormiston, R. A., and Hodges, D. H., "Linear Flap-Lag Dynamics of Hingeless Helicopter Rotor Blades in Hover." J. Am. Helicop. Soc., vol. 17, no. 2, Apr. 1972.
9. Lytwyn, R. T., Miao, W., and Woitsch, W., "Airborne and Ground Resonance of Hingeless Rotors." J. Am. Helicop. Soc., vol. 16, no. 2, Apr. 1971.
10. Burkam, J. E., and Miao, W.-L., "Exploration of Aeroelastic Stability Boundaries with a Soft-Inplane Hingeless-Rotor Model." J. Am. Helicop. Soc., vol. 17, no. 4, Oct. 1972.
11. Reichert, G., and Huber, H., "Influence of Elastic Coupling Effects on the Handling Qualities of a Hingeless Rotor Helicopter." AGARD Conf. Proc. No. 121, Hampton, Va., Sept. 1971.
12. Huber, H. B., "Effect of Torsion-Flap-Lag Coupling on Hingeless Rotor Stability." An. Nat. Forum Am. Helicop. Soc., May 1973.
13. Miao, W.-L., and Huber, H. B., "Rotor Aeroelastic Stability Coupled with Helicopter Body Motion." NASA SP-352, Feb. 1974.
14. Hansford, R. E., and Simons, I. A., "Torsion-Flap-Lag Coupling on Helicopter Rotor Blades." J. Am. Helicop. Soc., vol. 18, no. 4, Oct. 1973.
15. Ormiston, R. A., "Techniques for Improving the Stability of Soft-Inplane Hingeless Rotors." NASA TM X-62390, Oct. 1974.
16. Kaza, K. R. V., and Kvaternik, R. G., "Examination of the Flap-Lag Stability of Rigid Articulated Rotor Blades." J. Aircraft, vol. 16, no. 12, Dec. 1979.
17. Ormiston, R. A., and Bousman, W. G., "A Study of Stall-Induced Flap-Lag Instability of Hingeless Rotors." J. Am. Helicop. Soc., vol. 20, no. 1, Jan. 1975.
18. Bousman, W. G., Sharpe, D. L., and Ormiston, R. A., "An Experimental Study of Techniques for Increasing the Lead-Lag Damping of Soft Inplane Hingeless Rotors." An. Nat. Forum Am. Helicop. Soc., May 1976.
19. Hodges, D. H., and Ormiston, R. A., "Stability of Elastic Bending and Torsion of Uniform Cantilevered Rotor Blades in Hover." AIAA Paper 73-405, Mar. 1973.
20. Hodges, D. H., and Dowell, E. H., "Nonlinear Equations of Motion for the Elastic Bending and Torsion of Twisted Nonuniform Rotor Blades." NASA TN D-7818, Dec. 1974.

21. Friedmann, P., and Tong, P., "Nonlinear Flap-Lag Dynamics of Hingeless Helicopter Blades in Hover and in Forward Flight." J. Sound Vib., vol. 30, no. 1, 1973.
22. Friedmann, P., "Some Conclusions Regarding the Aeroelastic Stability of Hingeless Helicopter Blades in Hover and in Forward Flight." J. Am. Helicop. Soc., vol. 18, no. 4, Oct. 1973.
23. Friedmann, P., "Aeroelastic Instabilities of Hingeless Helicopter Blades." J. Aircraft, vol. 10, no. 10, Oct. 1973.
24. Hodges, D. H., and Ormiston, R. A., "Stability of Elastic Bending and Torsion of Uniform Cantilever Rotor Blades in Hover with Variable Structural Coupling." NASA TN D-8192, Apr. 1976.
25. Friedmann, P., and Straub, F., "Application of the Finite Element Method to Rotary Wing Aeroelasticity." J. Am. Helicop. Soc., vol. 25, no. 1, Jan. 1980.
26. Hodges, D. H., and Ormiston, R. A., "Stability of Hingeless Rotor Blades in Hover with Pitch-Link Flexibility." AIAA J., vol. 15, no. 4, Apr. 1977.
27. Friedmann, P., "Influence of Modeling and Blade Parameters on the Aeroelastic Stability of a Cantilevered Rotor." AIAA J., vol. 15, no. 2, Feb. 1977.
28. Kaza, K. R. V., and Kvaternik, R. G., "Nonlinear Aeroelastic Equations for Combined Flapwise Bending, Chordwise Bending, Torsion, and Extension of Twisted Nonuniform Rotor Blades in Forward Flight." NASA TM-74059, Aug. 1977.
29. Johnson, W., "Development of a Comprehensive Analysis for Rotorcraft." Vertica, vol. 5, nos. 2 and 3, 1981.
30. Warmbrodt, W., and Peterson, R. L., "Hover Test of a Full-Scale Hingeless Rotor." NASA TM-85990, Aug. 1984.
31. Peters, D. A., "Flap-Lag Stability of Helicopter Rotor Blades in Forward Flight." J. Am. Helicop. Soc., vol. 20, no. 4, Oct. 1975.
32. Friedmann, P., and Silverthorn, L. J., "Aeroelastic Stability of Coupled Flap-Lag Motion of Hingeless Helicopter Blades at Arbitrary Advance Ratios." J. Sound Vib., vol. 39, no. 4, 1975.
33. Friedmann, P., and Shamie, J., "Aeroelastic Stability of Trimmed Helicopter Blades in Forward Flight." Vertica., vol. 1, no. 3, 1977.
34. Friedmann, P., and Kottapalli, S. B. R., "Coupled Flap-Lag-Torsional Dynamics of Hingeless Rotor Blades in Forward Flight." J. Am. Helicop. Soc., vol. 27, no. 4, Oct. 1982.
35. Reddy, T. S. R., and Warmbrodt, W., "The Influence of Dynamic Inflow and Torsional Flexibility on Rotor Damping in Forward Flight from Symbolically Generated Equations." Am. Helicop. Soc. Specialists' Meeting on Rotorcraft Dynamics, Moffett Field, Calif., Nov. 1984.
36. Bielawa, R. L., "Aeroelastic Analysis for Helicopter Rotor Blades with Time-Variable, Nonlinear Structural Twist and Multiple Structural Redundancy." NASA CR-2638, 1976.
37. Bielawa, R. L., Cheney, M. C., and Novak, R. C., "Investigation of a Bearingless Helicopter Rotor Concept Having a Composite Primary Structure." NASA CR-2637, 1976.
38. Hodges, D. H., "A Theoretical Technique for Analyzing Aeroelastic Stability of Bearingless Rotors." AIAA J., vol. 17, no. 4, Apr. 1979.

39. Hodges, D. H., "An Aeromechanical Stability Analysis for Bearingless Rotor Helicopters." J. Am. Helicop. Soc., vol. 24, no. 1, Jan. 1979.
40. Lytwyn, R. T., "Aeroelastic Stability Analysis of Hingeless Rotor Helicopters in Forward Flight Using Blade and Airframe Normal Modes." An. Nat. Forum Am. Helicop. Soc., May 1980.
41. Warmbrodt, W., McCloud, J. L., III, Sheffler, M., and Staley, J., "Full-Scale Wind-Tunnel Test of the Aeroelastic Stability of a Bearingless Main Rotor." Vertica, vol. 6, no. 3, 1982.
42. Dawson, S., "An Experimental Investigation of a Bearingless Model Rotor in Hover." J. Am. Helicop. Soc., vol. 28, no. 4, Oct. 1983.
43. Bousman, W. G., and Dawson, S., "Experimentally Determined Flutter from Two- and Three-Bladed Model Bearingless Rotors in Hover." Am. Helicop. Soc. Specialists' Meeting on Rotorcraft Dynamics, Moffett Field, Calif., Nov. 1984.
44. Sivaneri, N. T., and Chopra, I., "Finite Element Analysis for Bearingless Rotor Blade Aeroelasticity." J. Am. Helicop. Soc., vol. 29, no. 2, Apr. 1984.
45. Chopra, I., "Dynamic Stability of a Bearingless Circulation Control Rotor Blade in Hover." Am. Helicop. Soc. Specialists' Meeting on Rotorcraft Dynamics, Moffett Field, Calif., Nov. 1984.
46. Ormiston, R. A., "Aeromechanical Stability of Soft Inplane Hingeless Rotor Helicopters." Eur. Rotorcraft and Powered Lift Aircraft Forum, Aix-en-Provence, France, Sept. 1977.
47. Bousman, W. G., "An Experimental Investigation of the Effects of Aeroelastic Couplings on Aeromechanical Stability of a Hingeless Rotor Helicopter." J. Am. Helicop. Soc., vol. 26, no. 1, Jan. 1981.
48. Yeager, W. T., Jr., Hamouda, M. H., and Mantay, W. R., "Aeromechanical Stability of a Hingeless Rotor in Hover and Forward Flight: Analysis and Wind Tunnel Tests." NASA TM-85683, Aug. 1983.
49. Hooper, W. E., "Parametric Study of Aeroelastic Stability of a Bearingless Rotor." Am. Helicop. Soc. Specialists' Meeting on Rotorcraft Dynamics, Moffett Field, Calif., Nov. 1984.
50. Piziali, R. A., "Rotor Aeroelastic Simulation--A Review." AGARD Conf. Proc. No. 122, Milan, Italy, Mar. 1973.
51. Yen, J. G., and Weller, W. H., "Analysis and Application of Compliant Rotor Technology." Eur. Rotorcraft and Powered Lift Aircraft Forum, England, Sept. 1980.
52. Gabel, R., "Current Loads Technology for Helicopter Rotors." AGARD Conf. Proc. No. 122, Milan, Italy, Mar. 1973.
53. Arcidiacono, P. J., and Carlson, R. G., "Helicopter Rotor Loads Predictions." AGARD Conf. Proc. No. 122, Milan, Italy, Mar. 1973.
54. Gallot, J., "Prediction of Helicopter Rotor Loads." AGARD Conf. Proc. No. 122, Milan, Italy, Mar. 1973.
55. Bennett, R. L., "Rotor System Design and Evaluation Using a General Purpose Helicopter Flight Simulation Program." AGARD Conf. Proc. No. 122, Milan, Italy, Mar. 1973.
56. McKenzie, K. T., and Howell, D. A. S., "The Prediction of Loading Actions on High Speed Semirigid Rotor Helicopters." AGARD Conf. Proc. No. 122, Milan, Italy, Mar. 1973.

57. Reichert, G., "Loads Prediction Methods for Hingeless Rotor Helicopters." AGARD Conf. Proc. No. 122, Milan, Italy, Mar. 1973.
58. Carlson, R. M., and Kerr, A. W., "Integrated Rotor/Body Loads Prediction." AGARD Conf. Proc. No. 122, Milan, Italy, Mar. 1973.
59. Staley, J. A., "Validation of Rotorcraft Flight Simulation Program through Correlation with Flight Data for Soft-in-Plane Hingeless Rotors." U.S. Army Air Mobility R&D Labs., TR 75-50, Jan. 1976.
60. Sheffler, M., "Analysis and Correlation with Theory of Rotor Lift-Limit Test Data." NASA CR-159139, Nov. 1979.
61. Yen J. G., and Glass, M., "Helicopter Rotor Load Prediction." Am. Helicop. Soc. Mideast Region Meet. on Helicop. Fatigue Method., Mar. 1980.
62. Jepson, D., Moffitt, R., Hilzinger, K., and Bissell, J., "Analysis and Correlation of Test Data from an Advanced Technology Rotor System." NASA CR-3714, Aug. 1983.
63. Sopher, R., Studwell, R. E., Cassarino, S., and Kottapalli, S. B. R., "Coupled Rotor/Airframe Vibration Analysis." NASA CR-3582, June 1982.
64. Reichert, G., "Helicopter Vibration Control--A Survey." Vertica, vol. 5, no. 1, 1981.
65. Cronkhite, J. D., "Development, Documentation, and Correlation of a NASTRAN Vibration Model of the AH-1G Helicopter Airframe." NASA TM X-3428, Oct. 1976.
66. Stoppel, J., and Degener, M., "Investigations of Helicopter Structural Dynamics and a Comparison with Ground Vibration Tests." J. Am. Helicop. Soc., vol. 27, no. 2, Apr. 1982.
67. Gabel, R., Reed, D., Ricks, R., and Kesack, W., "Planning, Creaging, and Documenting a NASTRAN Finite Element Model of a Modern Helicopter." Am. Helicop. Soc. Specialists' Meet. on Rotorcraft Dynamics, Moffett Field, Calif., Nov. 1984.
68. Gabel, R., and Reichert, G., "Pendulum Absorbers Reduce Transition Vibration." An. Nat. Forum Am. Helicop. Soc., May 1975.
69. Ham, N. D., "Helicopter Individual Blade Control and Its Applications." An. Nat. Forum Am. Helicop. Soc., May 1983.
70. Kretz, M., "Research in Multicyclic and Active Control of Rotary Wings." Vertica, vol. 1, no. 2, 1976.
71. Gupta, N. K., and DuVal, R. W., "A New Approach to Active Control of Rotorcraft Vibration." J. Guid. Control, vol. 5, no. 2, Mar.-Apr. 1982.
72. Jacob, H. G., and Lehmann, G., "Optimization of Blade Pitch Angle for Higher Harmonic Rotor Control." Vertica, vol. 7, no. 3, 1983.
73. McCloud, J. L., III, and Kretz, M., "Multicyclic Jet-Flap Control for Alleviation of Helicopter Blade Stresses and Fuselage Vibration." NASA SP-352, Feb. 1974.
74. Kretz, M., Aubrun, J.-N., and Larche, M., "Wind Tunnel Tests of the Dorand DH 2011 Jet Flap Rotor." NASA CR-114693 and CR-114694, June 1973.
75. Johnson, W., "Self-Tuning Regulators for Multicyclic Control of Helicopter Vibration." NASA TP-1996, Mar. 1982.
76. Hammond, C. E., "Wind Tunnel Results Showing Rotor Vibratory Loads Reduction Using Higher Harmonic Blade Pitch." J. Am. Helicop. Soc., vol. 28, no. 1, Jan. 1983.

77. Molusis, J. A., Hammond, C. E., and Cline, J. H., "A Unified Approach to the Optimal Design of Adaptive and Gain Scheduled Controllers to Achieve Minimum Helicopter Rotor Vibration." J. Am. Helicop. Soc., vol. 28, no. 2, Apr. 1983.
78. Wood, E. R., Powers, R. W., Cline, J. H., and Hammond, C. E., "On Developing and Flight Testing a Higher Harmonic Control System." An. Nat. Forum Am. Helicop. Soc., May 1983.
79. Gupta, B. P., Wood, E. R., Logan, A. H., and Cline, J. H., "Recent Higher Harmonic Control Development and OH-6A Flight Testing." An. Nat. Forum Am. Helicop. Soc., May 1985.
80. Johnson, W., "The Influence of Unsteady Aerodynamics in Hingeless Rotor Ground Resonance." J. Aircraft, vol. 19, no. 8, Aug. 1982.
81. Gaonkar, G. H., and Peters, D. A., "A Review of Dynamic Inflow and Its Effect on Experimental Correlations." Am. Helicop. Soc. Specialists' Meet. Rotorcraft Dynamics, Moffett Field, Calif., Nov. 1984.
82. Peters, D. A., "Hingeless Rotor Frequency Response with Unsteady Inflow." NASA SP-352, Feb. 1974.
83. Miller, R. H., "Rotor Blade Harmonic Air Loading." AIAA J., vol. 2, no. 7, July 1964.
84. Pitt, D. M., and Peters, D. A., "Theoretical Prediction of Dynamic-Inflow Derivatives." Vertica, vol. 5, no. 1, 1981.
85. Curtiss, H. C., Jr., and Shupe, N. K., "A Stability and Control Theory for Hingeless Rotors." An. Nat. Forum Am. Helicop. Soc., May 1971.
86. Peters, D. A., and Gaonkar, G. H., "Theoretical Flap-Lag Damping with Various Dynamic Inflow Models." J. Am. Helicop. Soc., vol. 25, no. 3, July 1980.
87. Yasue, M., "Gust Response and Its Alleviation for a Hingeless Helicopter Rotor in Cruising Flight." MIT, ASRL TR 189-1, Jan. 1977.
88. Sivaneri, N. T., and Chopra, I., "Dynamic Stability of a Rotor Blade Using Finite Element Analysis." AIAA J., vol. 20, no. 5, May 1982.
89. Rutkowski, M. J., "The Vibration Characteristics of a Coupled Helicopter Rotor-Fuselage by a Finite Element Analysis." NASA TP-2118, Jan. 1983.
90. Lefrancq, J. P., and Masure, B., "A Complete Method for Computation of Blade Mode Characteristics and Responses in Forward Flight." Eur. Rotorcraft and Powered Lift Forum, Germany, Sept. 1981.
91. Borri, M., Lanz, M., and Mantegazza, P., "A General Purpose Program for Rotor Blade Dynamics." Eur. Rotorcraft and Powered Lift Aircraft Forum, Germany, Sept. 1981.
92. Borri, M., Lanz, M., Mantegazza, P., Orlandi, D., and Russo, A., "STAHR: A Program for Stability and Trim Analysis of Helicopter Rotors." Eur. Rotorcraft and Powered Lift Aircraft Forum, France, Sept. 1982.
93. Giavotto, V., Borri, M., Russo, A., and Ceriotta, A., "The Role of Aeroelasticity in the Preliminary Design of Helicopter Rotors." AGARD Conf. Proc. No. 354, Apr. 1983.
94. Hodges, D. H., "Nonlinear Equations for Dynamics of Pretwisted Beams Undergoing Small Strains and Large Rotations." NASA TP, 1985 (to be published).
95. Mansfield, E. H., and Sobey, A. J., "The Fibre Composite Helicopter Blade." The Aeronaut. Q., vol. 30, no. 2, May 1979.

96. Worndle, R., "Calculation of the Cross Section Properties and the Shear Stresses of Composite Rotor Blades." Vertica, vol. 26, no. 2, 1982.
97. Hong, C.-H., and Chopra, I., "Aeroelastic Stability Analysis of a Composite Blade." An. Nat. Forum Am. Helicop. Soc., May 1984.
98. Strehlow, H., and Enenkl, B., "Aeroelastic Design Considerations in the Development of Helicopters." AGARD Conf. Proc. No. 354, Apr. 1983.
99. Anderson, W. D., "Investigation of Reactionless Mode Stability Characteristics of a Stiff Inplane Hingeless Rotor System." An. Nat. Forum Am. Helicop. Soc., May 1973.
100. Anderson, W. D., and Johnston, J. F., "Comparison of Flight Data and Analysis for Hingeless Rotor Regressive Inplane Mode Stability." NASA SP-352, Feb. 1974.
101. Reichert, G., and Weiland, E., "Long Term Experience with a Hingeless/Composite Rotor." AGARD Conf. Proc. No. 233, Moffett Field, Calif., May 1977.
102. Kloppel, V., Kampa, K., and Isselhorst, B., "Aeromechanical Aspects in the design of Hingeless/Bearingless Rotor Systems." Eur. Rotorcraft Forum, Italy, Sept. 1983.
103. Balmford, D. E. H., "Ground and Flight Test Experience with the Westland Scout Hingeless Rotor Helicopter." AGARD Conf. Proc. No. 121, Hampton, Va., Sept. 1971.
104. Berrington, D. K., "Design and Development of the Westland Sea Lynx." J. Am. Helicop. Soc., vol. 19, no. 1, Jan. 1974.
105. Burgess, R. K., "Development of the ABC Rotor." AGARD Conf. Proc. No. 121, Hampton, Va., Sept. 1971.
106. Young, H. R., and Simon, D. R., "The Advancing Blade Concept (ABC) Rotor Program." AGARD Conf. Proc. No. 233, Moffett Field, Calif., May 1977.
107. Abbe, J. T. L., Blackwell, R. H., and Jenney, D. S., "Advancing Blade Concept (ABC) Dynamics." An. Nat. Forum Am. Helicop. Soc., May 1977.
108. Linden, A. W., and Ruddell, A. J., "An ABC Status Report." An. Nat. Forum Am. Helicop. Soc., May 1981.
109. Ruddell, A. J., et al., "Advancing Blade Concept (ABC) Technology Demonstrator." U.S. Army Aviation R&D Cmd., TR 81-D-5, Apr. 1981.
110. Huber, H., and Masue, T., "Flight Characteristics Design and Development of the MBB/KHI BK 117 Helicopter." Eur. Rotorcraft and Powered Lift Aircraft Forum, Germany, Sept. 1981.
111. Bousman, W. G., Ormiston, R. A., and Mirick, P. H., "Design Considerations for Bearingless Rotor Hubs." An. Nat. Forum Am. Helicop. Soc., May 1983.
112. Donham, R. E., Cardinale, S. V., and Sachs, I. B., "Ground and Air Resonance Characteristics of a Soft Inplane Rigid Rotor System." J. Am. Helicop. Soc., vol. 14, no. 4, Oct. 1969.
113. Staley, J. A., Gabel, R., and MacDonald, H. I., "Full-Scale Ground and Air Resonance Testing of the Army-Boeing Vertol Bearingless Main Rotor." An. Nat. Forum Am. Helicop. Soc., May 1979.
114. Dixon, P. G. C., "Design, Development, and Flight Demonstration of the Loads and Stability Characteristics of a Bearingless Main Rotor." U.S. Army Aviation R&D Cmd., TR 80-D-3, June 1980.

115. Sheffler, M., Warmbrodt, W., and Staley, J., "Evaluation of the Effect of Elastomeric Damping Material on the Stability of a Bearingless Main Rotor System." Am. Helicop. Soc. Mideast Region Meet. on Rotor System Design, Philadelphia, Pa., Oct. 1980.
116. McHugh, F. J., Staley, J. A., and Sheffler, M. W., "Dynamic Stability of Low Effective Flap Hinge BMR Concepts." Am. Helicop. Soc. Mideast Region Meet. on Rotor System Design, Philadelphia, Pa., Oct. 1980.
117. Cassier, A., "Development of the Triflex Rotor Head." J. Am. Helicop. Soc., vol. 26, no. 3, July 1981.
118. Metzger, R., "Smooth and Simple: The Bell Model 680 Bearingless Main Rotor." Vertiflite, vol. 29, no. 4, May-June 1983.
119. Weller, W. H., "Correlation and Evaluation of Inplane Stability Characteristics for an Advanced Bearingless Main Rotor Model." NASA CR-166448, May 1983.
120. Seitz, G., and Singer, G., "Structural and Dynamic Tailoring of Hingeless/Bearingless Rotors." Eur. Rotorcraft Forum, Italy, Sept. 1983.
121. Maloney, P. F., and Porterfield, J. D., "Elastic Pitch Beam Tail Rotor." U.S. Army Air Mobility R&D Lab., TR 76-35, Dec. 1976.
122. Fenaughty, R. R., and Noehren, W. L., "Composite Bearingless Tail Rotor for UTTAS." J. Am. Helicop. Soc., vol. 22, no. 3, July 1977.
123. Shaw, J., Jr., and Edwards, W. T., "The YUH-61A Tail Rotor: Development of a Stiff-Inplane Bearingless Flexstrap Design." J. Am. Helicop. Soc., vol. 23, no. 2, Apr. 1978.
124. Huber, H., Frommlet, H., and Buchs, W., "Development of a Bearingless Helicopter Tailrotor." Vertica, vol. 5, no. 2, 1981.
125. Blachere, C., and D'Ambra, F., "Tail Rotor Studies for Satisfactory Performance, Strength, and Dynamic Behavior." Vertica, vol. 6, no. 4, 1982.
126. Banerjee, D., Johnston, R. A., and Messinger, R. H., "Wind Tunnel Test of a Soft/Stiff Inplane Bearingless Rotor." J. Am. Helicop. Soc., vol. 29, no. 2, Apr. 1984.
127. Chopra, I., and Johnson, W., "Flap-Lag-Torsion Aeroelastic Stability of Circulation-Controlled Rotors in Hover." J. Am. Helicop. Soc., vol. 24, no. 2, Apr. 1979.
128. Richardson, D. A., and Alwang, J. R., "Engine/Airframe/Drive Train Dynamic Interface Documentation." U.S. Army Res. and Tech. Labs., TR 78-11, Apr. 1978.
129. Needham, J. F., and Banerjee, D., "Engine/Airframe/Drive Train Dynamic Interface Documentation." U.S. Army Res. and Tech. Labs., TR 78-12, May 1978.
130. Twomey, W. J., and Ham, E. H., "Review of Engine/Airframe/Drive Train Dynamic Interface Development Problems." U.S. Army Res. and Tech. Labs., TR 78-13, June 1978.
131. Bowes, M. A., "Engine/Airframe/Drive Train Dynamic Interface Documentation." U.S. Army Res. and Tech. Labs., TR 78-14, June 1978.
132. Hanson, H. W., Balke, R. W., Edwards, B. D., Riley, W. W., and Downs, B. D., "Engine/Airframe/Drive Train Dynamic Interface Documentation." U.S. Army Res. and Tech. Labs., TR 78-15, Oct. 1978.
133. Warmbrodt, W., and Hull, R., "Development of a Helicopter Rotor/Propulsion System Dynamics Analysis." AIAA Paper 82-1078, June 1982.

134. Fredrickson, C., Rumford, K., and Stephenson, C., "Factors Affecting Fuel Control Stability of a Turbine Engine/Helicopter Rotor Drive System." J. Am. Helicop. Soc., vol. 17, no. 1, Jan. 1972.
135. Fredrickson, C., "Engine/Airframe Interface Dynamics Experience." NASA SP-352, Feb. 1974.
136. Thibert, F., and Maquin, F., "Dynamic Behavior of Transmission Systems." Eur. Rotorcraft and Powered Lift Aircraft Forum, France, Sept. 1982.
137. Silverthorn, L. J., "Whirl Mode Stability of the Main Rotor of the YAH-64 Advanced Attack Helicopter." An. Nat. Forum Am. Helicop. Soc., May 1982.
138. Neff, J. R., "Pitch-Flap-Lag Instability of Elastic Modes of an Articulated Rotor Blade." An. Nat. Forum Am. Helicop. Soc., May 1984.
139. Johnson, W., "An Assessment of the Capability to Calculate Tilting Prop-Rotor Aircraft Performance, Loads, and Stability." NASA TP-2291, Mar. 1984.
140. Johnson, W., "Theory and Comparison with Tests of Two Full-Scale Prop-Rotors." NASA SP-352, Feb. 1974.
141. Johnson, W., "Analytical Modeling Requirements for Tilting Proprotor Aircraft Dynamics." NASA TN D-8013, July 1975.
142. Johnson, W., "The Influence of Pitch-Lag Coupling on the Predicted Aeroelastic Stability of the XV-15 Tilting Proprotor Aircraft." NASA TM X-73213, Feb. 1977.
143. Johnson, W., "The Influence of Engine/Transmission/Governor on Tilting Prop-rotor Aircraft Dynamics." NASA TM X-62455, June 1975.
144. Johnson, W., "Assessment of Aerodynamic and Dynamic Models in a Comprehensive Analysis for Rotorcraft." Comput. & Math., May 1985.
145. Bilger, J. M., Marr, R. L., and Zahedi, A., "Results of Structural Dynamic Testing of the XV-15 Tilt Rotor Research Aircraft." J. Am. Helicop. Soc., vol. 27, no. 2, Apr. 1982.

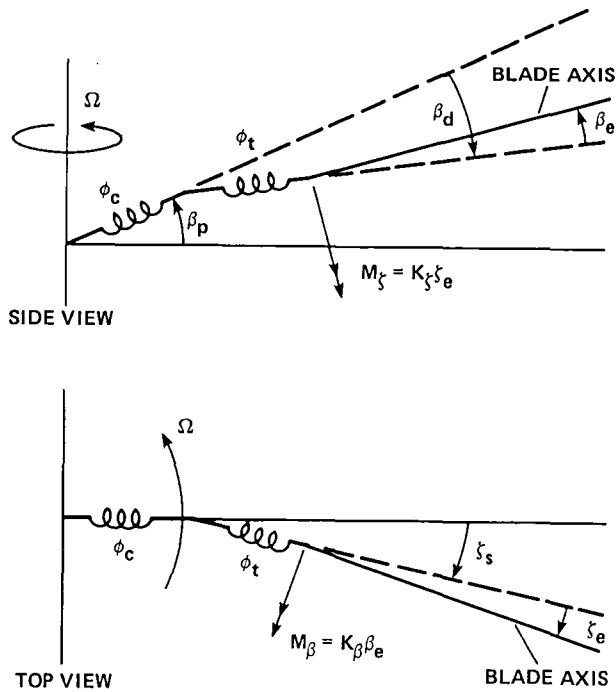


Fig. 1. Origin of effective pitch/lag and pitch/flap coupling.

SOFT-INPLANE HINGELESS ROTOR, NO DAMPING

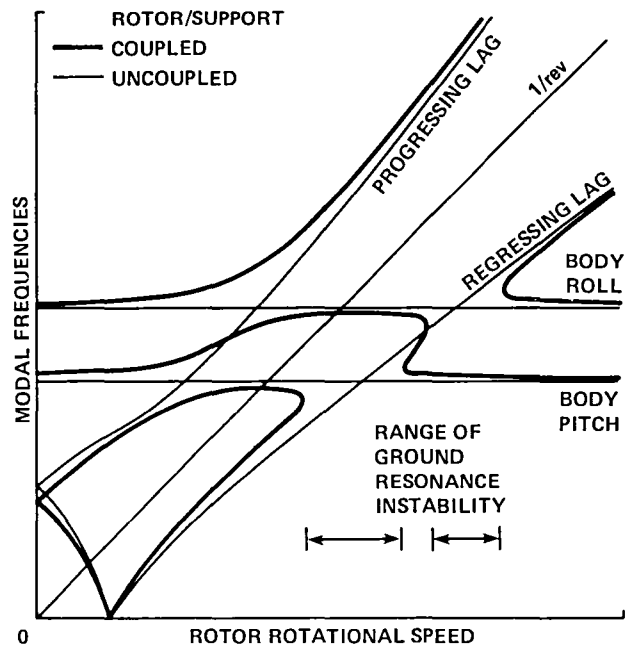


Fig. 2. Coleman diagram for ground resonance.

HINGELESS ROTOR HOVER THEORY, $K_{P_\zeta} = 0$, $R = 0$

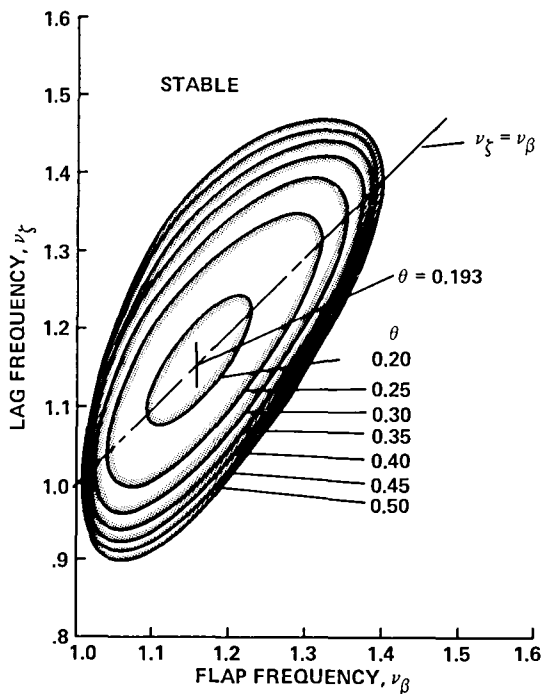


Fig. 3. Calculated flap-lag stability boundaries (Ref. 8).

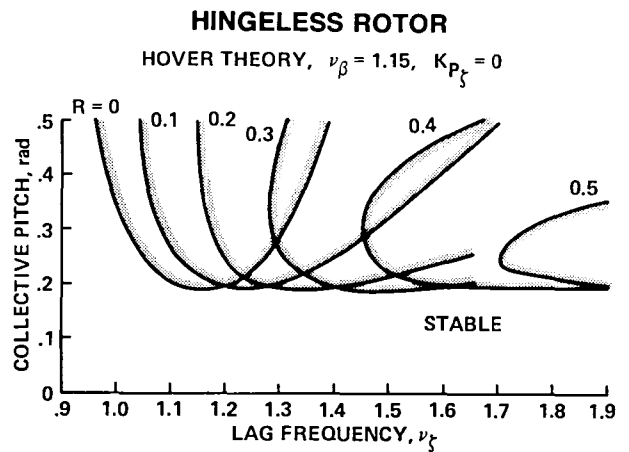


Fig. 4. Calculated flap-lag stability boundaries (Ref. 8).

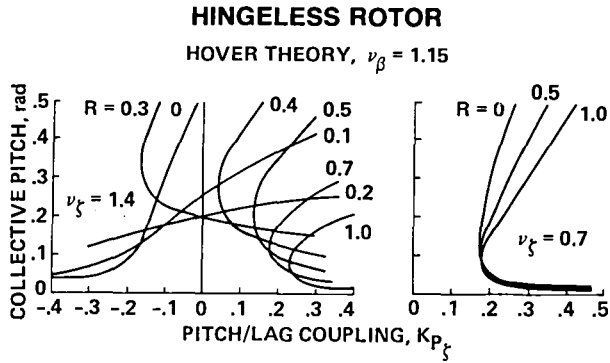


Fig. 5. Calculated flap-lag stability boundaries (Ref. 8).

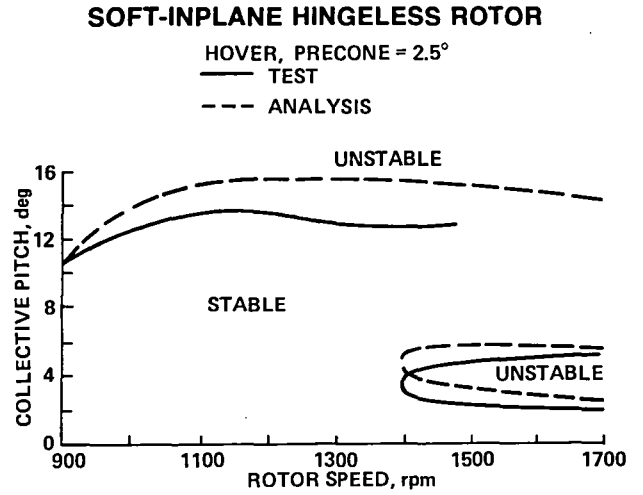


Fig. 6. Soft-inplane hingeless rotor stability boundaries (Ref. 10).

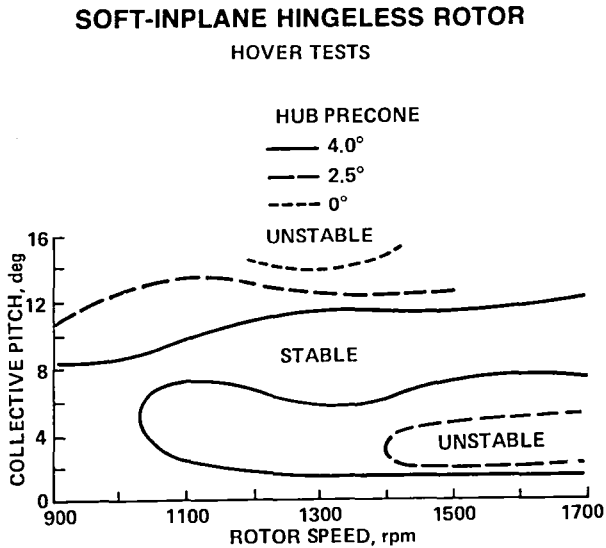


Fig. 7. Measured soft-inplane hingeless rotor stability boundaries (Ref. 10).

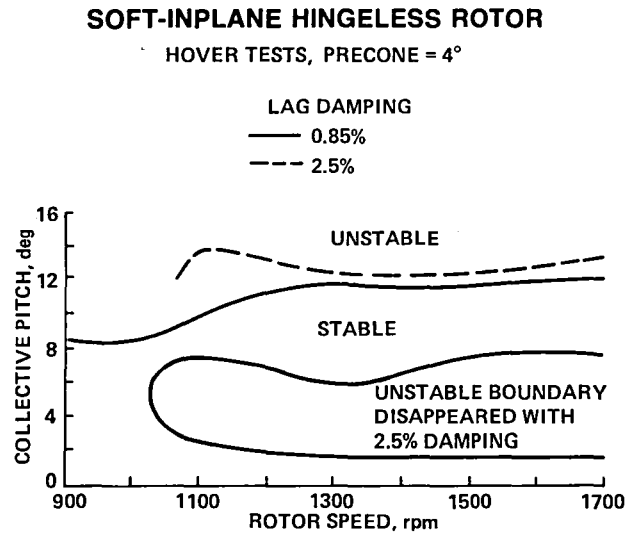


Fig. 8. Measured soft-inplane hingeless rotor stability boundaries (Ref. 10).

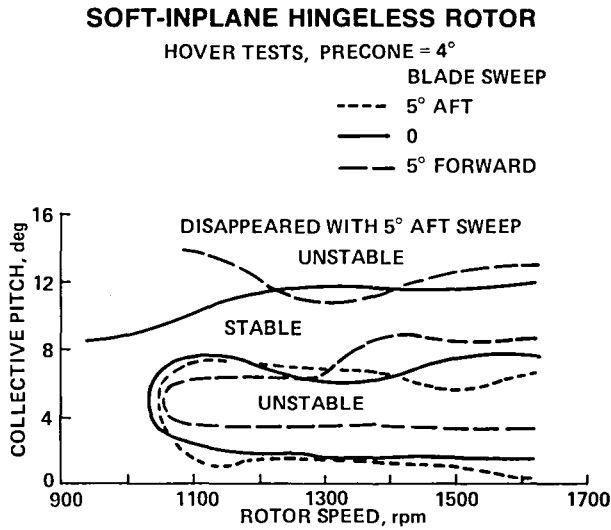


Fig. 9. Measured soft-inplane hingeless rotor stability boundaries (Ref. 10).

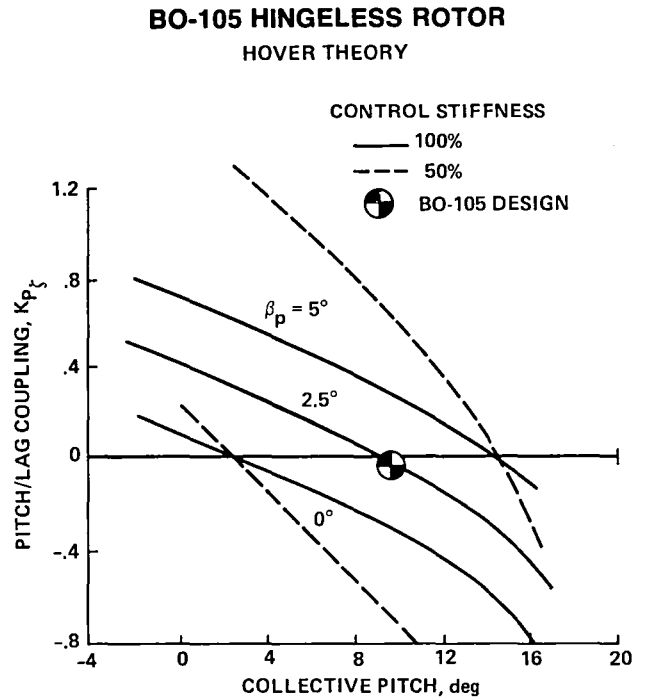


Fig. 10. Calculated pitch/lag coupling for BO-105 helicopter (Ref. 12).

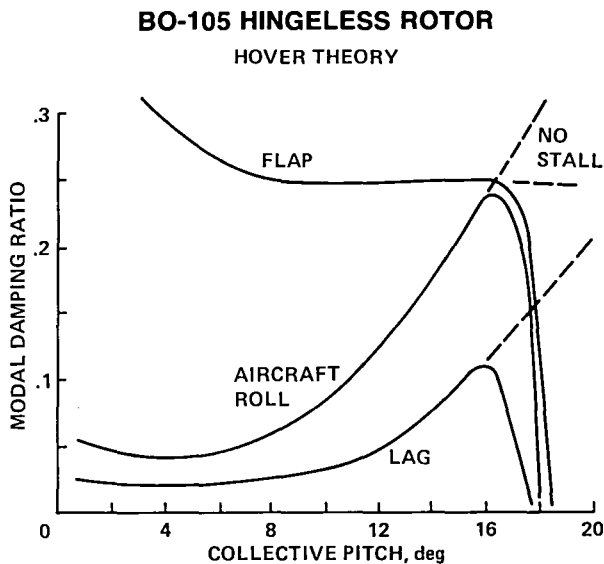


Fig. 11. Calculated flap-lag instability produced by stall (Ref. 12).

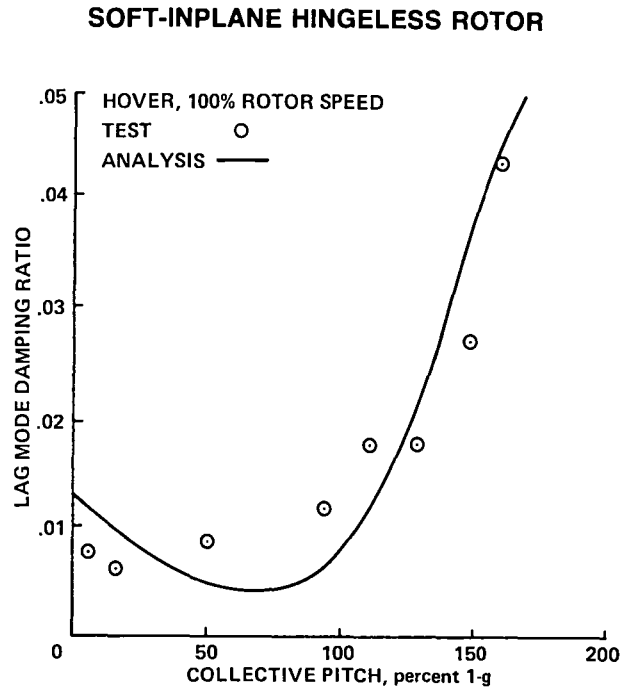


Fig. 12. Soft-inplane hingeless rotor air resonance damping (Ref. 13).

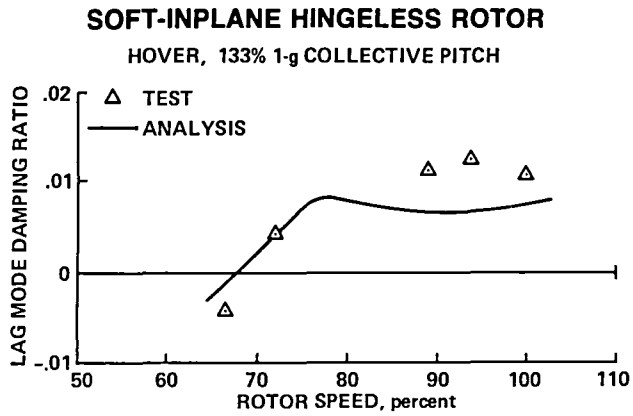


Fig. 13. Soft-inplane hingeless rotor air resonance damping (Ref. 13).

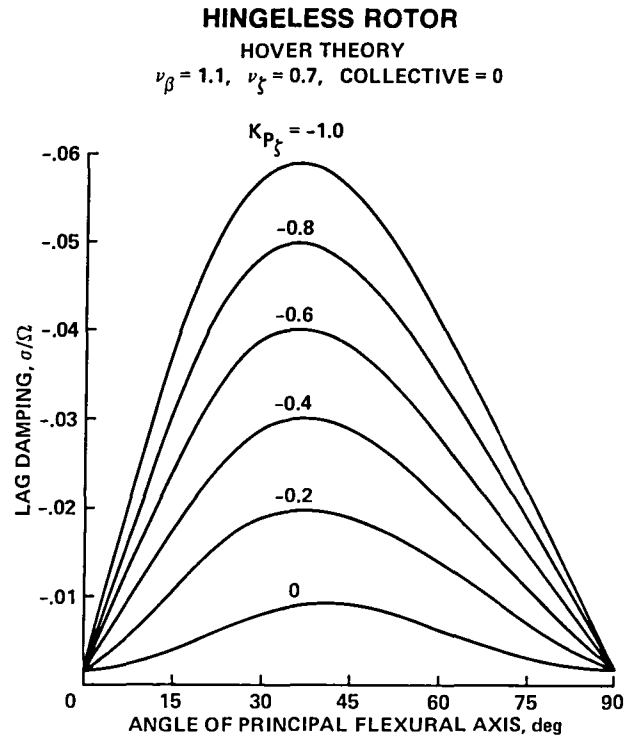


Fig. 14. Calculated hingeless rotor stability (Ref. 15).

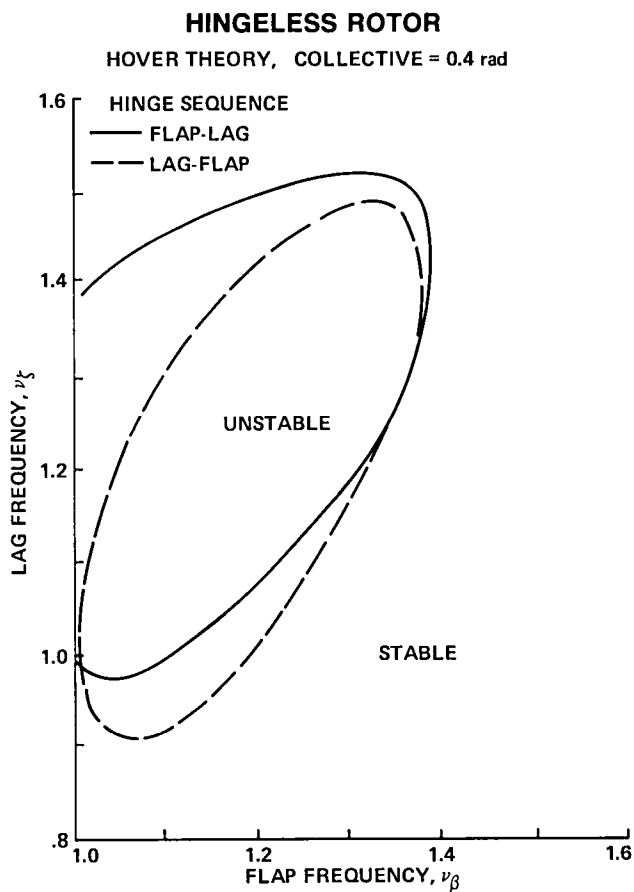


Fig. 15. Calculated flap-lag stability (Ref. 16).

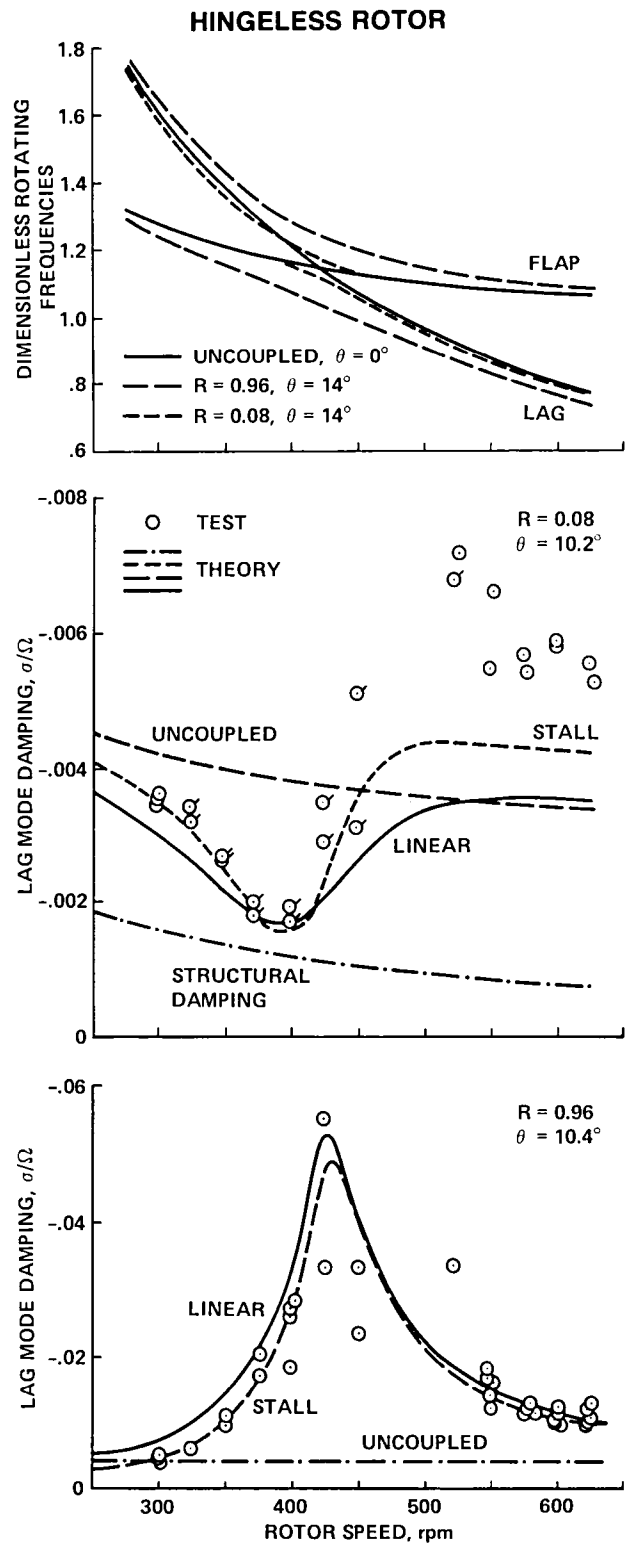


Fig. 16. Flap-lag stability (Ref. 17).

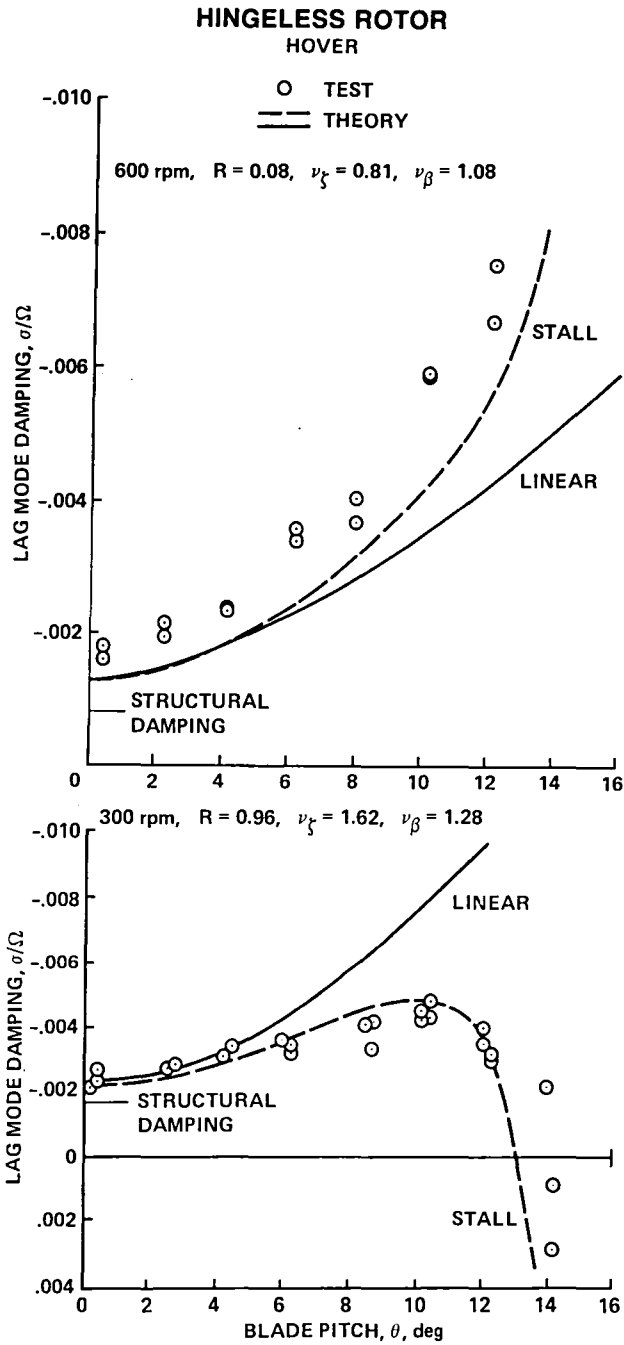


Fig. 17. Flap-lag stability produced by stall (Ref. 17).

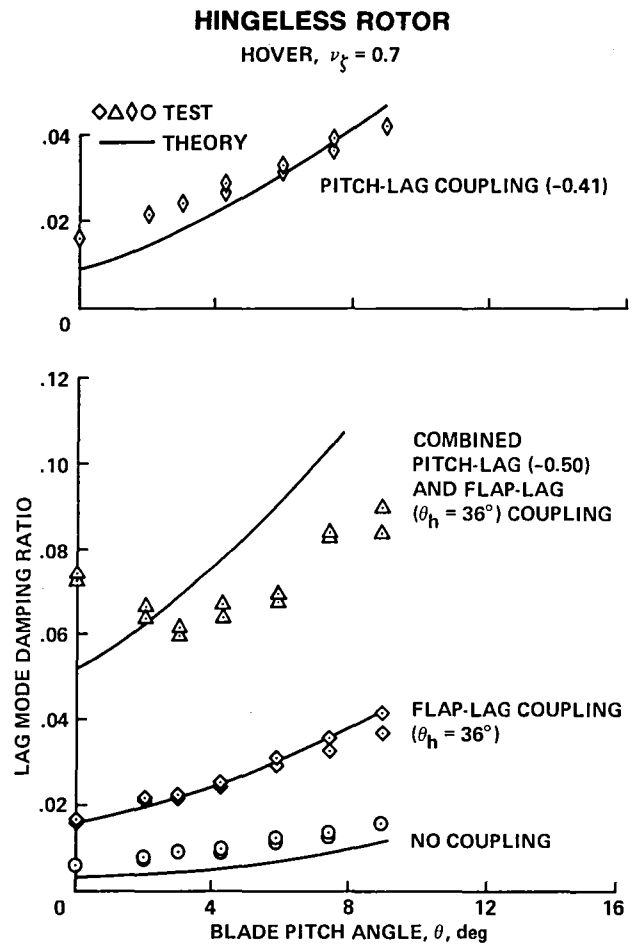


Fig. 18. Flap-lag stability (Ref. 18).

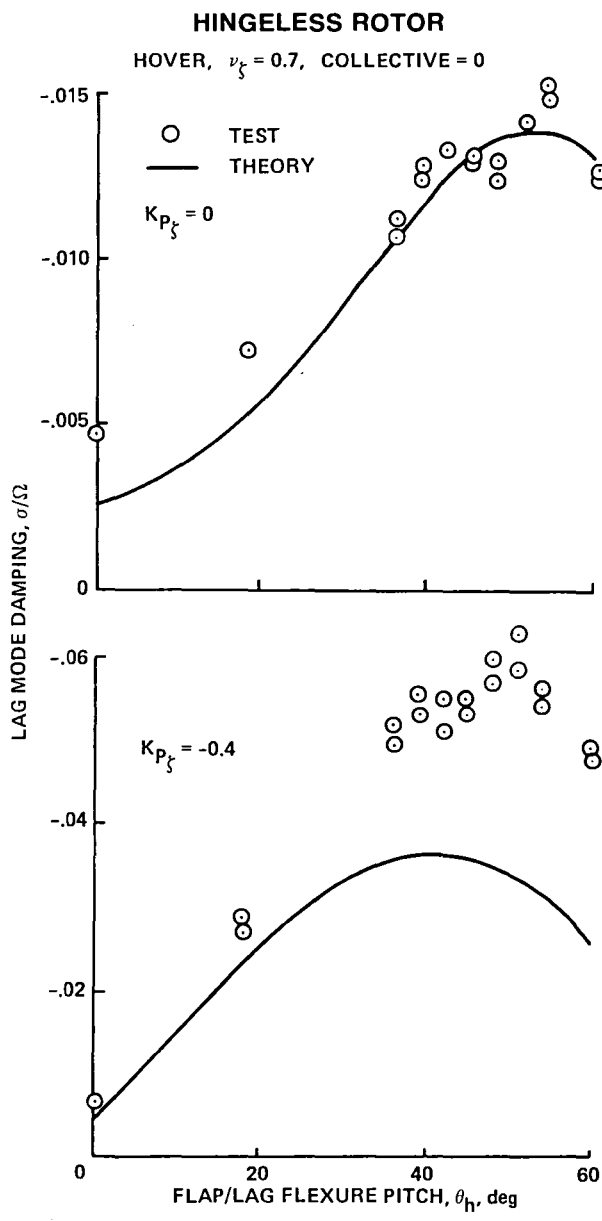


Fig. 19. Flap-lag stability (Ref. 18).

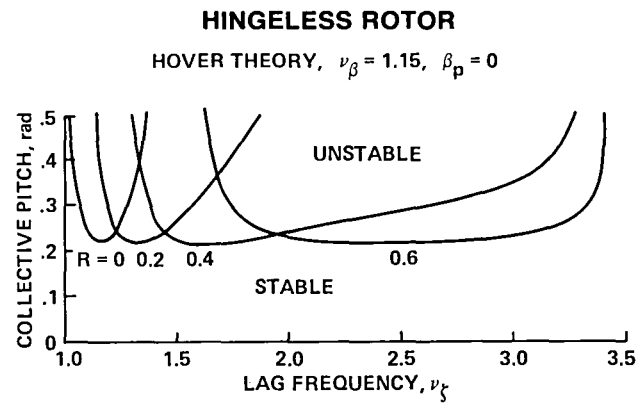


Fig. 20. Calculated elastic flap-lag stability boundaries (Ref. 24).

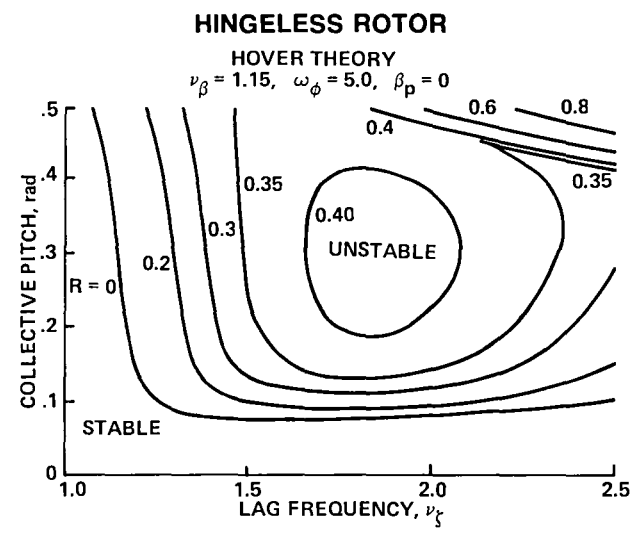


Fig. 21. Calculated flap-lag-torsion stability boundaries (Ref. 24).

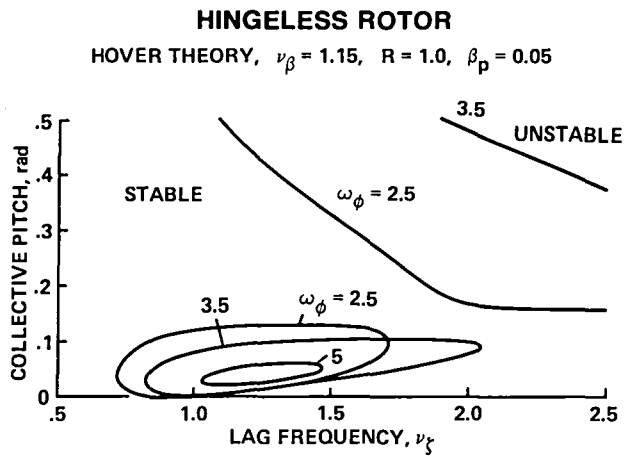


Fig. 22. Calculated flap-lag-torsion stability boundaries (Ref. 24).

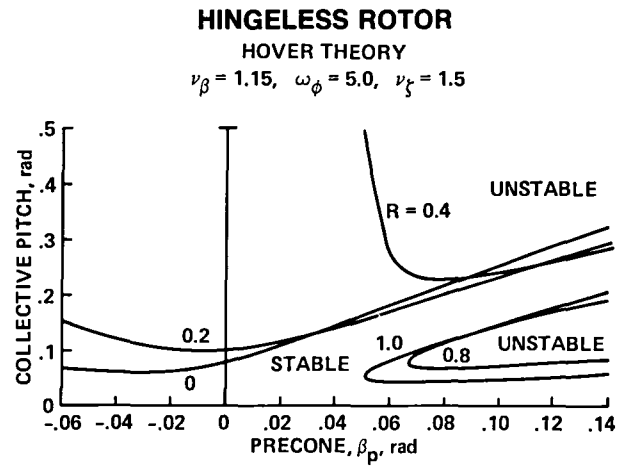


Fig. 23. Calculated flap-lag-torsion stability boundaries (Ref. 24).

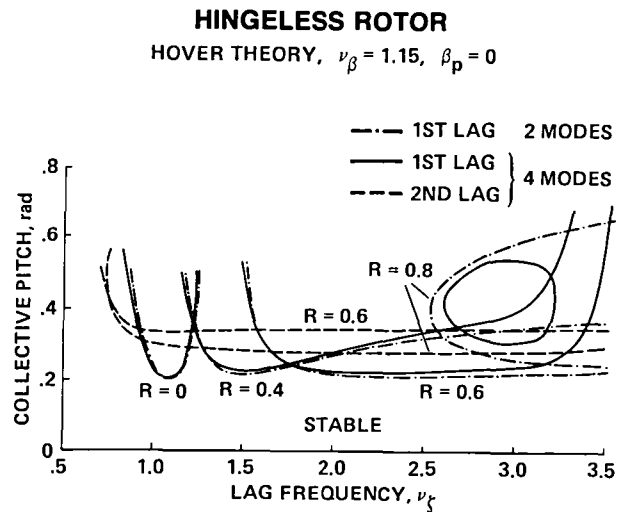


Fig. 24. Calculated elastic flap-lag stability boundaries (Ref. 25).

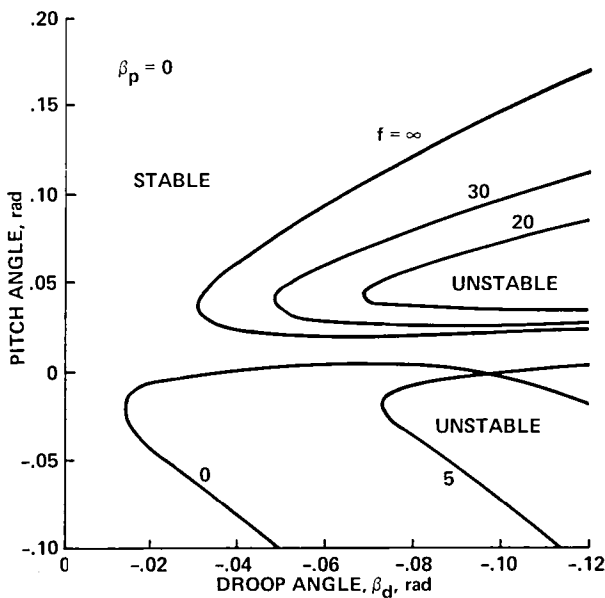
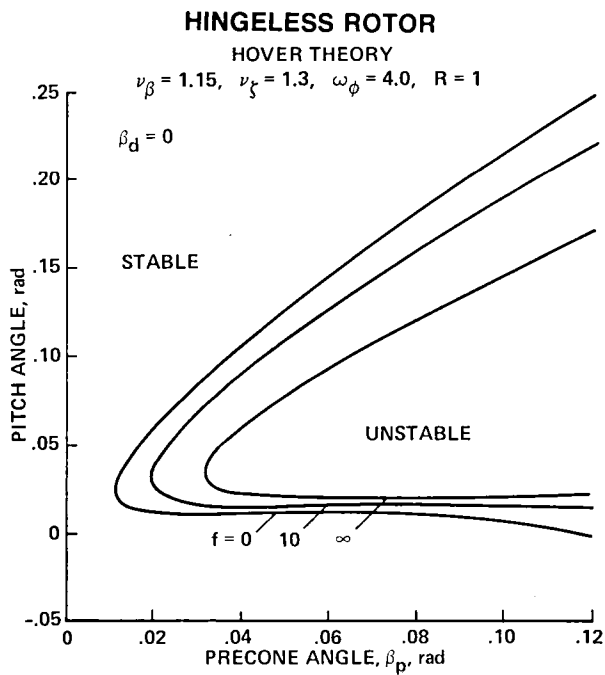


Fig. 25. Calculated pitch-flap-lag-torsion stability boundaries (Ref. 26).

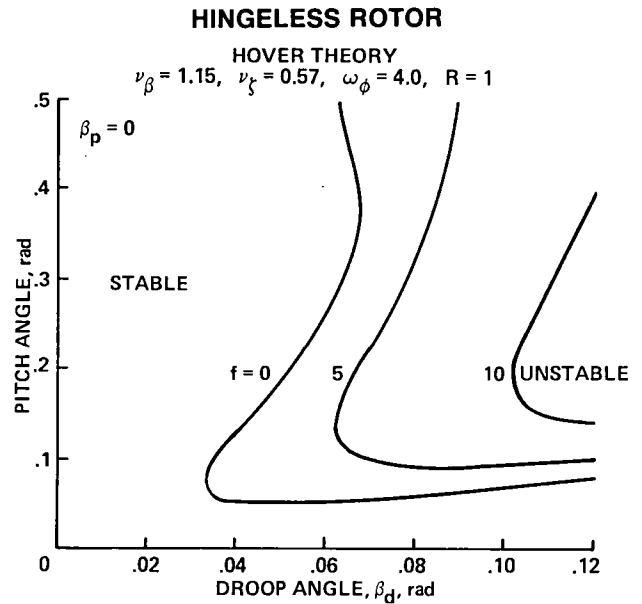


Fig. 26. Calculated pitch-flap-lag-torsion stability boundaries (Ref. 26).

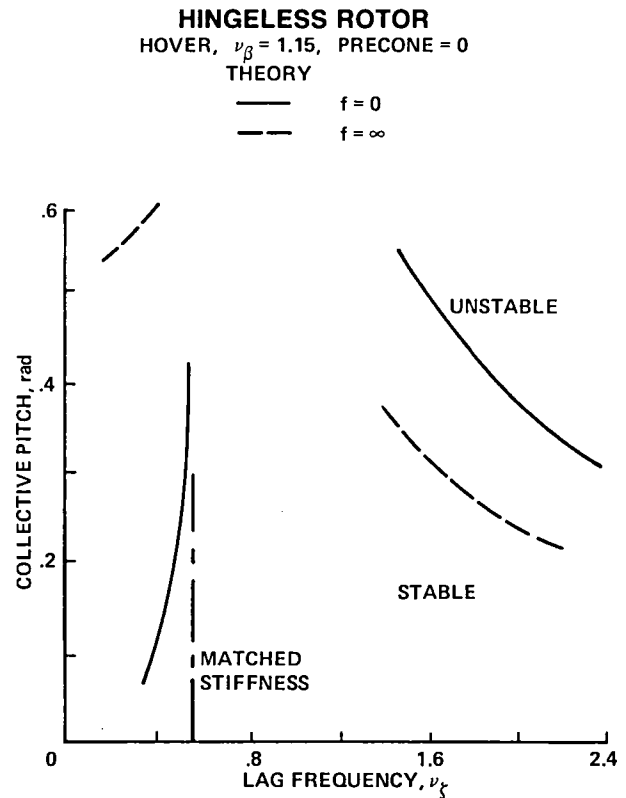


Fig. 27. Calculated pitch-flap-lag-torsion stability boundaries (Ref. 27).

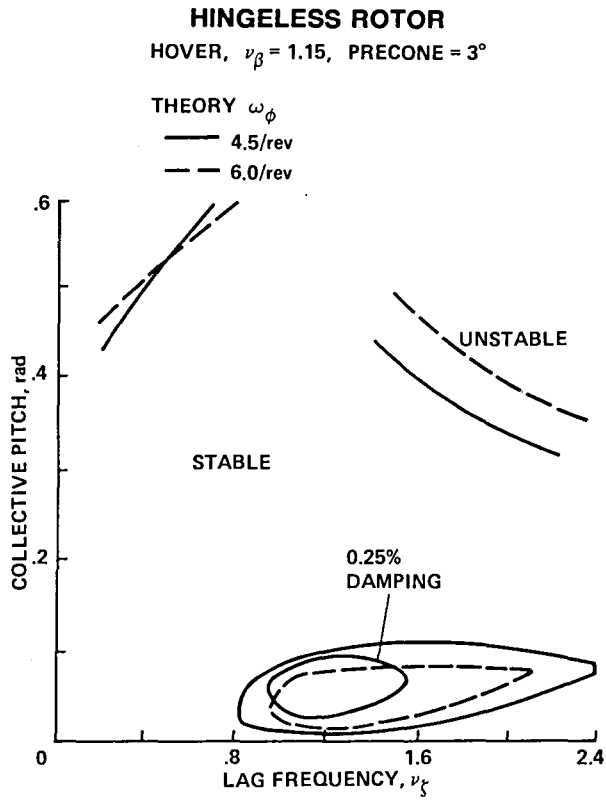


Fig. 28. Calculated flap-lag-torsion stability boundaries (Ref. 27).

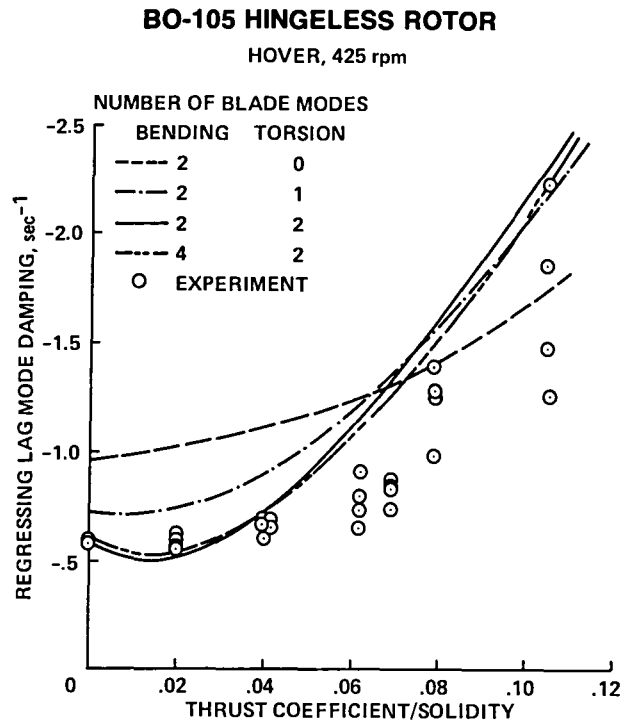


Fig. 29. Soft-inplane hingeless rotor stability (Ref. 30).

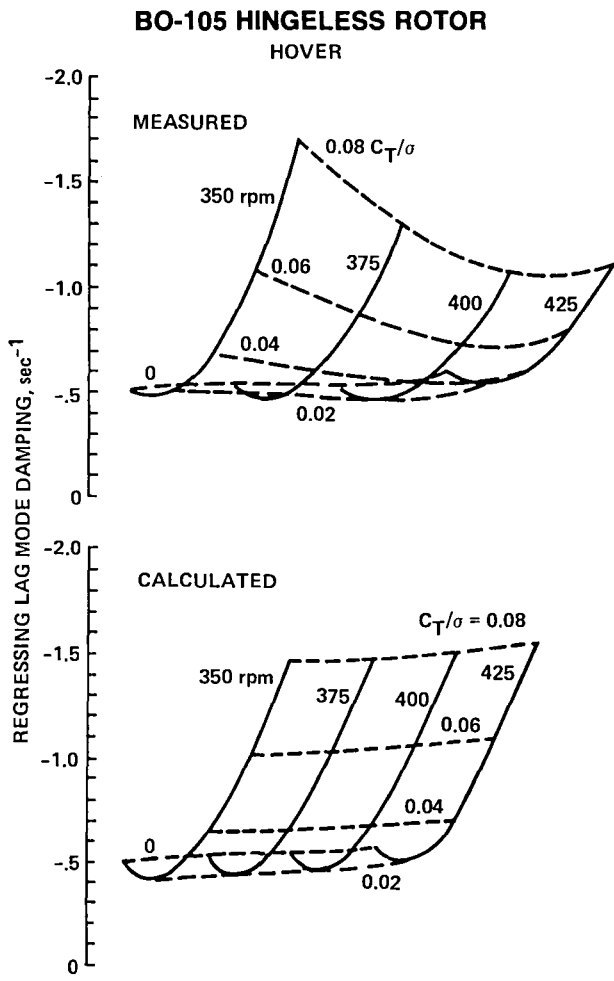


Fig. 30. Soft-inplane hingeless rotor stability (Ref. 30).

SOFT-INPLANE HINGELESS ROTOR
V = 150 knots, 100% ROTOR SPEED

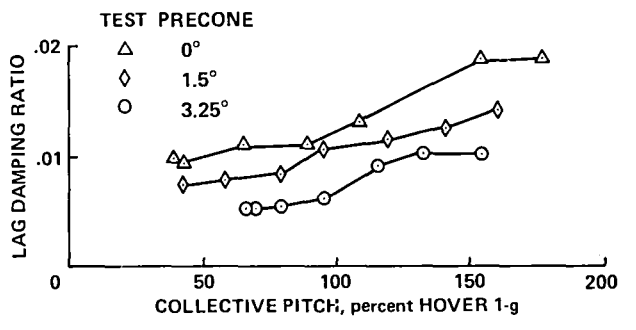


Fig. 31. Measured soft-inplane hingeless rotor air resonance stability (Ref. 13).

SOFT-INPLANE HINGELESS ROTOR
WIND TUNNEL TEST, 1-g LEVEL FLIGHT

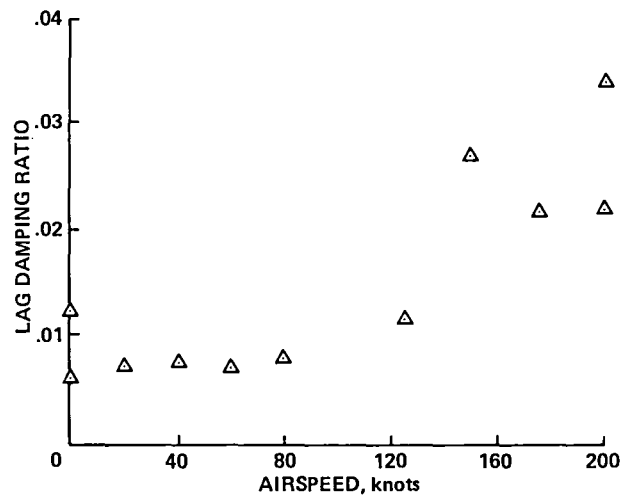


Fig. 32. Measured soft-inplane hingeless rotor air resonance stability (Ref. 13).

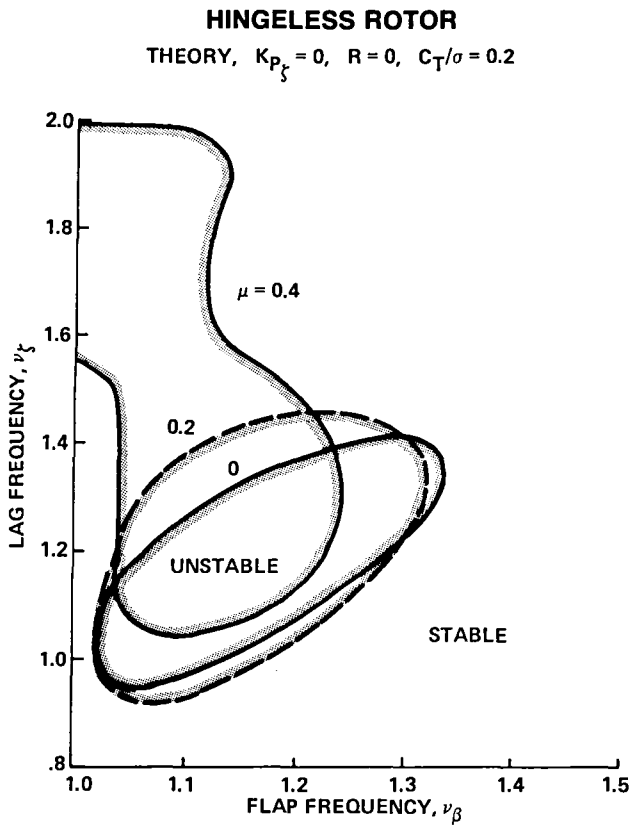


Fig. 33. Calculated flap-lag stability boundaries (Ref. 31).

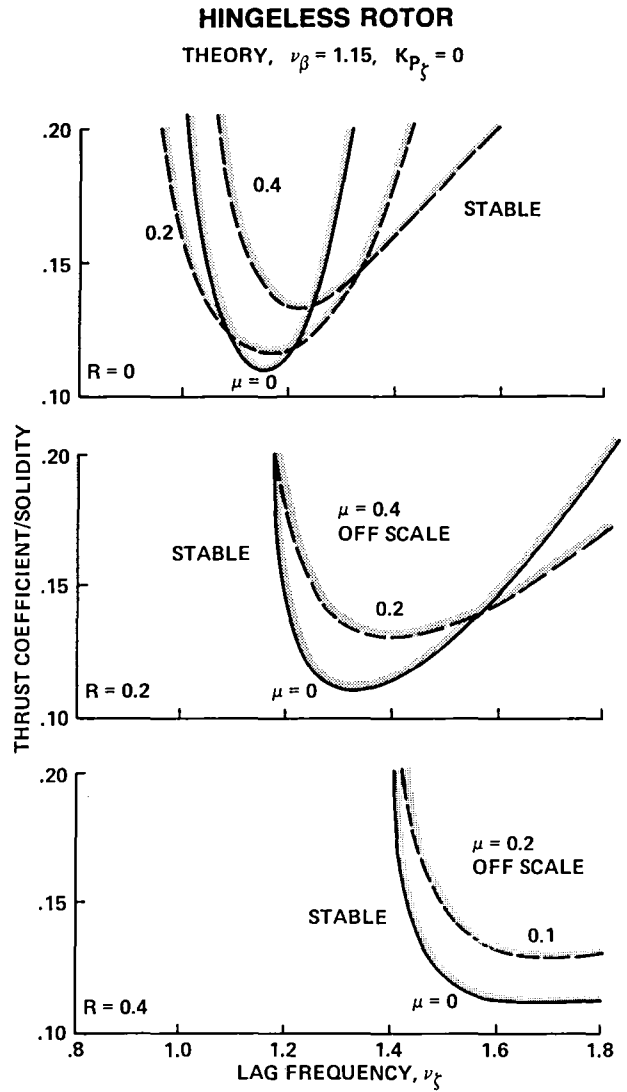


Fig. 34. Calculated flap-lag stability boundaries (Ref. 31).

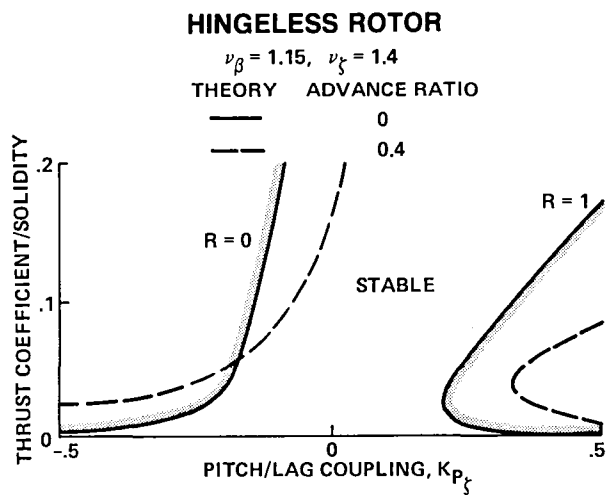


Fig. 35. Calculated flap-lag stability boundaries (Ref. 31).

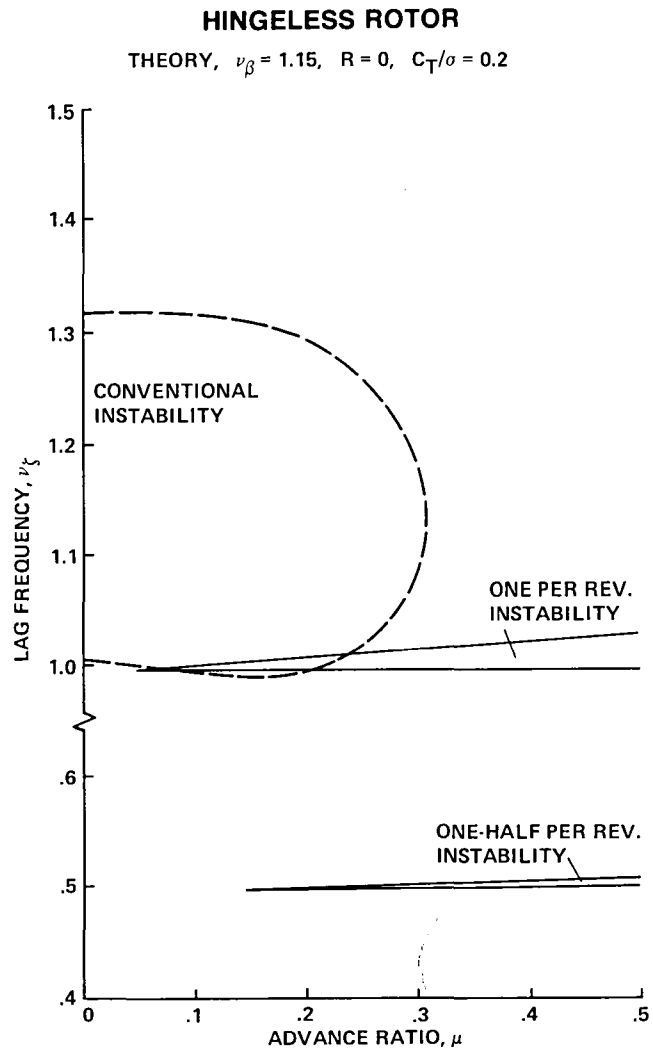


Fig. 36. Calculated flap-lag stability boundaries (Ref. 31).

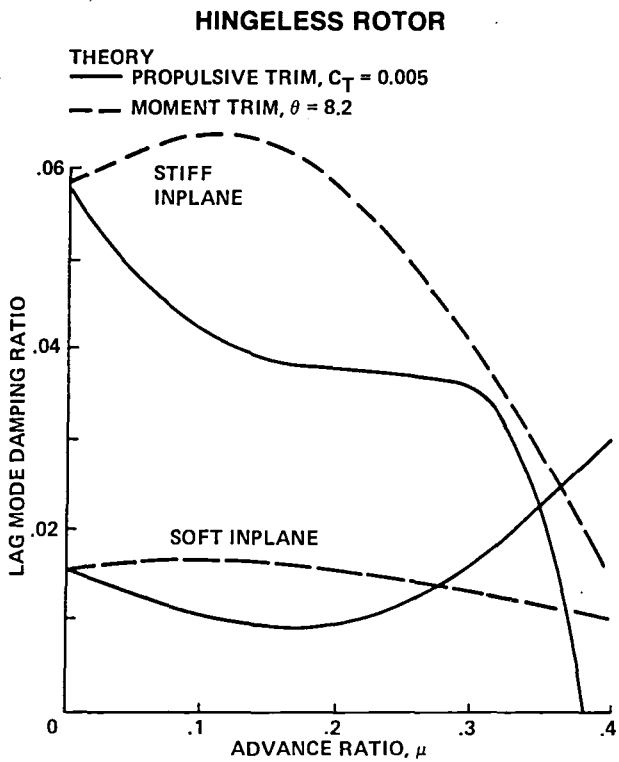


Fig. 37. Calculated elastic flap-lag-torsion stability (Ref. 34).

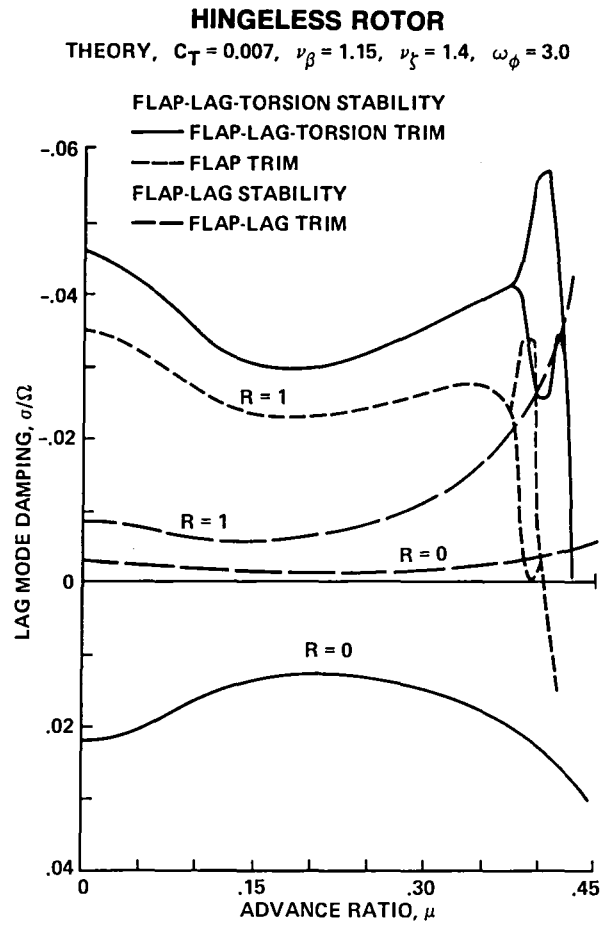


Fig. 38. Calculated elastic flap-lag-torsion stability (Ref. 35).

BEARINGLESS ROTOR

HOVER, 1-g THRUST, $\nu_\beta = 1.09$, $\nu_\zeta = 0.68$

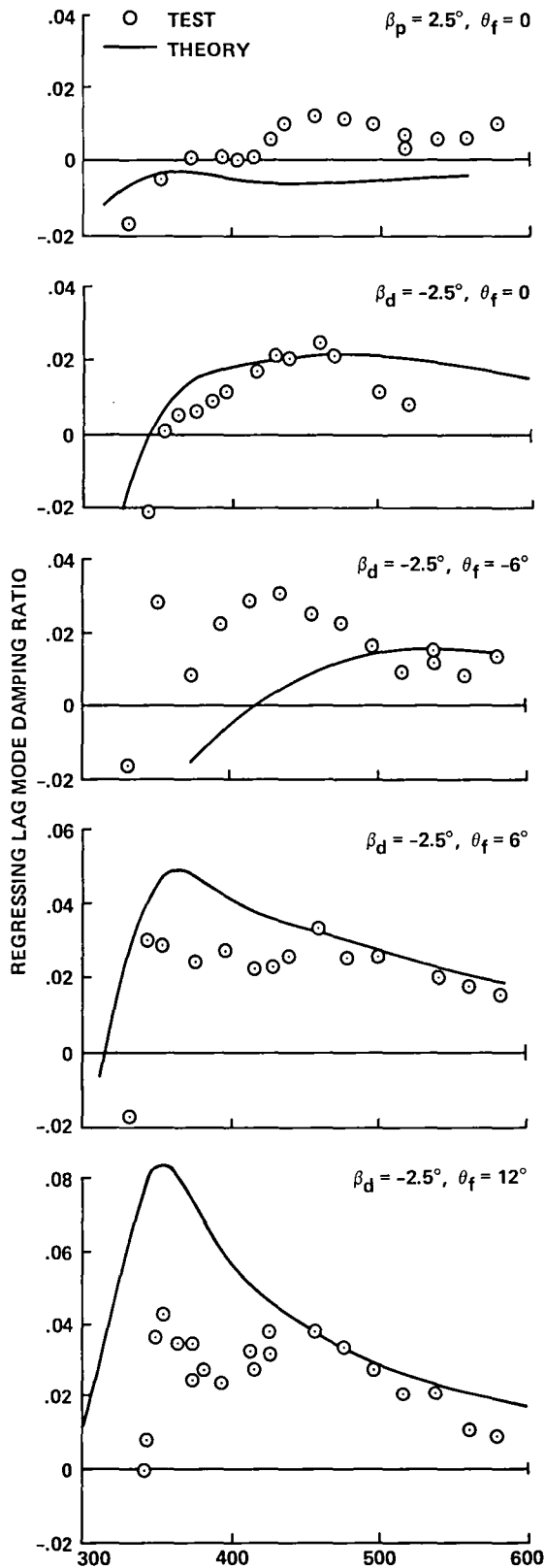


Fig. 39. Bearingless rotor stability (Ref. 39).

BEARINGLESS MAIN ROTOR (BMR)

HOVER, 425 rpm

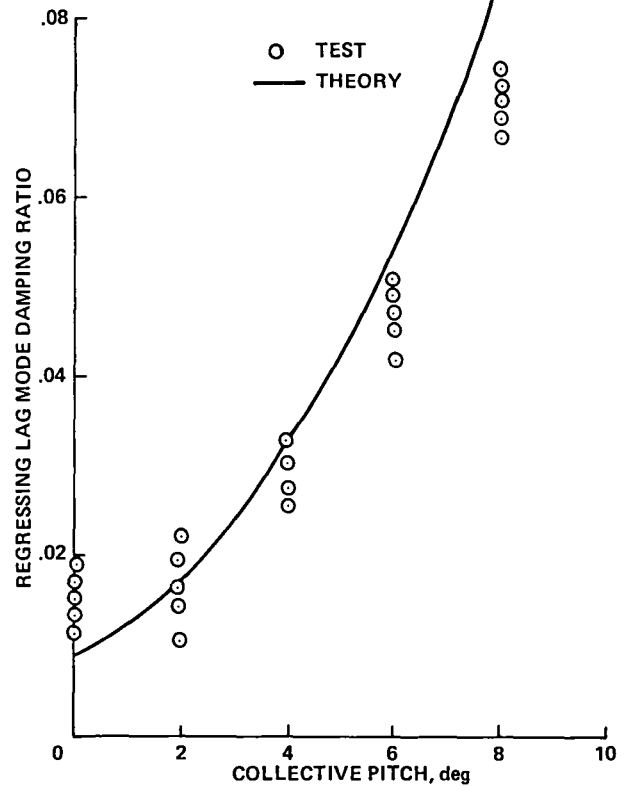


Fig. 40. Bearingless Main Rotor (BMR) stability (Ref. 40).

BEARINGLESS MAIN ROTOR (BMR)

LEVEL FLIGHT, 425 rpm

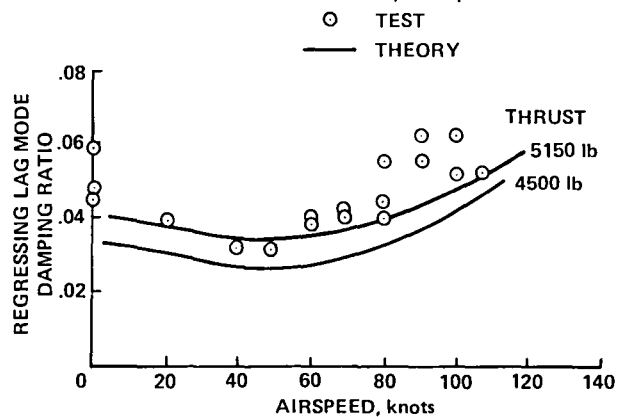


Fig. 41. Bearingless Main Rotor (BMR) stability (Ref. 40).

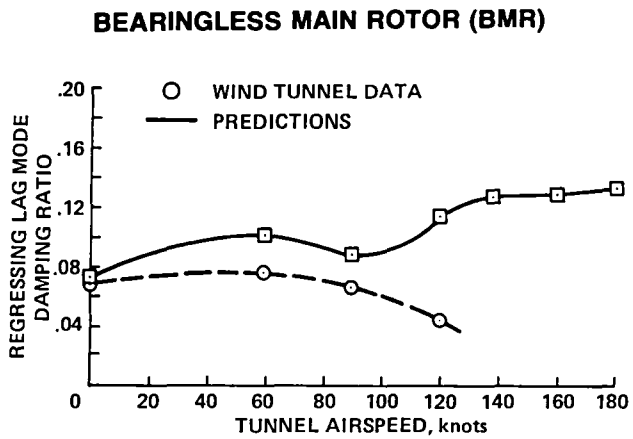


Fig. 42. Bearingless Main Rotor (BMR) stability (Ref. 41).

SOFT-INPLANE BEARINGLESS ROTOR

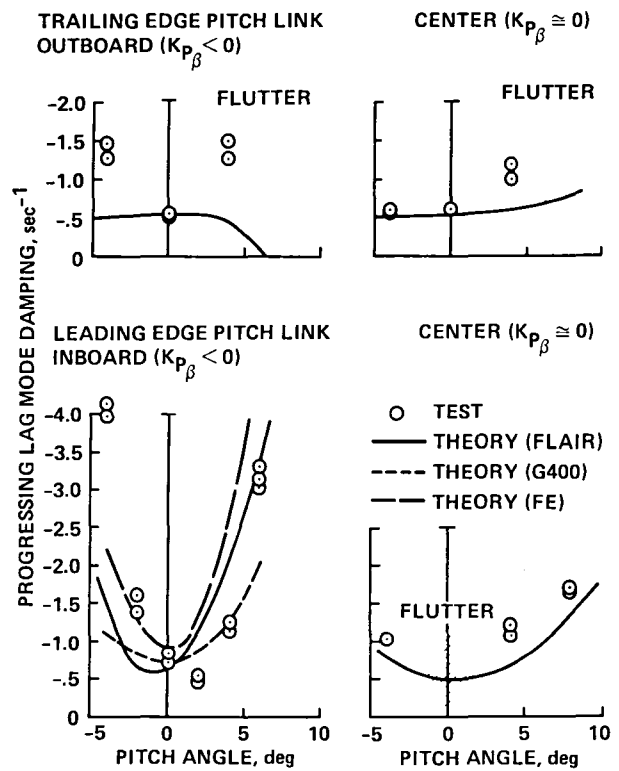


Fig. 43. Bearingless rotor stability (Ref. 42).

SOFT-INPLANE BEARINGLESS ROTOR
HOVER, INBOARD TRAILING-EDGE PITCH LINK

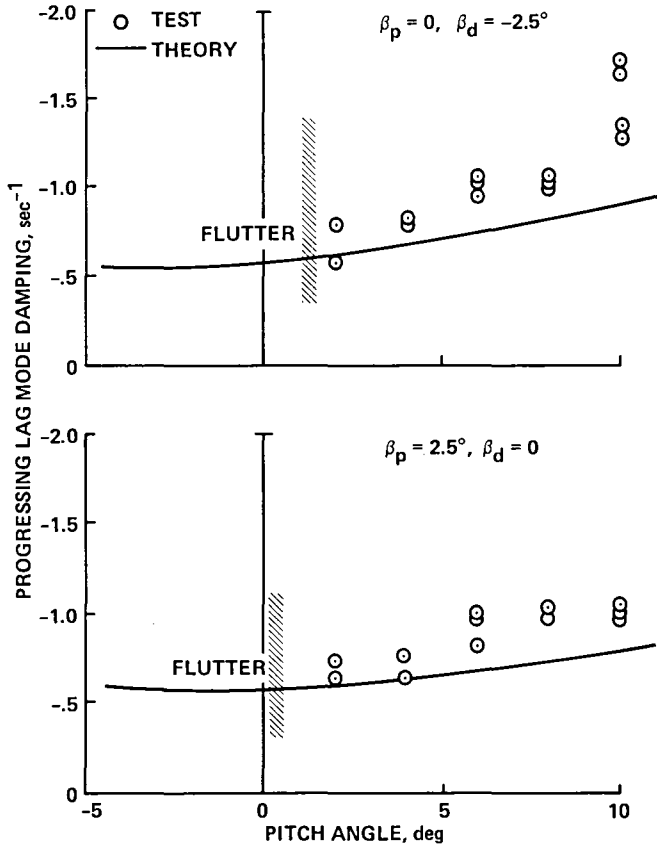


Fig. 44. Bearingless rotor stability (Ref. 42).

BEARINGLESS ROTOR
HOVER THEORY

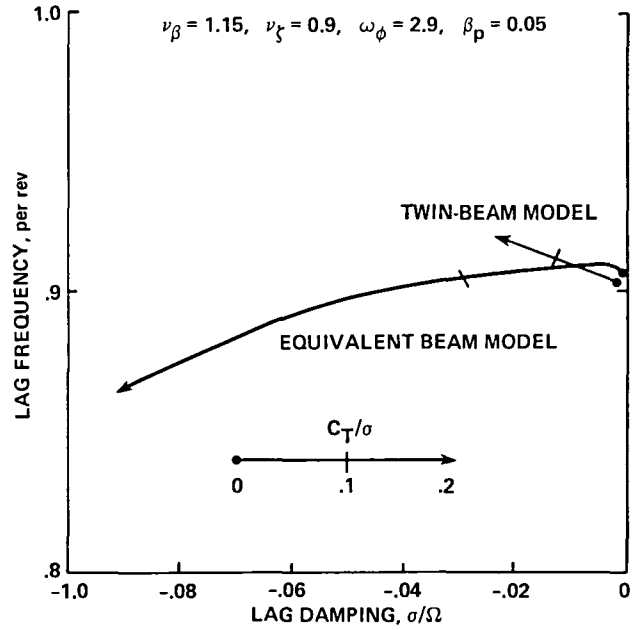


Fig. 45. Calculated bearingless rotor root locus (Ref. 44).

BEARINGLESS ROTOR
HOVER THEORY

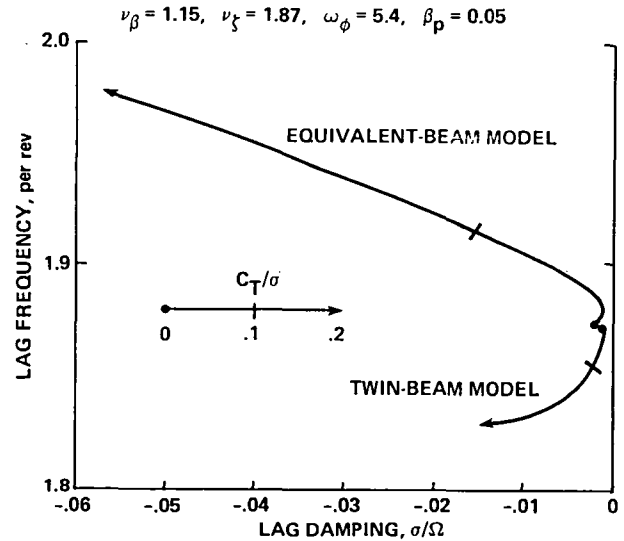


Fig. 46. Calculated bearingless rotor root locus (Ref. 44).

HINGELESS ROTOR
HOVER, SOFT FLAP FLEXURE

PITCH/LAG COUPLING, $K_{P\zeta} = 0$

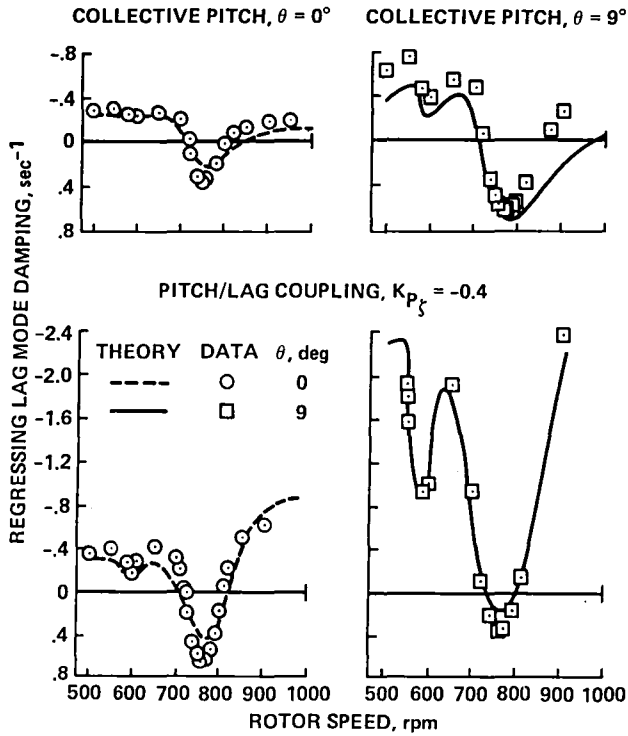


Fig. 47. Hingeless rotor ground resonance stability (Ref. 47).

HINGELESS ROTOR

HOVER, PRECONE = 0, DROOP = 0

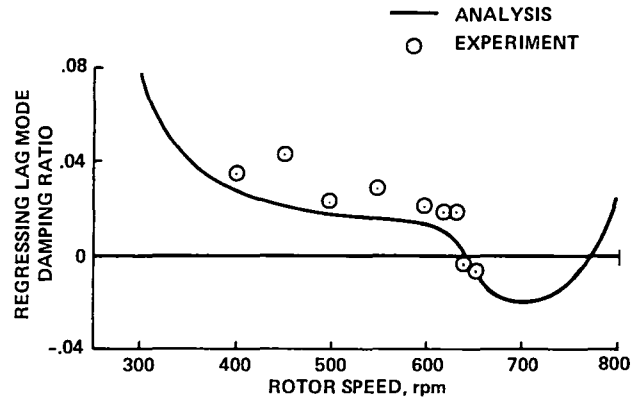


Fig. 48. Hingeless rotor ground resonance stability (Ref. 48).

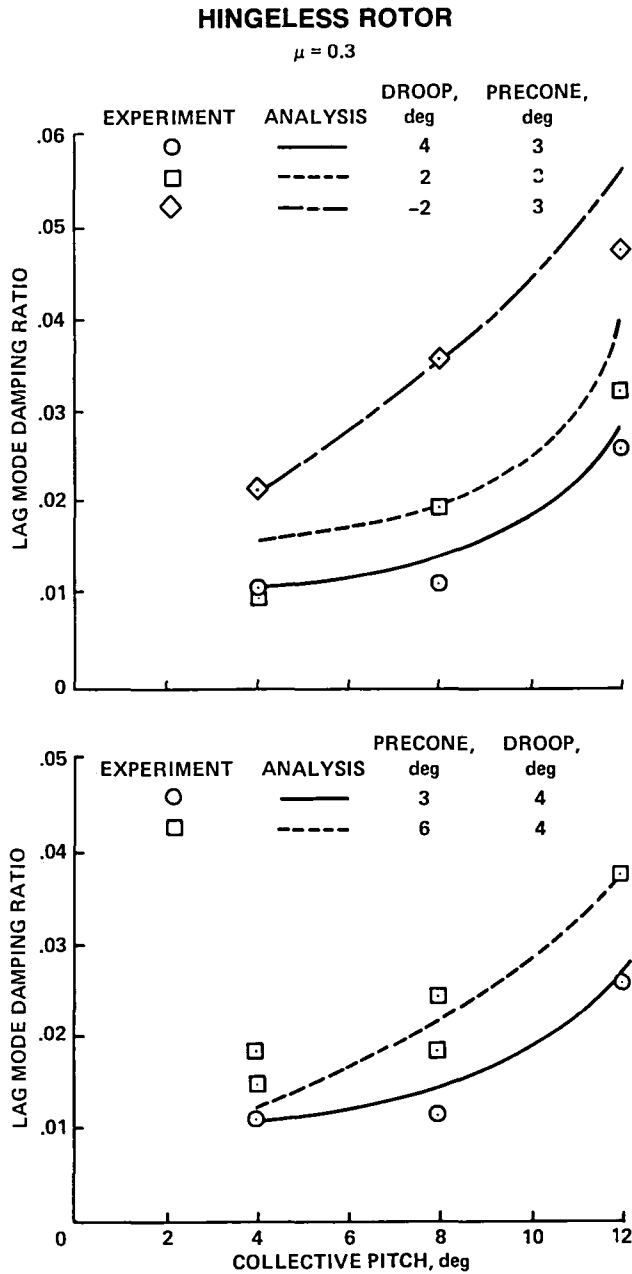


Fig. 49. Hingeless rotor ground resonance stability (Ref. 48).

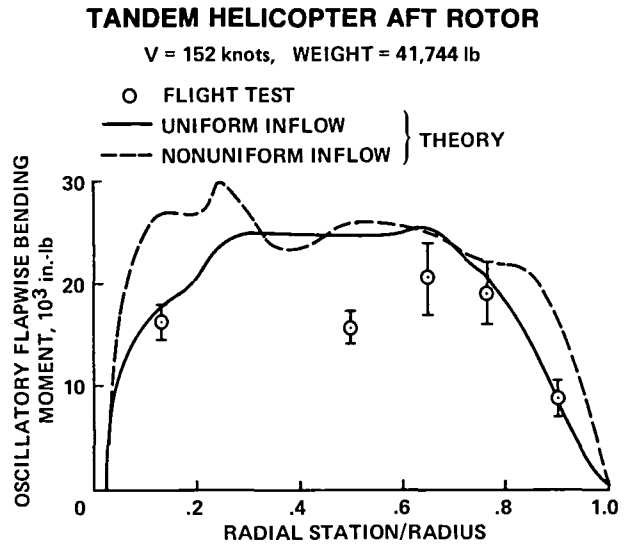


Fig. 50. Articulated rotor blade loads (Ref. 52).

ARTICULATED ROTOR

$C_T/\sigma = 0.076, \mu = 0.36$

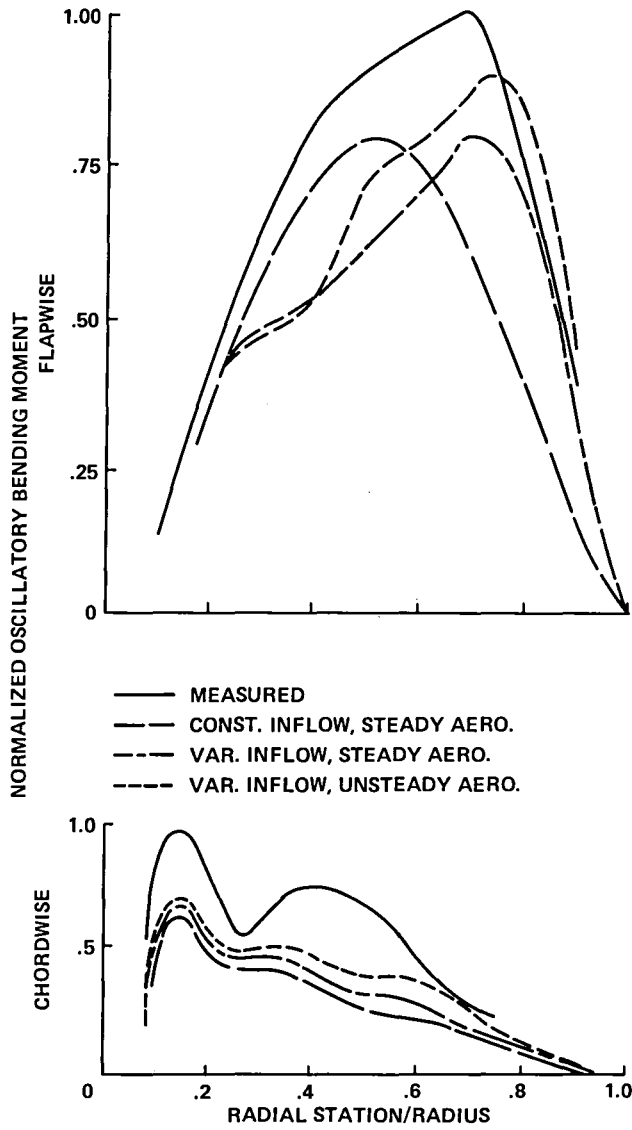


Fig. 51. Articulated rotor blade loads (Ref. 53).

SEMI-RIGID ROTOR

$V = 130$ knots

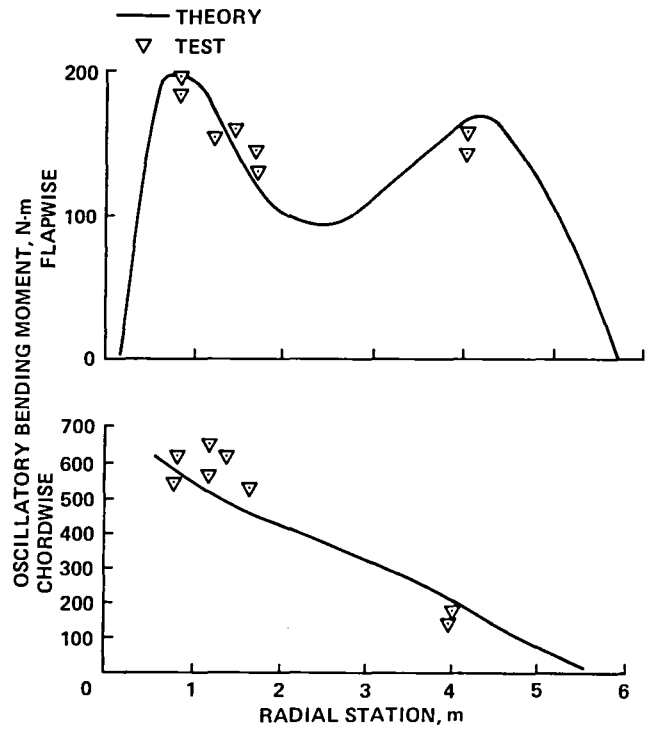


Fig. 52. Semi-rigid rotor blade loads (Ref. 54).

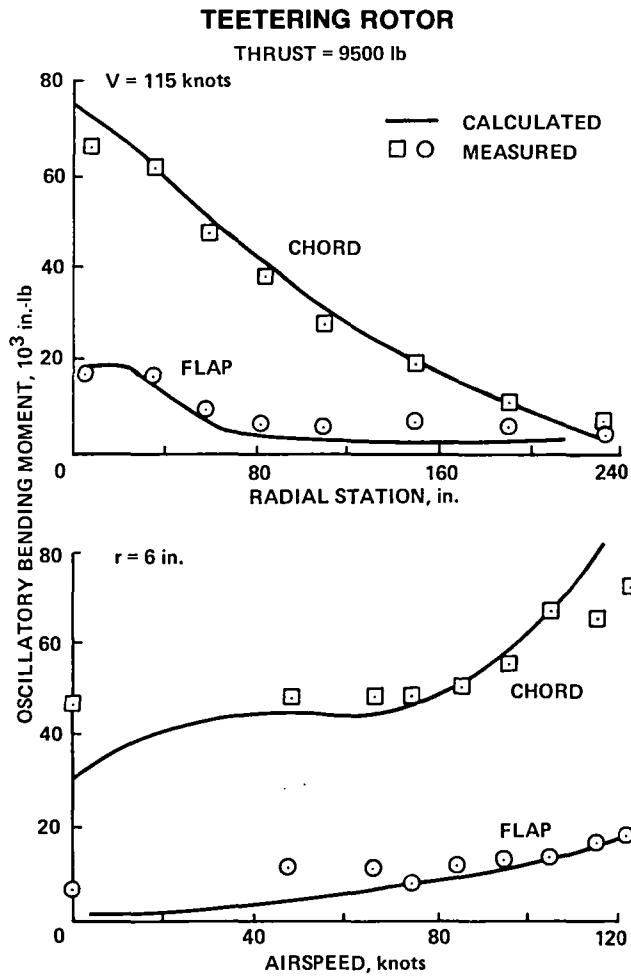


Fig. 53. Teetering rotor blade loads (Ref. 55).

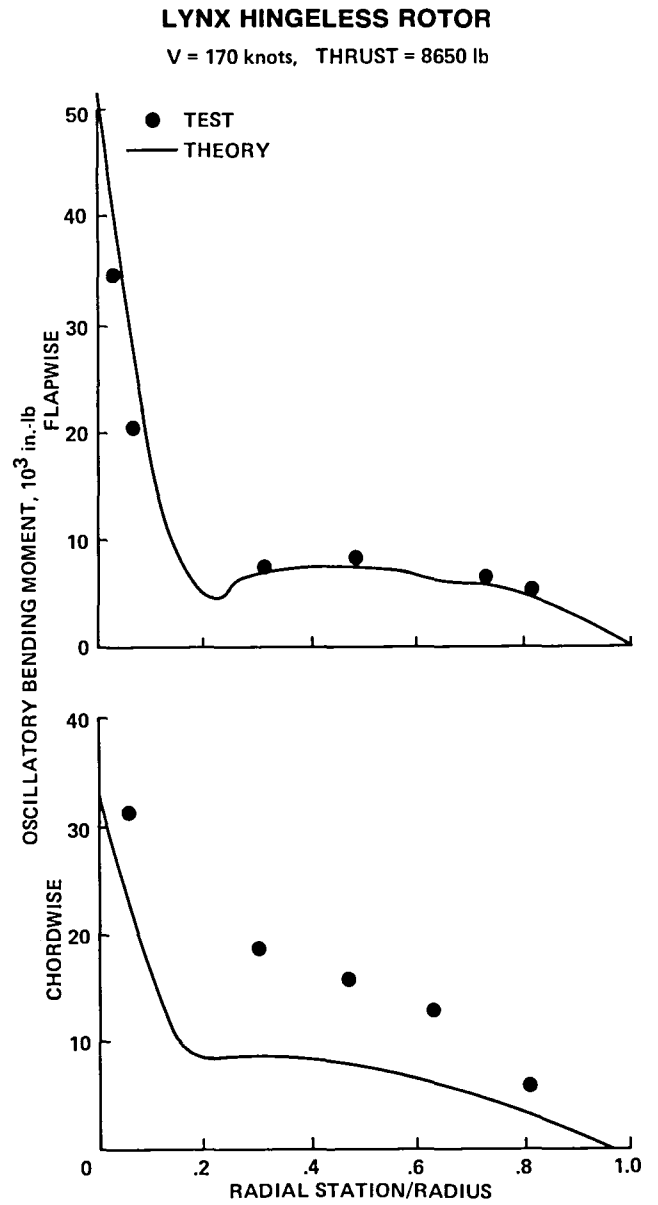


Fig. 54. Hingeless rotor blade loads (Ref. 56).

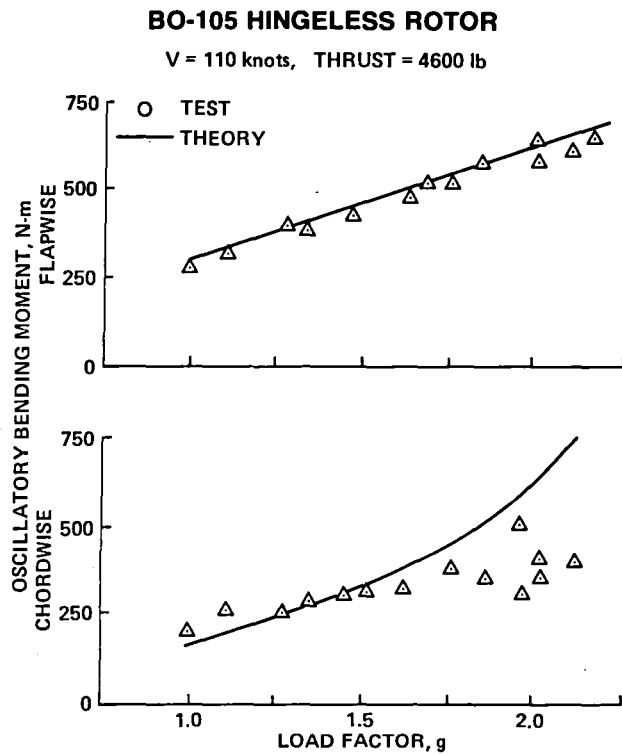


Fig. 55. Hingeless rotor blade loads (Ref. 57).

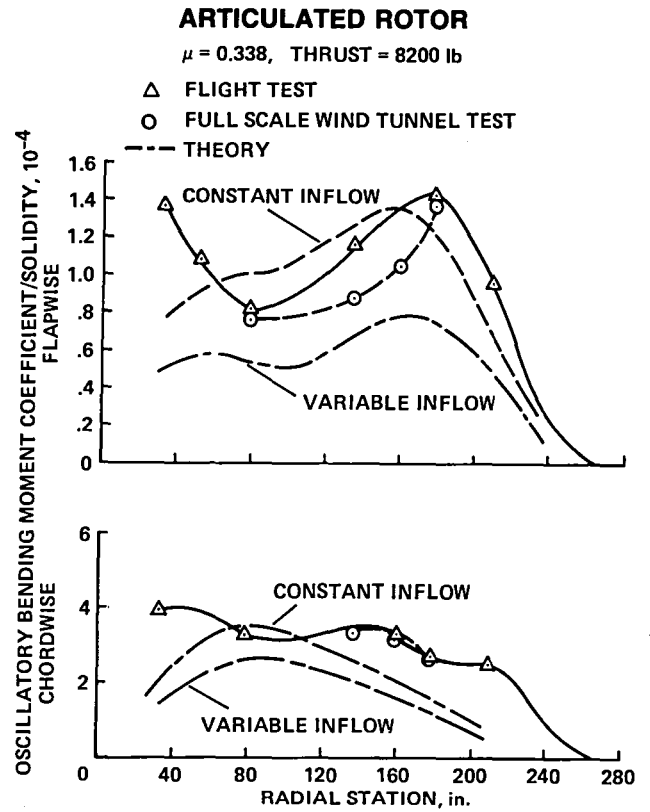


Fig. 56. Articulated rotor blade loads (Ref. 62).

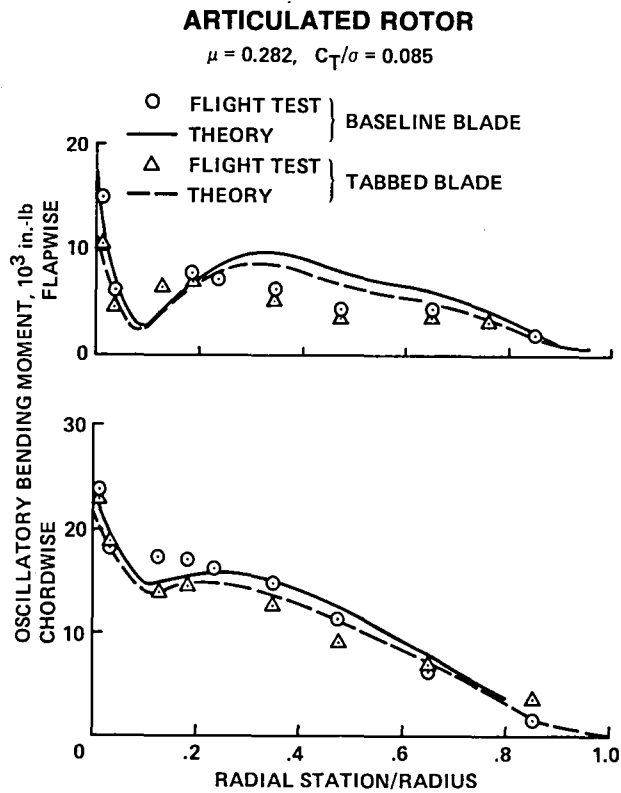


Fig. 57. Articulated rotor blade loads (Ref. 51).

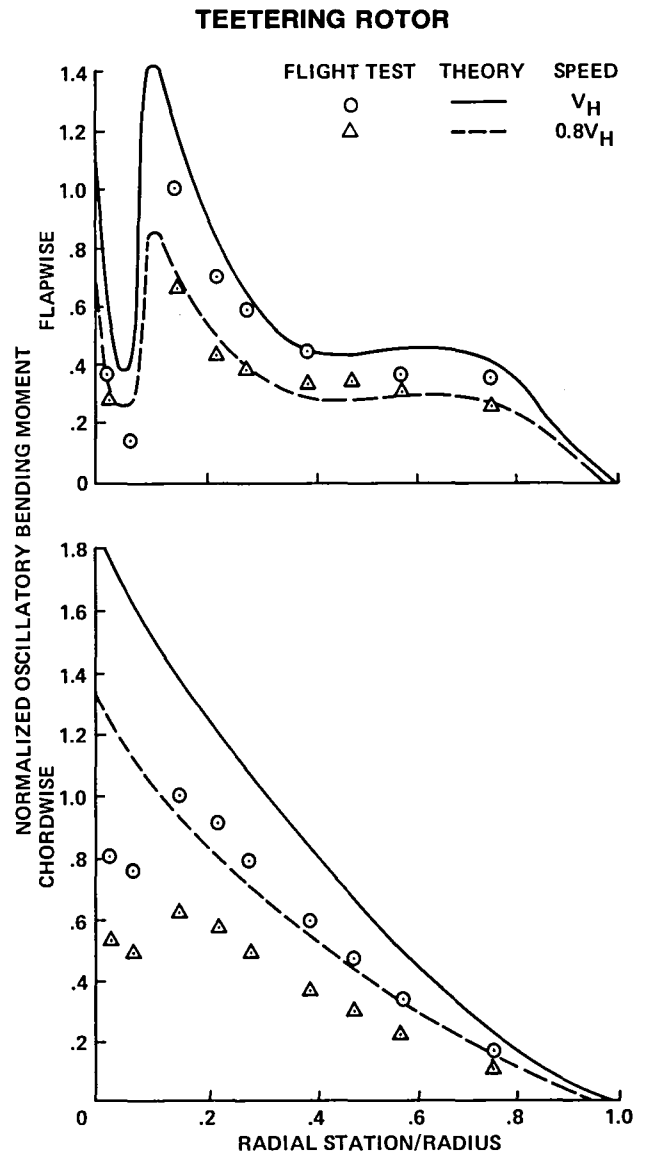


Fig. 58. Teetering rotor blade loads (Ref. 61).

BO-105 HINGELESS ROTOR
 V = 118 knots

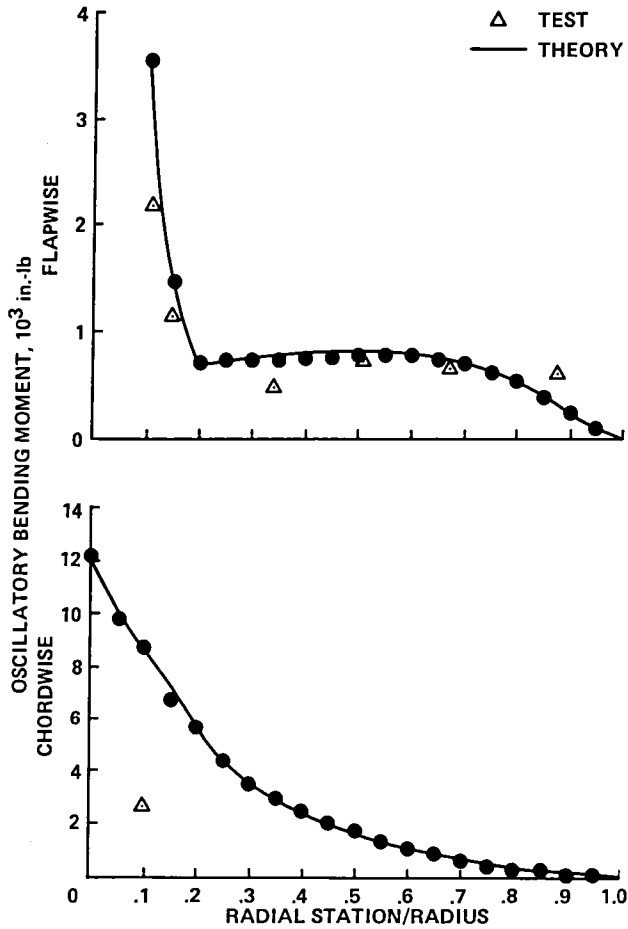


Fig. 59. Hingeless rotor blade loads (Ref. 59).

ARTICULATED ROTOR

$\mu = 0.53, C_T/\sigma = 0.11, r/R = 0.5$

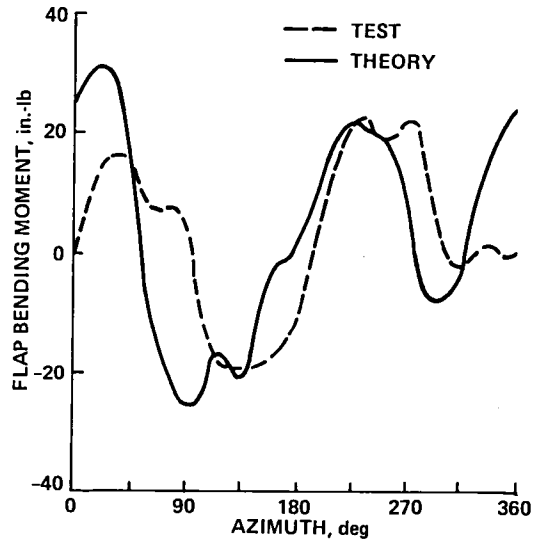


Fig. 60. Articulated rotor blade loads (Ref. 60).

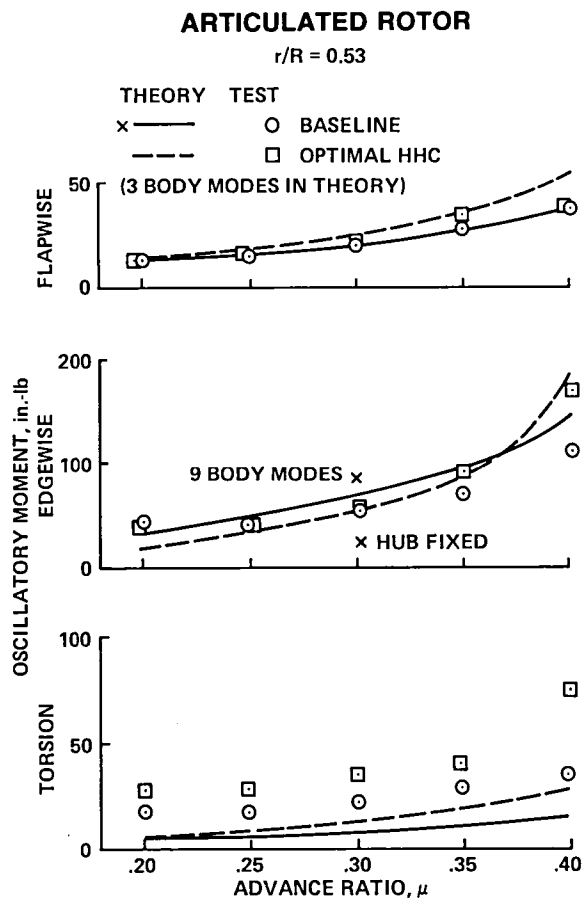


Fig. 61. Articulated rotor blade loads (Ref. 63).

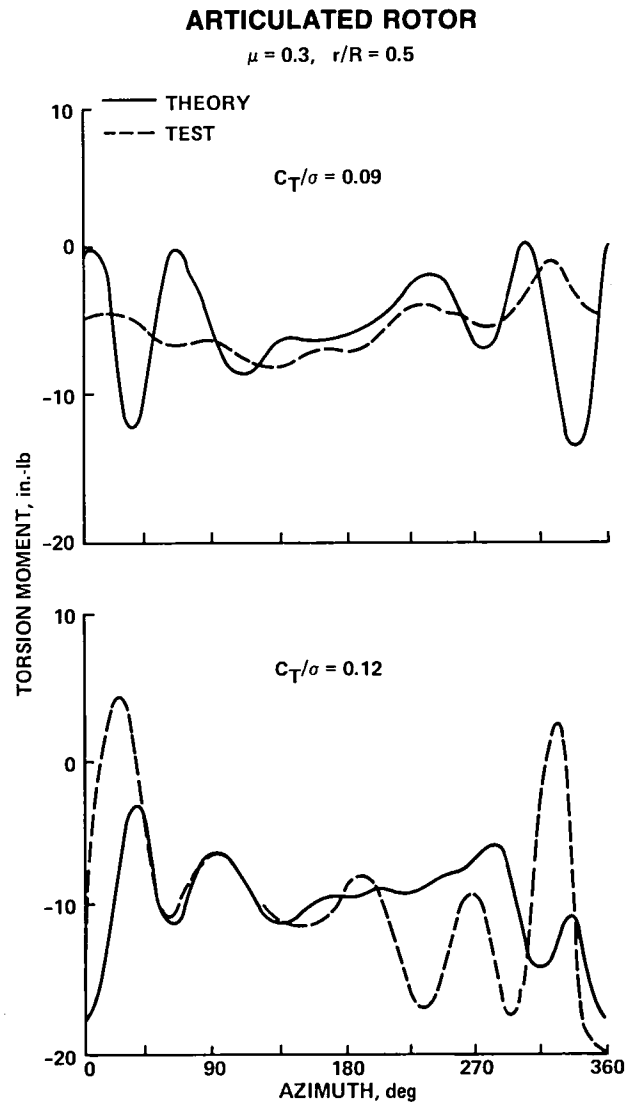


Fig. 62. Articulated rotor blade loads (Ref. 60).

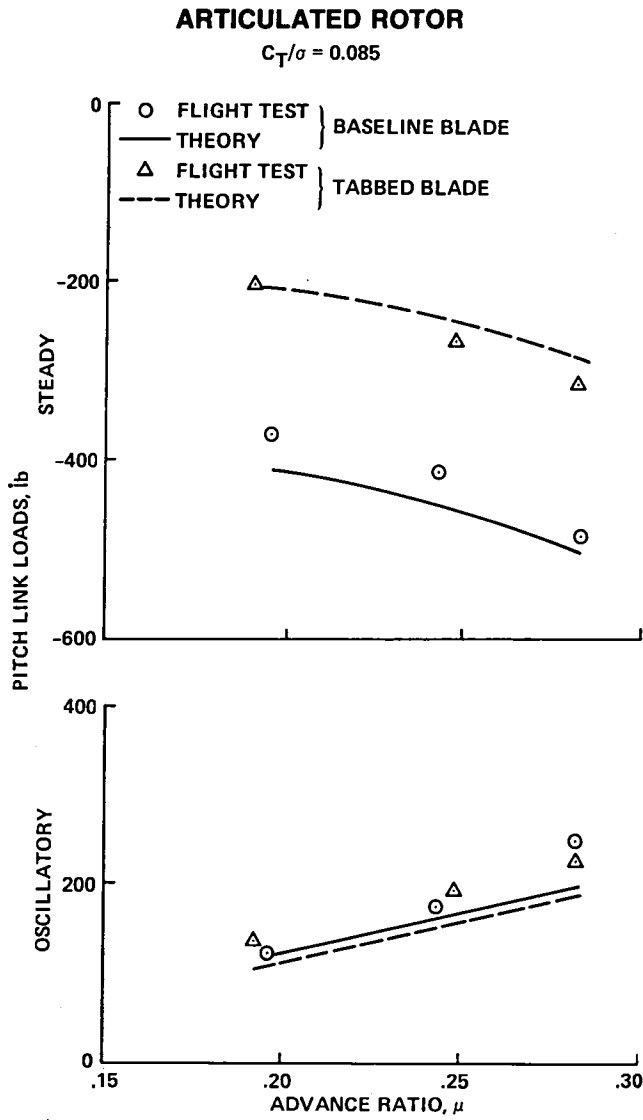


Fig. 63. Articulated rotor blade loads (Ref. 51).

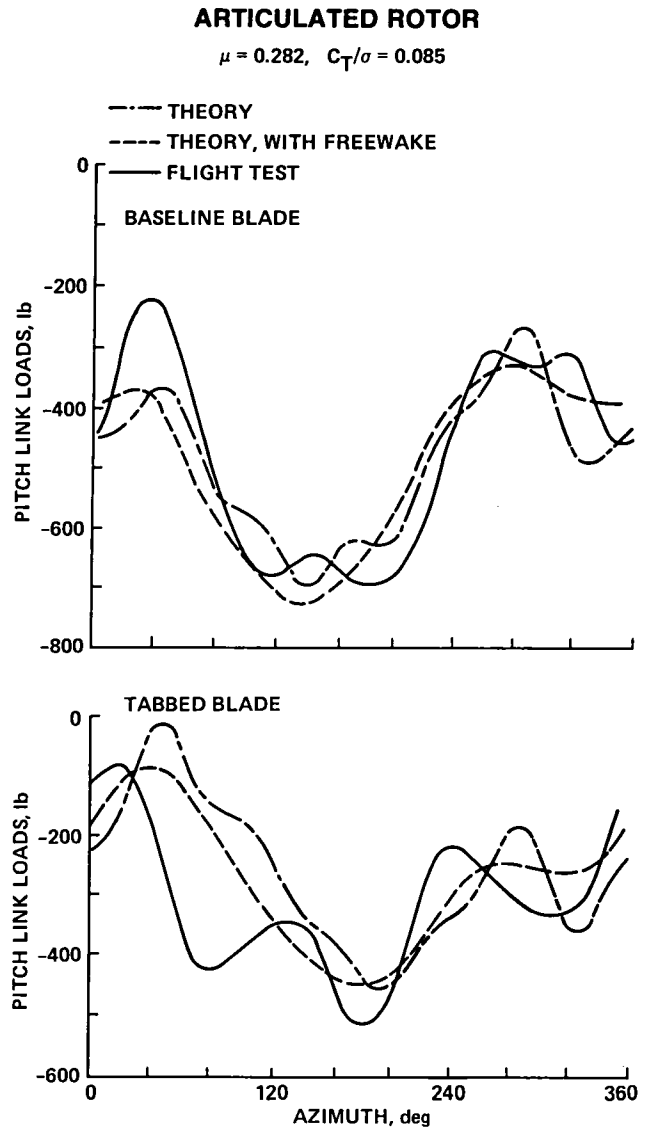


Fig. 64. Articulated rotor blade loads (Ref. 51).

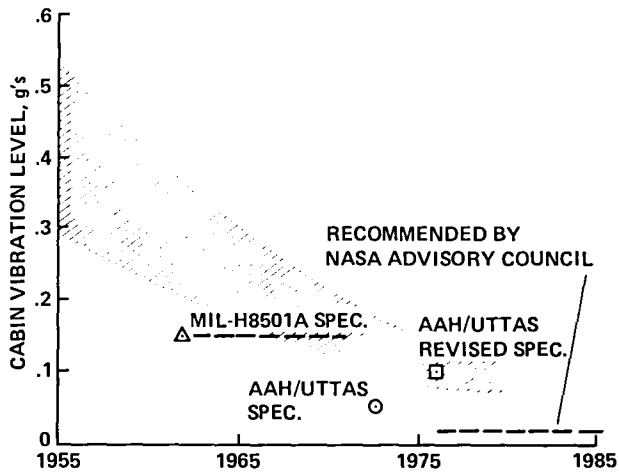


Fig. 65. Trend of helicopter vibration levels (Ref. 64).

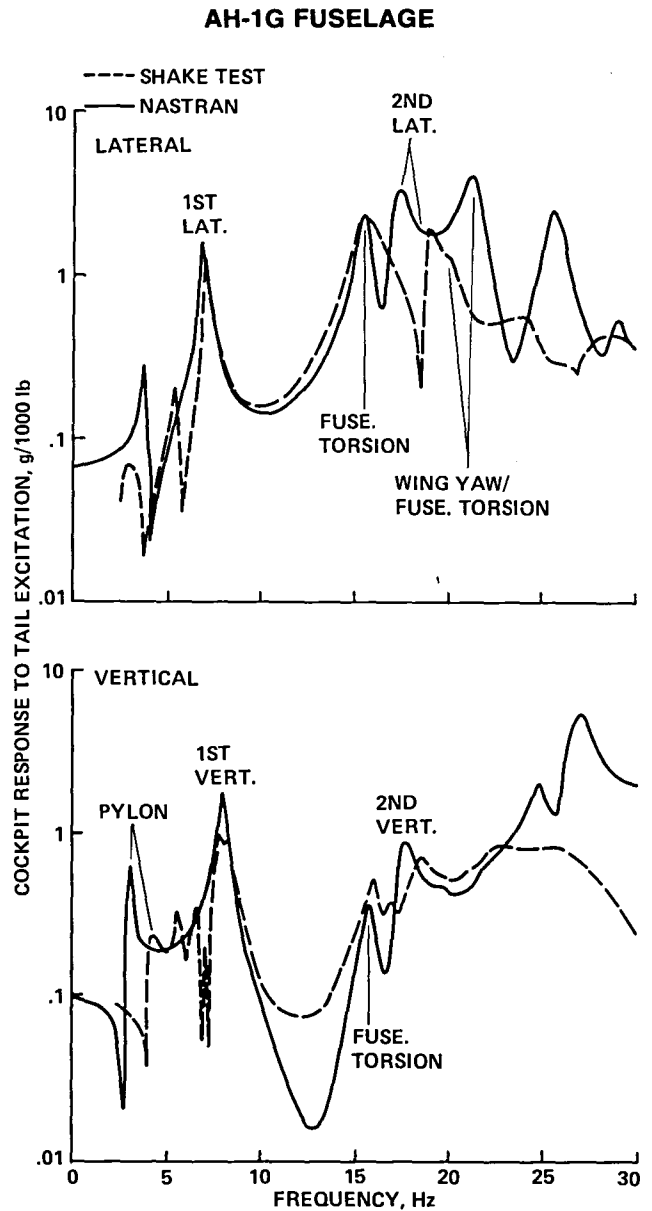


Fig. 66. Airframe structural dynamics (Ref. 65).

AH-1G FUSELAGE

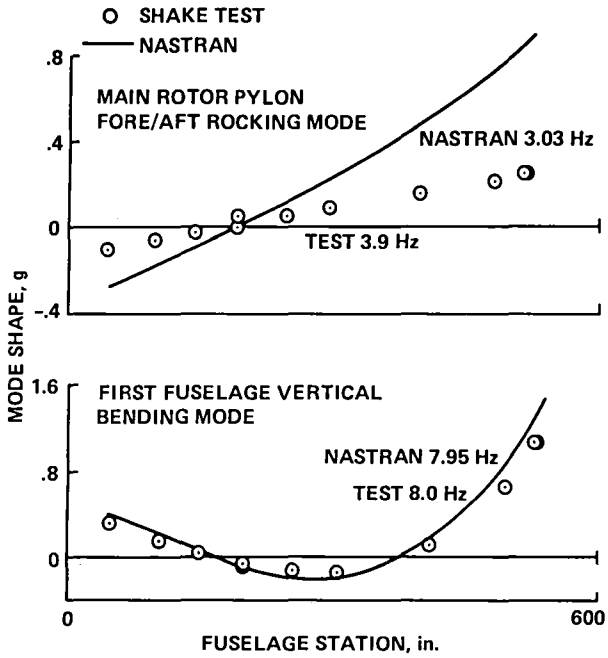


Fig. 67. Airframe structural dynamics (Ref. 65).

BO-105 FUSELAGE

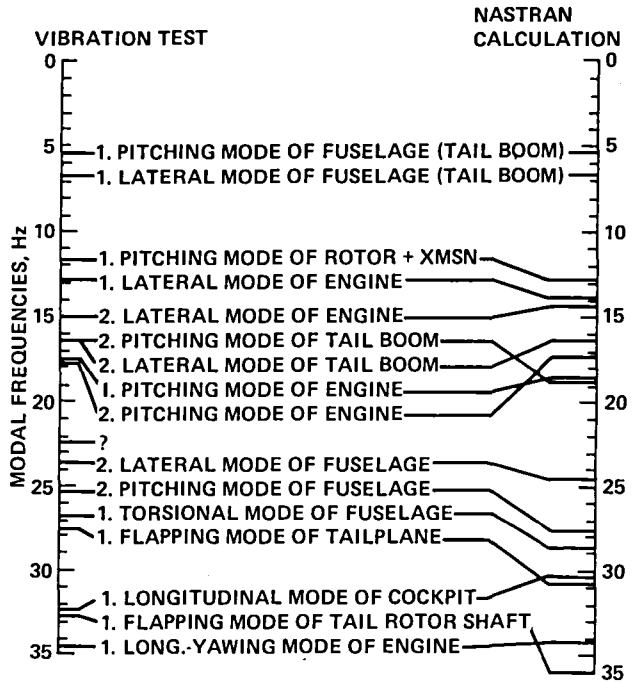


Fig. 68. Airframe structural dynamics (Ref. 66).

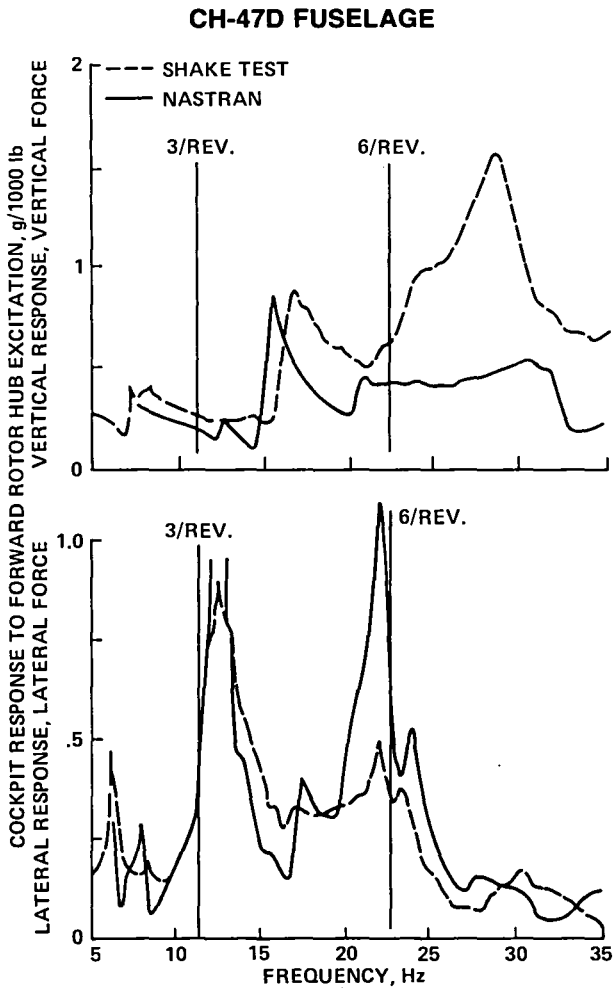


Fig. 69. Airframe structural dynamics (Ref. 67).

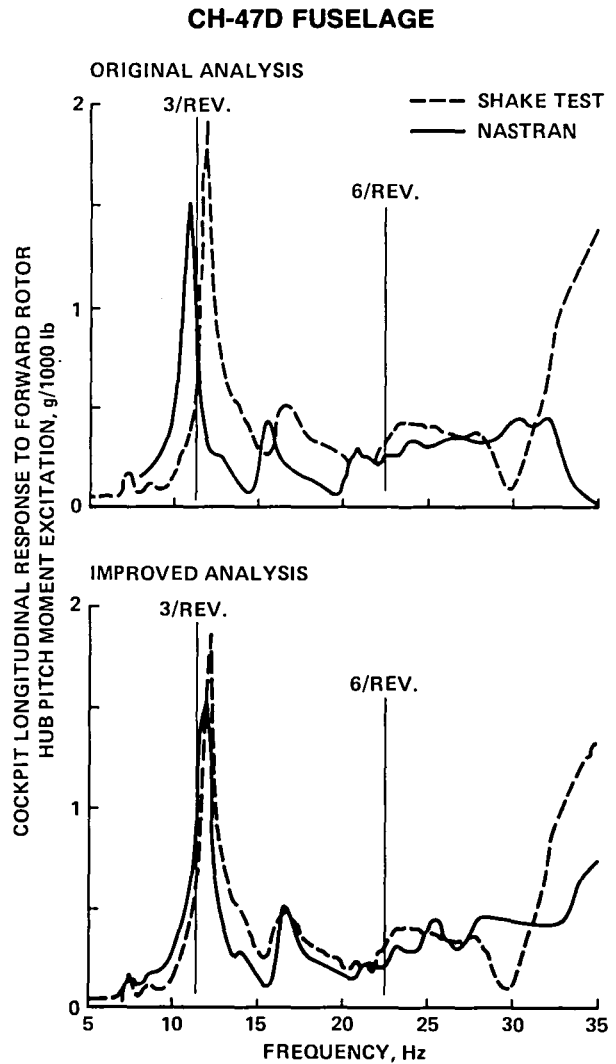


Fig. 70. Airframe structural dynamics (Ref. 67).

ARTICULATED ROTOR

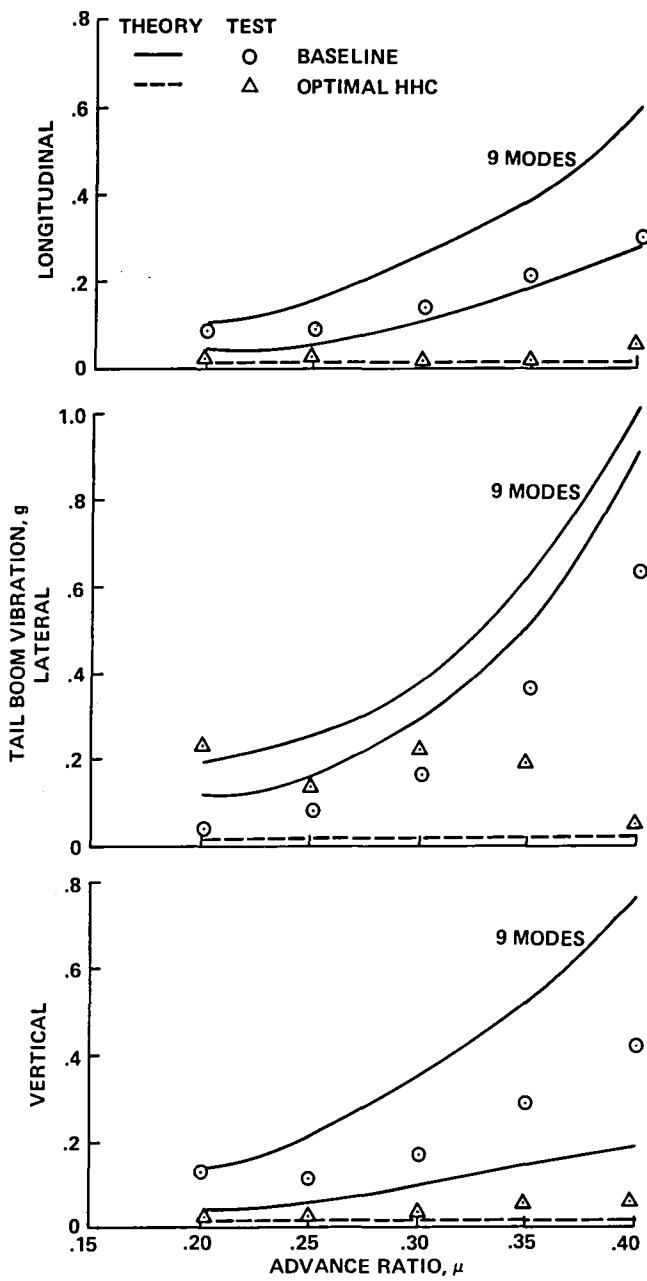


Fig. 71. Articulated rotor vibration (Ref. 63).

ARTICULATED ROTOR

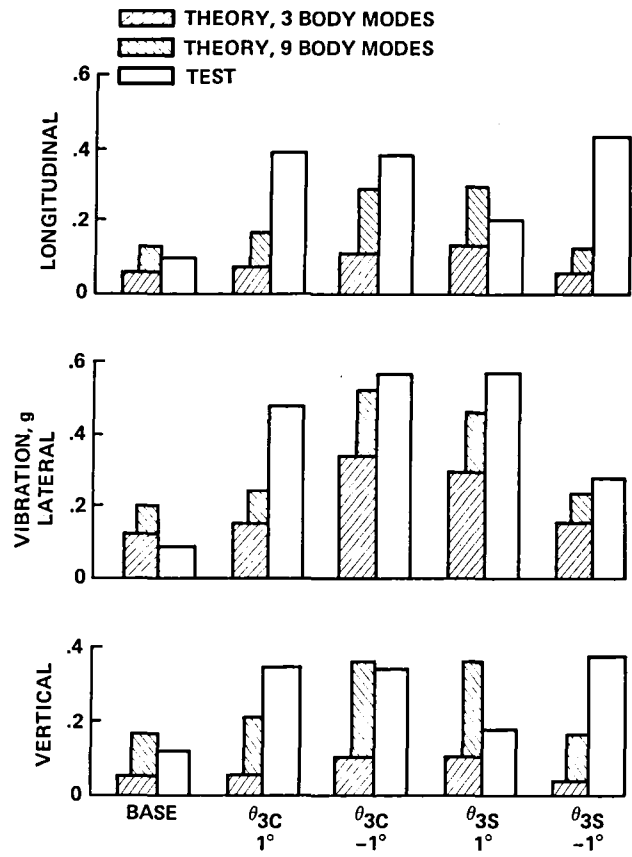


Fig. 72. Articulated rotor vibration (Ref. 63).

BO-105 HINGELESS ROTOR

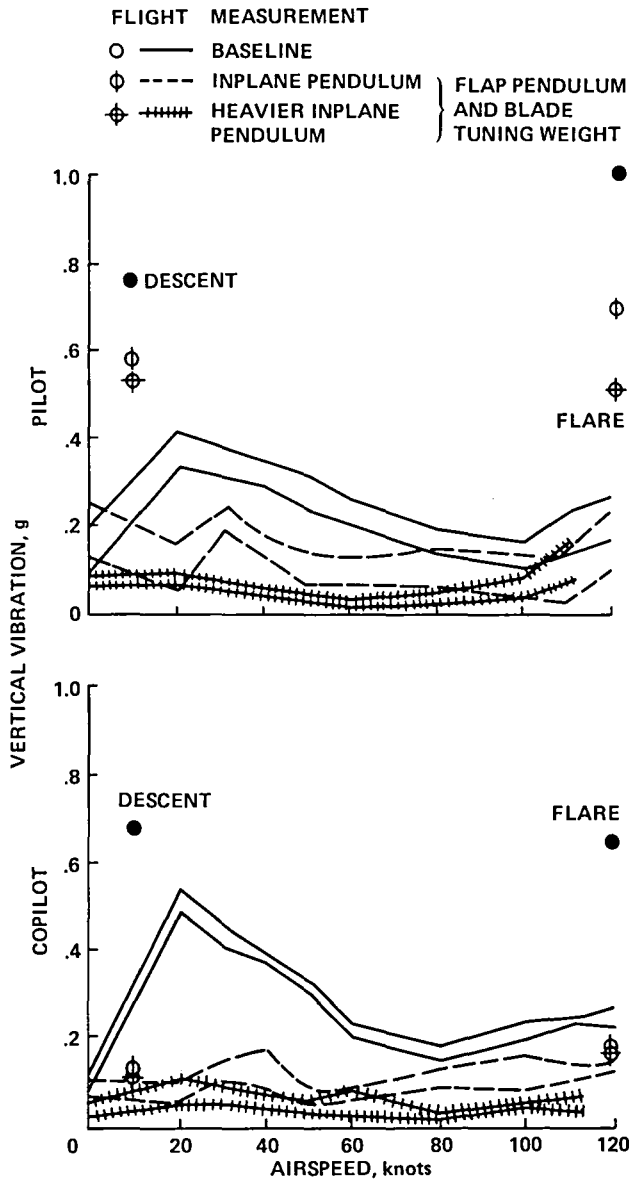


Fig. 73. Measured hingeless rotor vibration reduction (Ref. 68).

BO-105 HINGELESS ROTOR

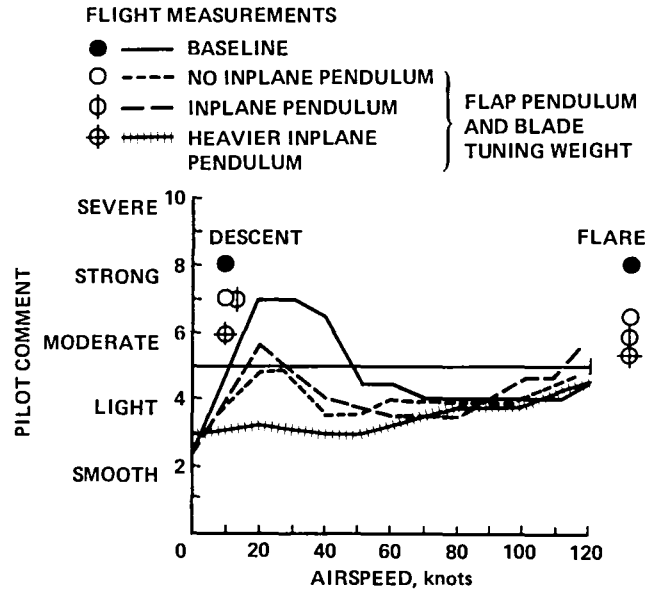


Fig. 74. Measured hingeless rotor vibration reduction (Ref. 68).

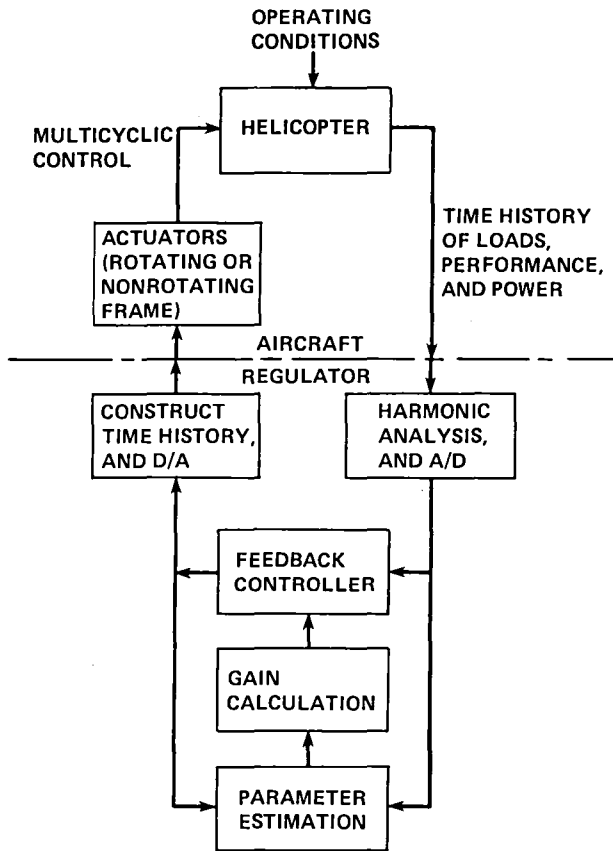


Fig. 75. Schematic of helicopter higher harmonic control system (Ref. 75).

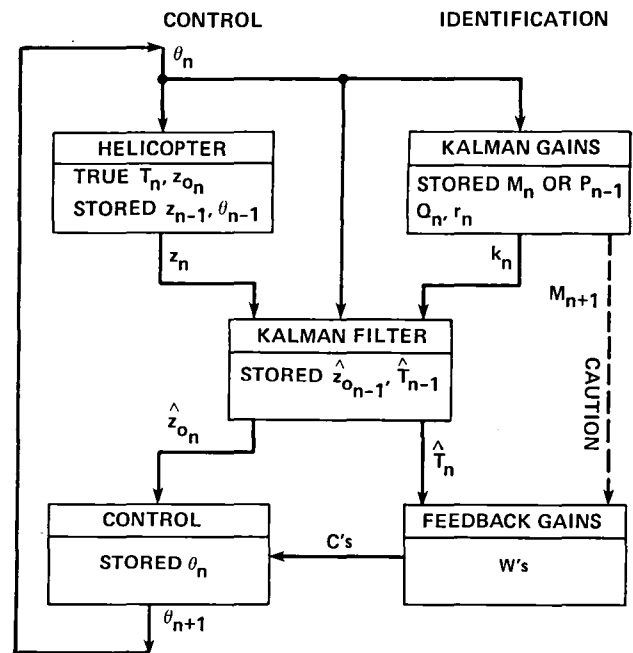


Fig. 76. Self-tuning regulator (adaptive open-loop version) for higher harmonic control of helicopter vibration (Ref. 75).

WIND TUNNEL MEASUREMENTS

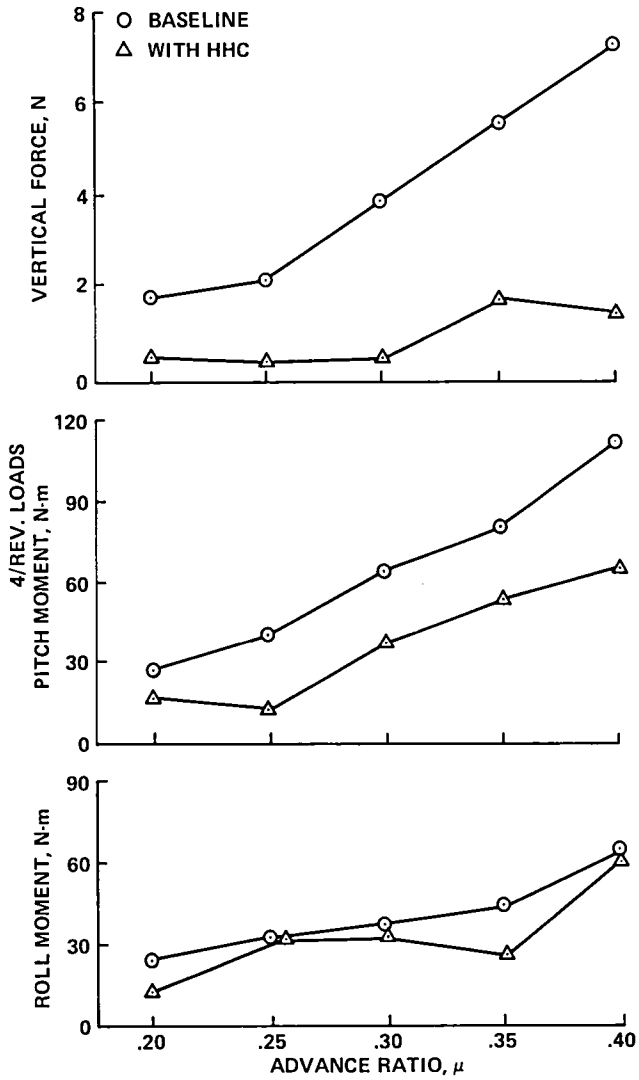


Fig. 77. Measured higher harmonic control of helicopter vibration (Ref. 76).

WIND TUNNEL MEASUREMENTS

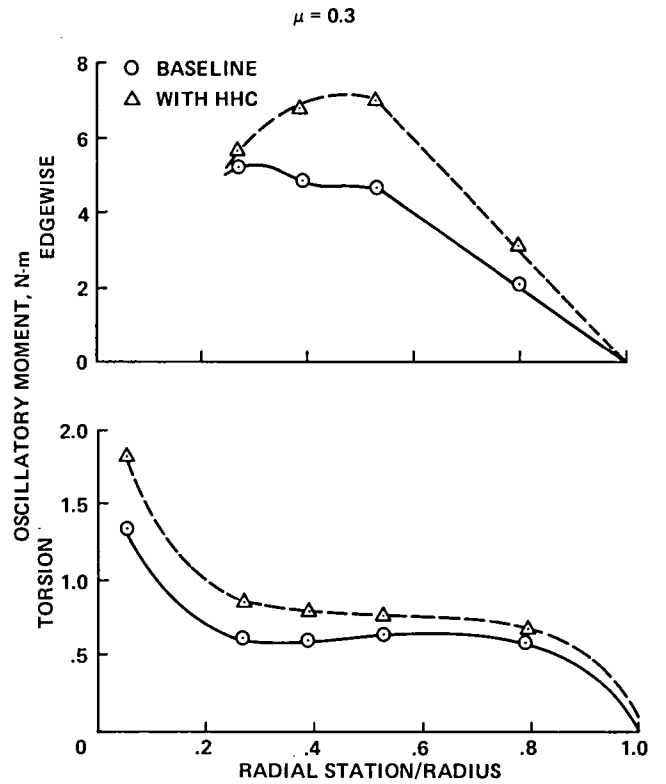


Fig. 78. Measured higher harmonic control of helicopter vibration (Ref. 76).

WIND TUNNEL MEASUREMENT

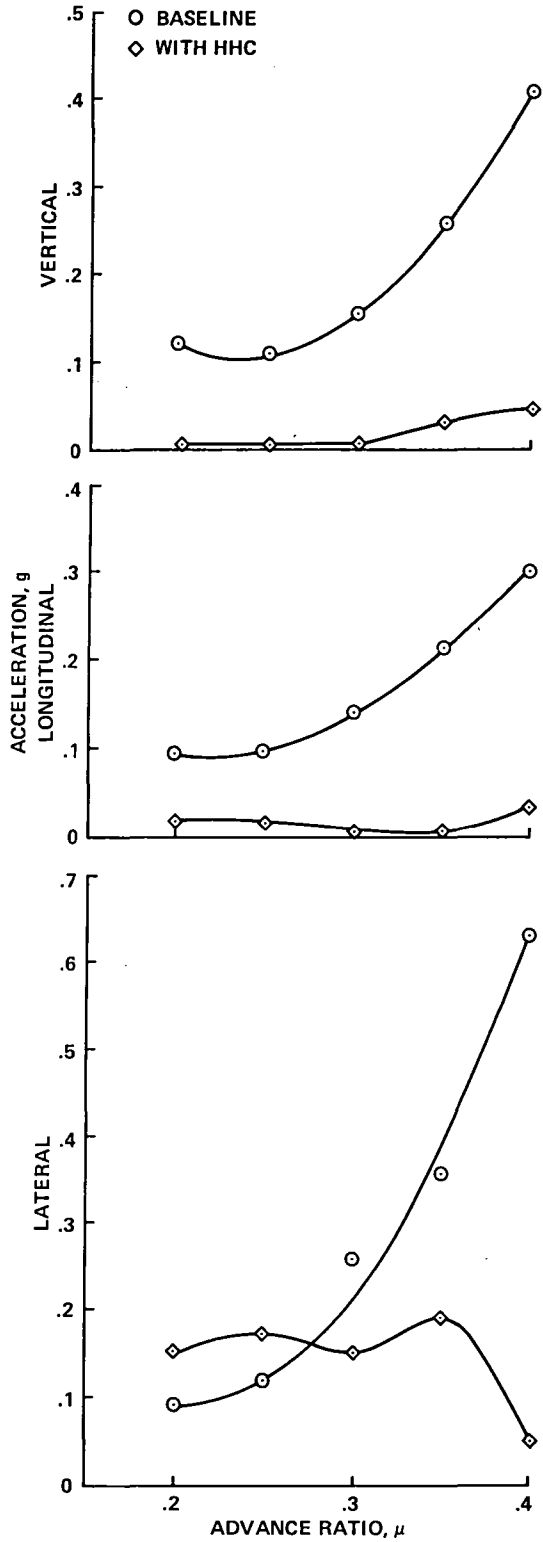


Fig. 79. Measured higher harmonic control of helicopter vibration (Ref. 77).

FLIGHT TEST MEASUREMENTS

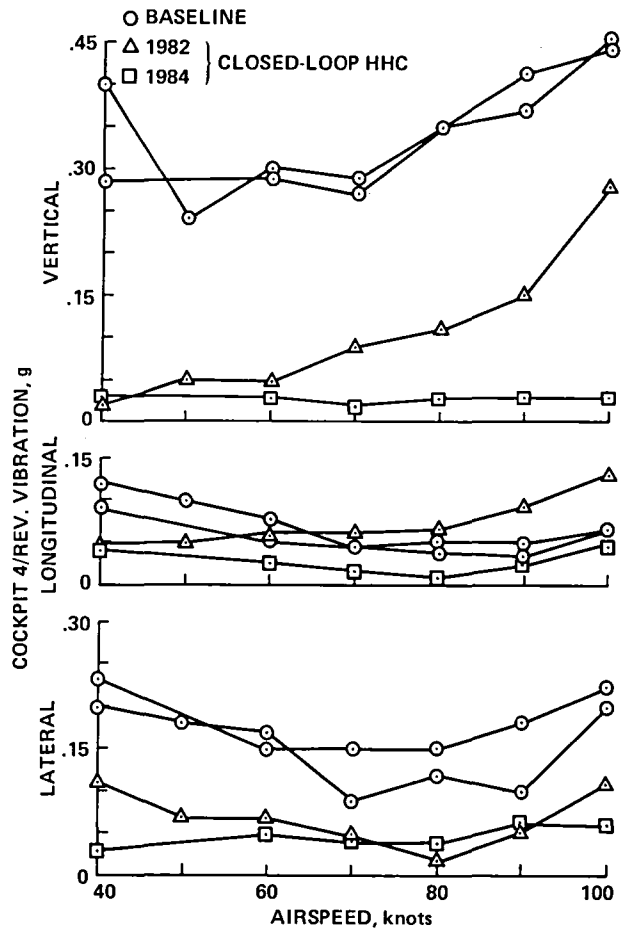


Fig. 80. Measured higher harmonic control of helicopter vibration (Refs. 78 and 79).

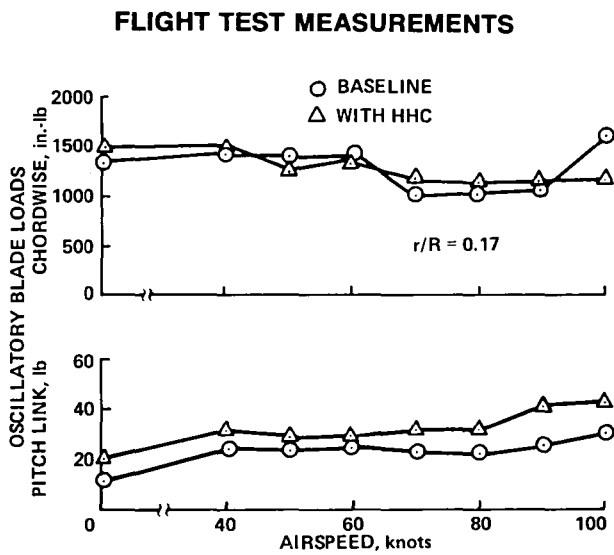


Fig. 81. Measured higher harmonic control of helicopter vibration (Ref. 78).

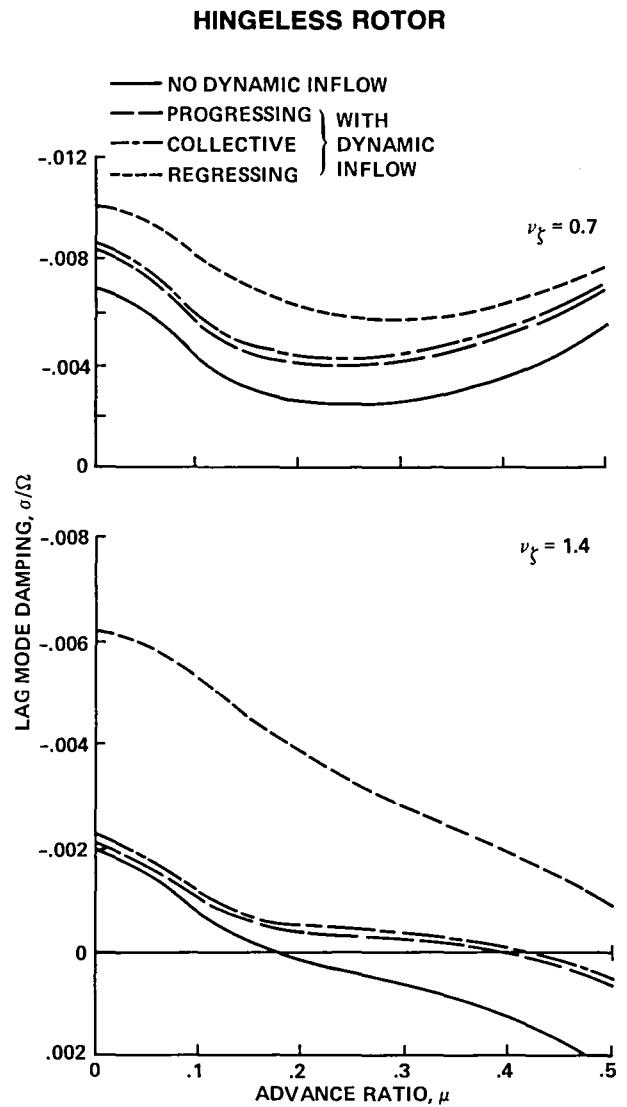


Fig. 82. Calculated flap-lag stability with dynamic inflow (Ref. 86).

HINGELESS ROTOR

HOVER, 650 rpm

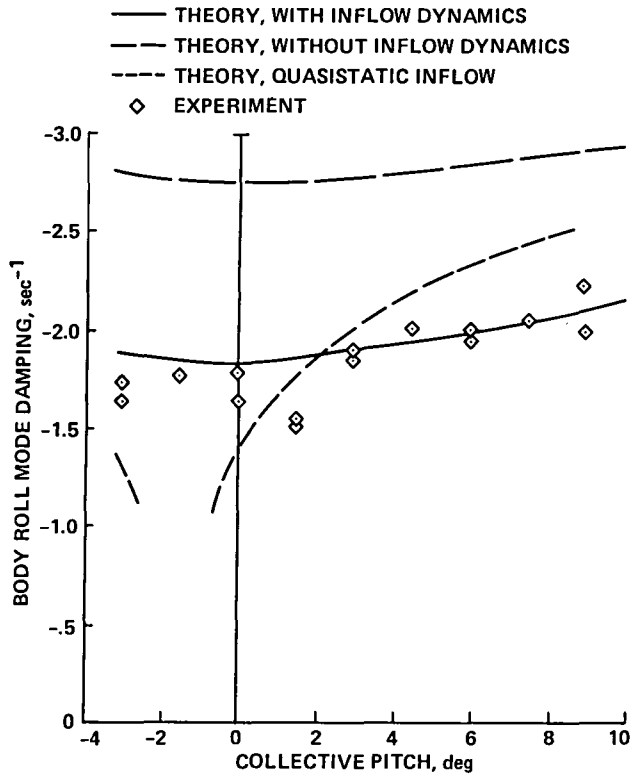


Fig. 83. Ground resonance stability with dynamic inflow (Ref. 80).

MATCHED STIFFNESS HINGELESS ROTOR

HOVER

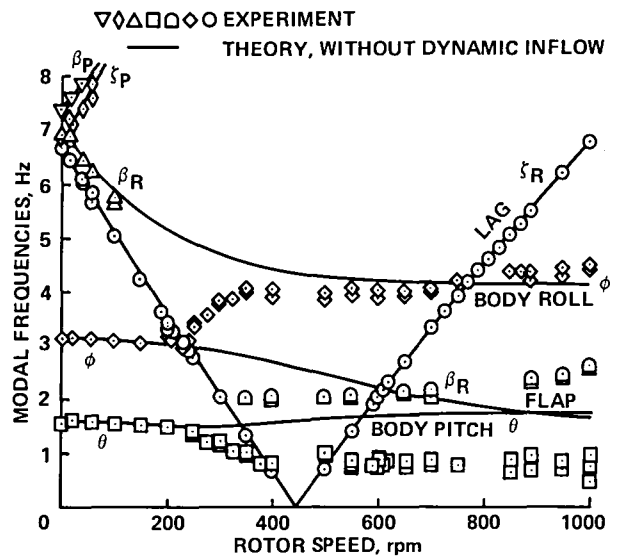


Fig. 84. Ground resonance stability with dynamic inflow (Ref. 80).

MATCHED STIFFNESS HINGELESS ROTOR

HOVER

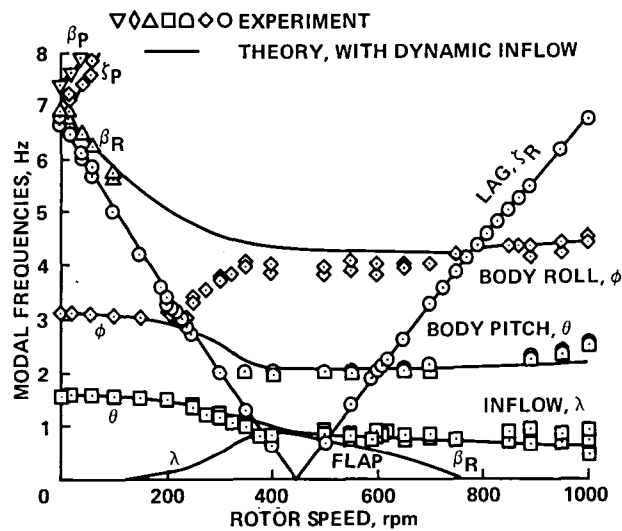


Fig. 85. Ground resonance stability with dynamic inflow (Ref. 80).

BO-105 HINGELESS ROTOR

HOVER, 425 rpm

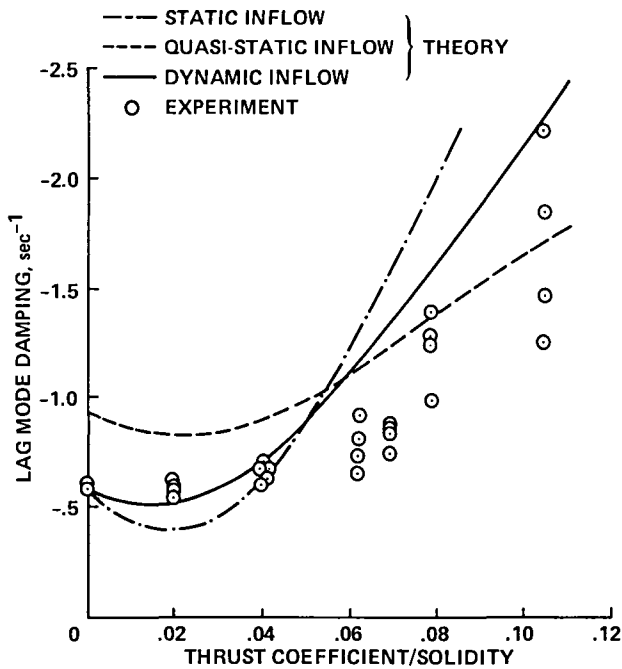


Fig. 86. Soft-inplane hingeless rotor stability with dynamic inflow (Ref. 30).

CENTRIFUGAL FORCE KNOWN

	CENTRIFUGAL FORCE KNOWN				ORDER OF DISPLACEMENT	ORDER OF LOAD
INPLANE	vv'			vv'	3	1
VERTICAL	ww'			ww'	3	1
TORSION	$\hat{\phi}$			$\hat{\phi}$	1	0

CENTRIFUGAL FORCE UNKNOWN

	CENTRIFUGAL FORCE UNKNOWN				ORDER OF DISPLACEMENT	ORDER OF LOAD
AXIAL	u	u		u	3	2
INPLANE	vv'			vv'	3	1
VERTICAL	ww'			ww'	3	1
TORSION	$\hat{\phi}$	$\hat{\phi}$		$\hat{\phi}$	2	1

Fig. 87. Finite element beam degrees of freedom.

HINGELESS COMPOSITE ROTOR

HOVER, $C_T/\sigma = 0.1$

SYMMETRIC LAMINATES ON SPAR SIDES

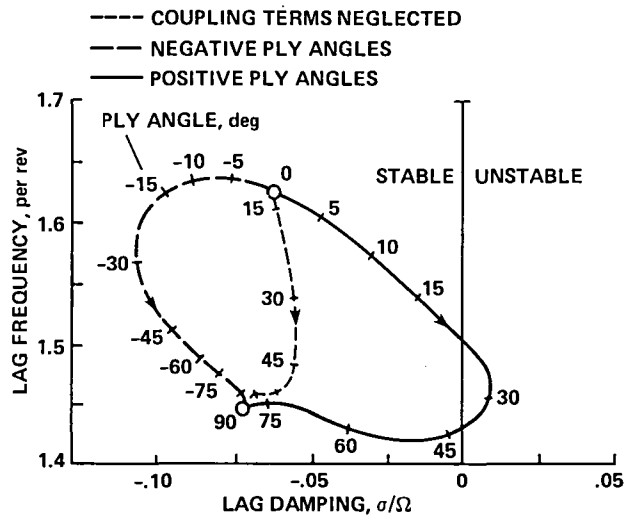


Fig. 88. Calculated hingeless rotor root locus with composite materials (Ref. 97).

HINGELESS COMPOSITE ROTOR

HOVER, $C_T/\sigma = 0.1$

ANTISYMMETRIC LAMINATES ON SPAR SIDES

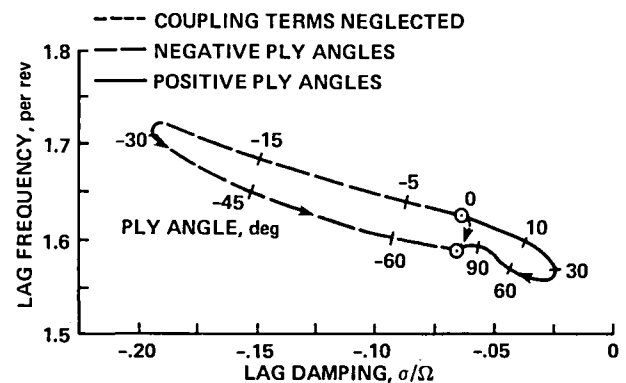


Fig. 89. Calculated hingeless rotor root locus with composite materials (Ref. 97).

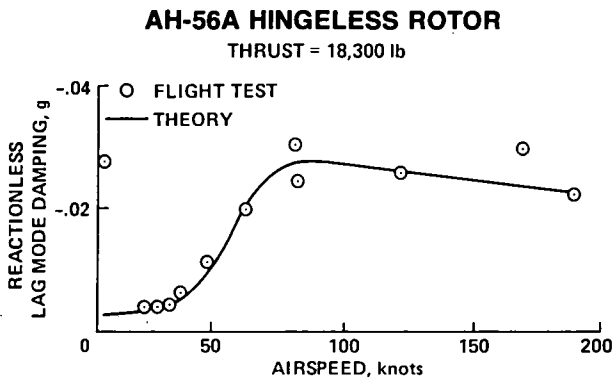


Fig. 90. AH-56A helicopter stability (Ref. 58).

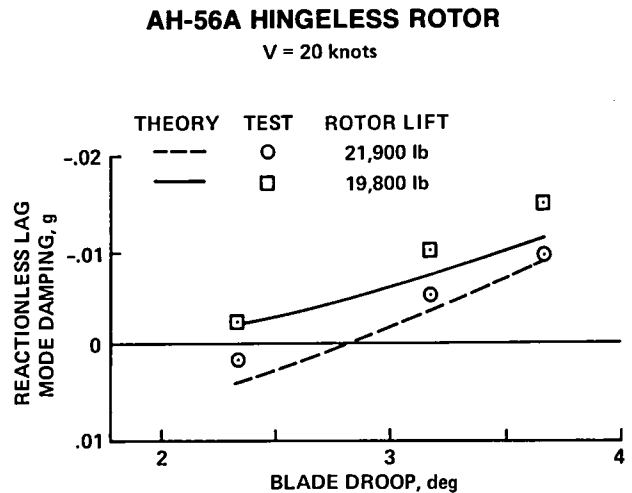


Fig. 91. AH-56A helicopter stability (Ref. 99).

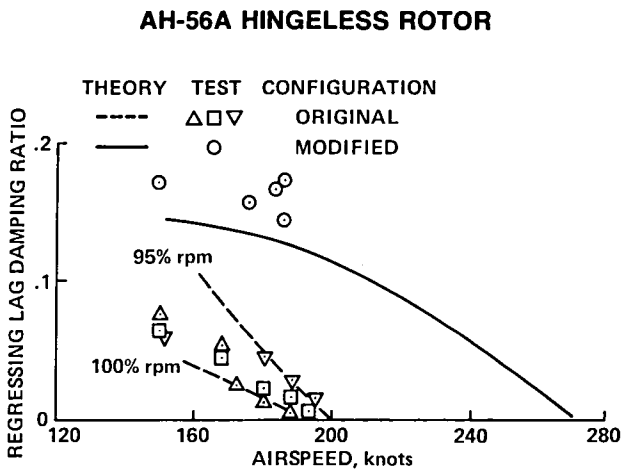


Fig. 92. AH-56A helicopter stability (Ref. 100).

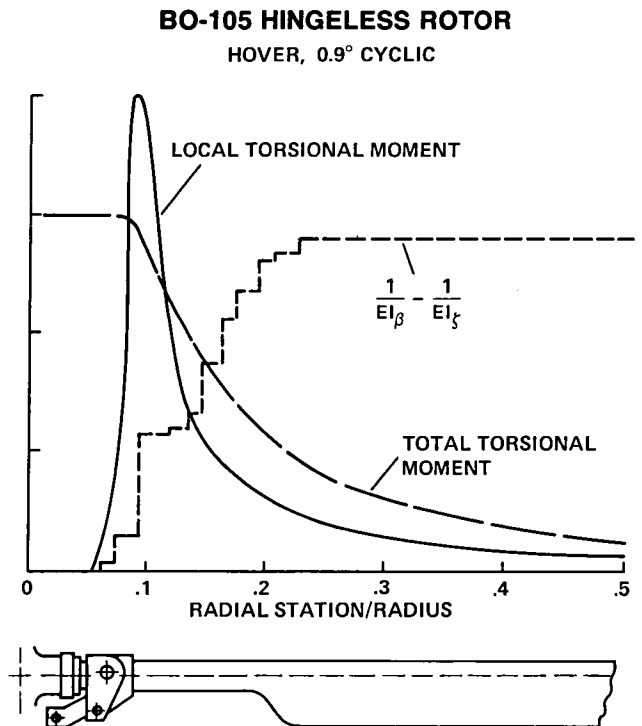


Fig. 93. Calculated BO-105 helicopter torsional moments produced by bending (Ref. 12).

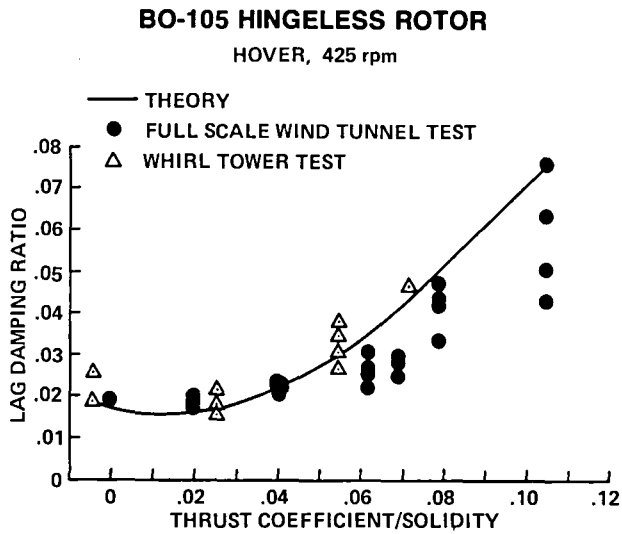


Fig. 94. BO-105 helicopter stability (Ref. 30).

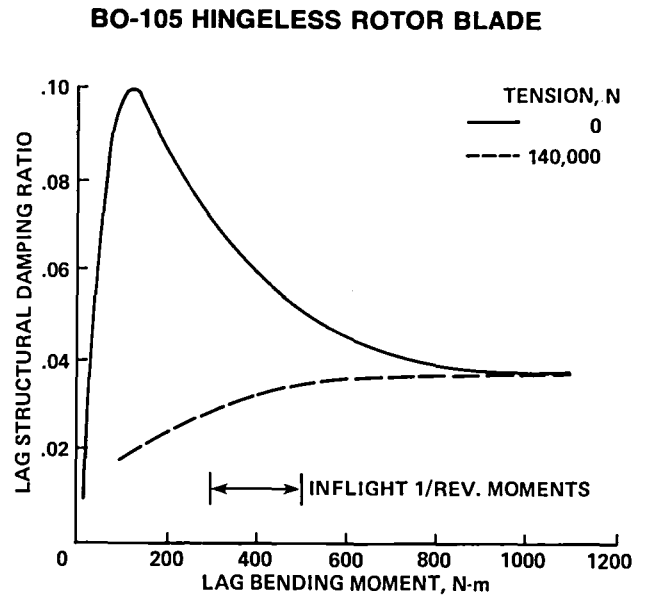


Fig. 95. Measured BO-105 blade structural lag damping (Ref. 98).

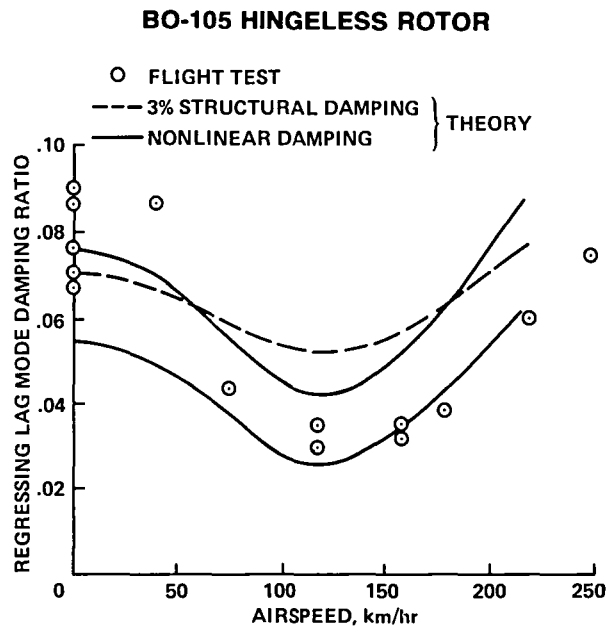


Fig. 96. BO-105 helicopter stability (Ref. 102).

LYNX HINGELESS ROTOR

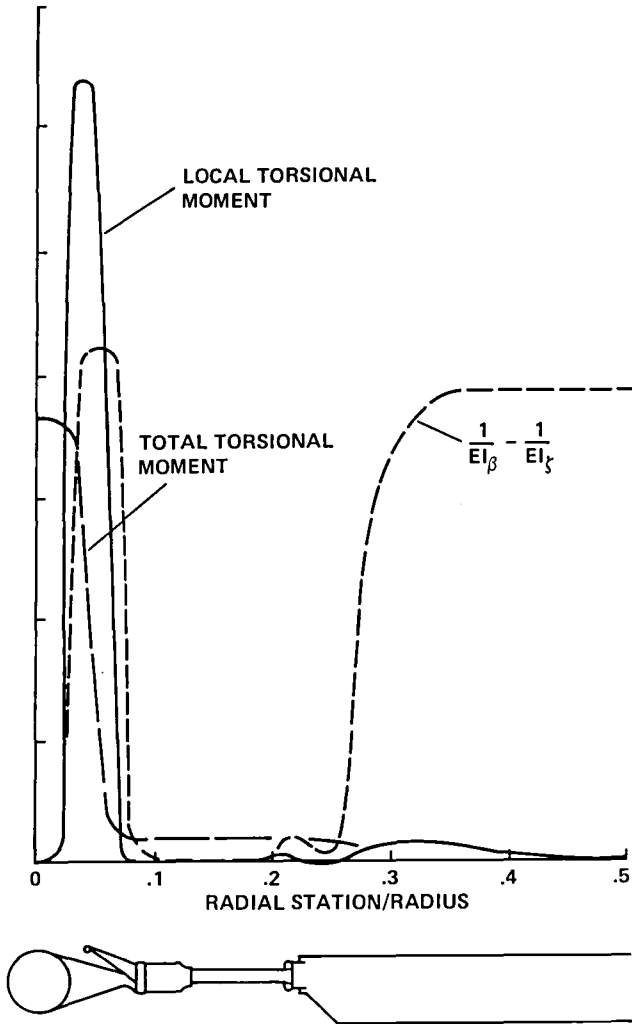


Fig. 97. Calculated Lynx helicopter torsional moments produced by bending (Ref. 14).

ABC HINGELESS ROTOR HELICOPTER

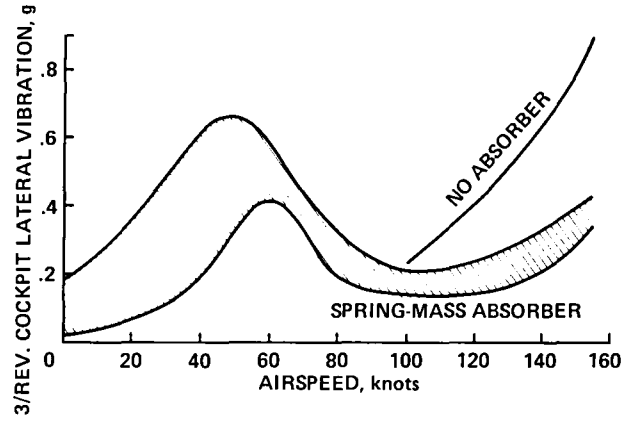


Fig. 98. Measured ABC helicopter vibration (Ref. 106).

ABC HINGELESS ROTOR HELICOPTER

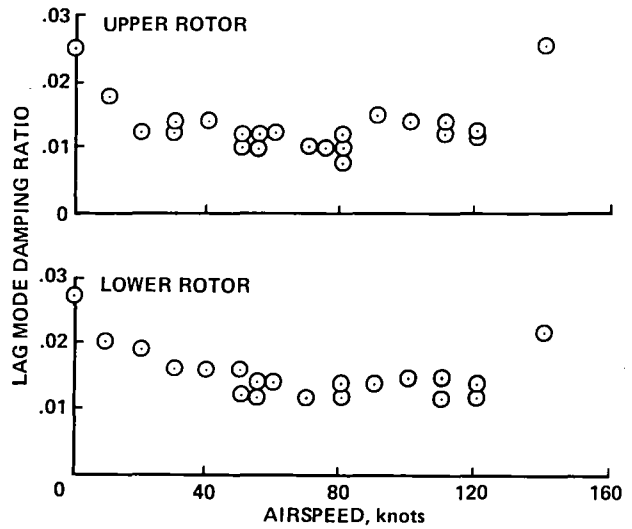


Fig. 99. Measured ABC helicopter stability (Ref. 107).

ABC HINGELESS ROTORCRAFT

NO VIBRATION TREATMENT

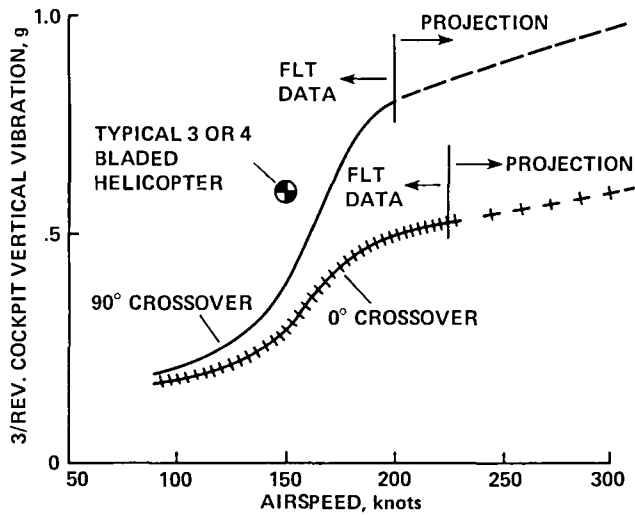


Fig. 100. Measured ABC rotorcraft vibration (Ref. 109).

BK-117 HINGELESS ROTOR

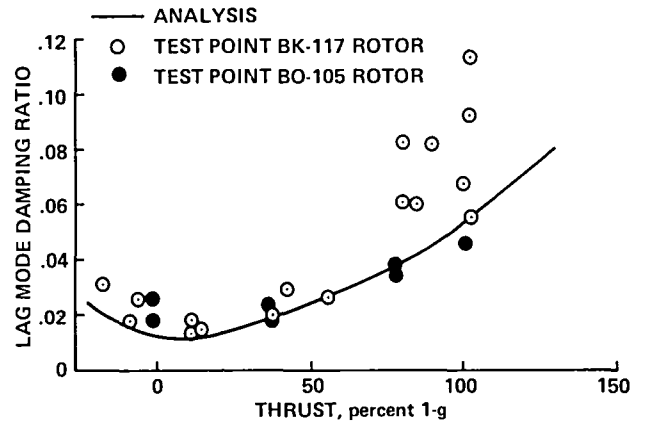


Fig. 101. BK-117 helicopter stability (Ref. 110).

BK-117 HINGELESS ROTOR

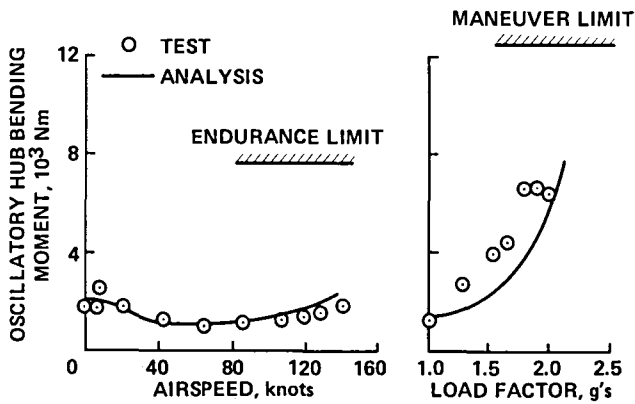


Fig. 102. BK-117 helicopter loads (Ref. 110).

BK-117 HINGELESS ROTOR

THRUST = 2850 kg

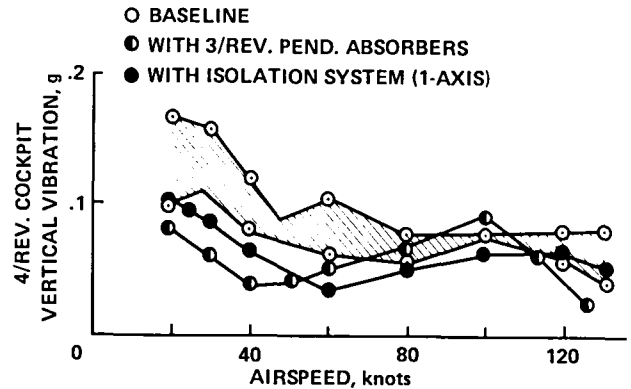


Fig. 103. Measured BK-117 helicopter vibration (Ref. 110).

XH-51A BEARINGLESS ROTOR

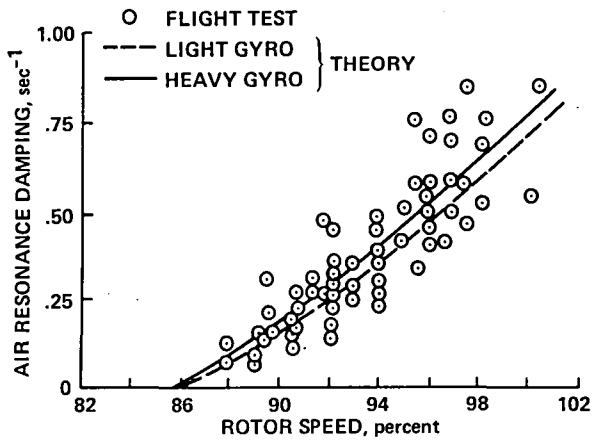


Fig. 104. XH-51A bearingless helicopter stability (Ref. 112).

BMR BEARINGLESS ROTOR

V = 60 knots, 100% ROTOR SPEED

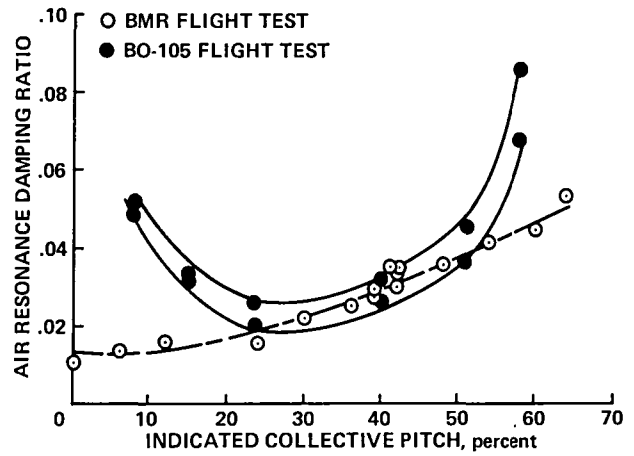


Fig. 105. Measured BMR bearingless helicopter stability (Ref. 113).

BMR BEARINGLESS ROTOR

LEVEL FLIGHT, 100% ROTOR SPEED

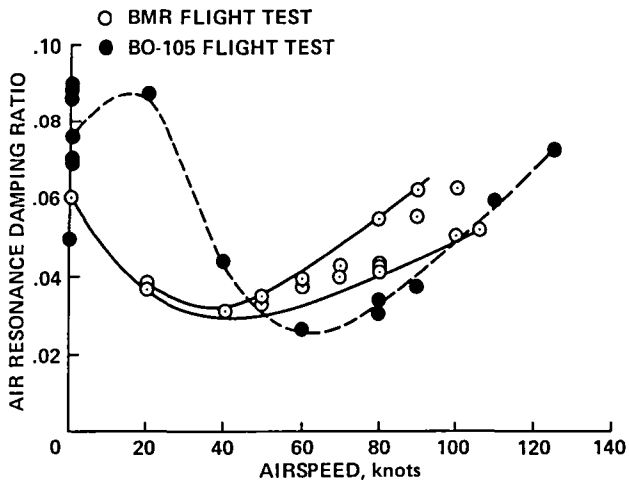


Fig. 106. Measured BMR bearingless helicopter stability (Ref. 113).

BMR BEARINGLESS ROTOR

TEST ON CONCRETE, 100% ROTOR SPEED

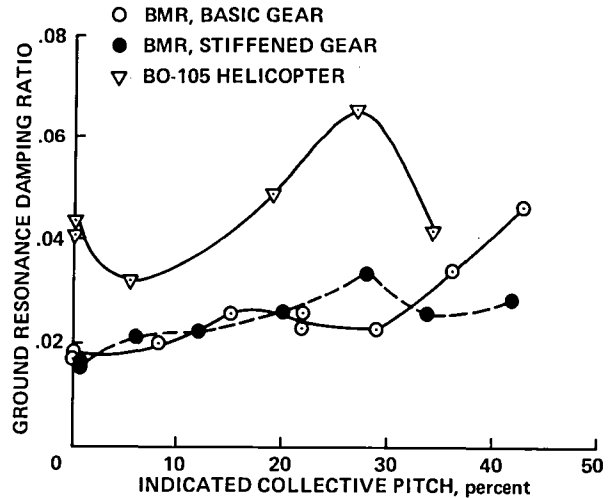


Fig. 107. Measured BMR bearingless helicopter stability (Ref. 113).

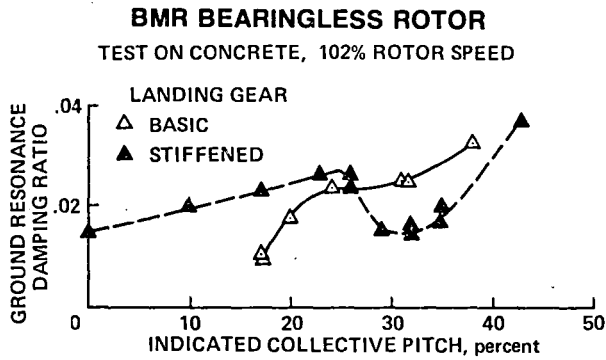


Fig. 108. Measured BMR bearingless helicopter stability (Ref. 113).

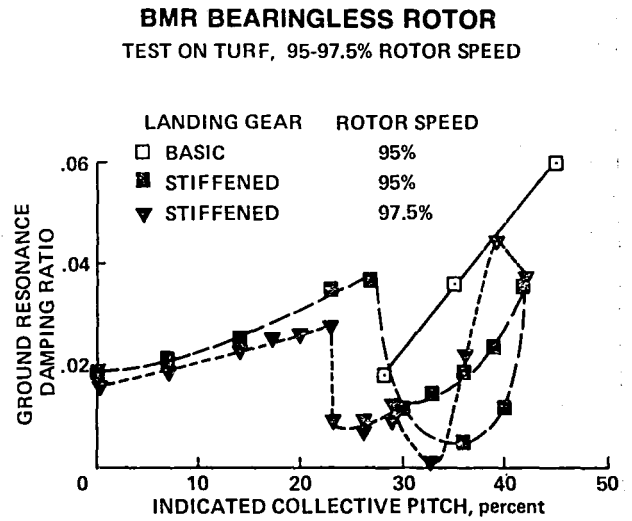


Fig. 109. Measured BMR bearingless helicopter stability (Ref. 113).

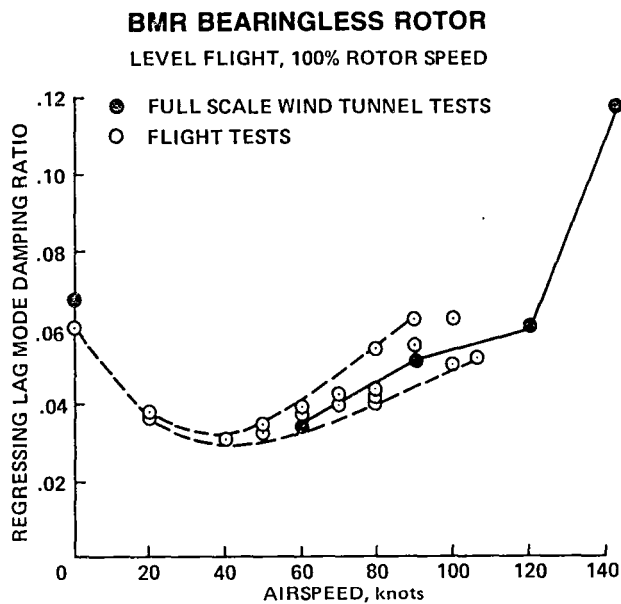


Fig. 110. Measured BMR bearingless helicopter stability (Ref. 41).

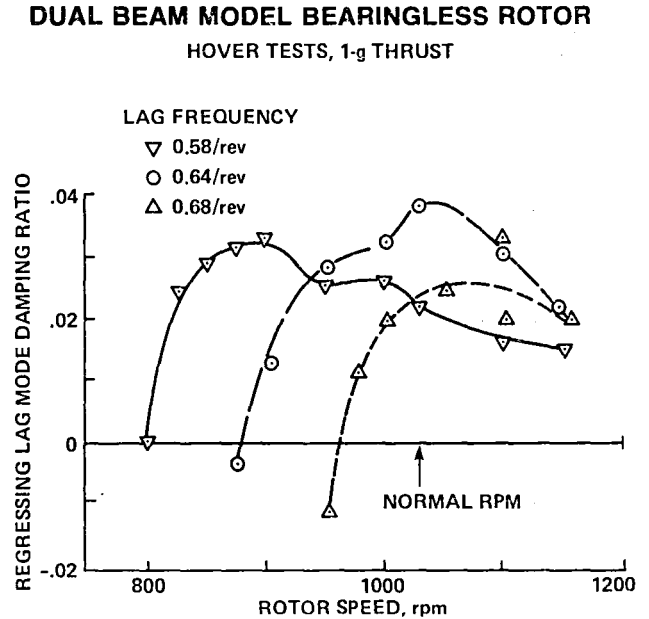


Fig. 111. Measured model bearingless rotor stability (Ref. 116).

SINGLE FLEX STRAP MODEL BEARINGLESS ROTOR
HOVER TESTS, 1-g THRUST

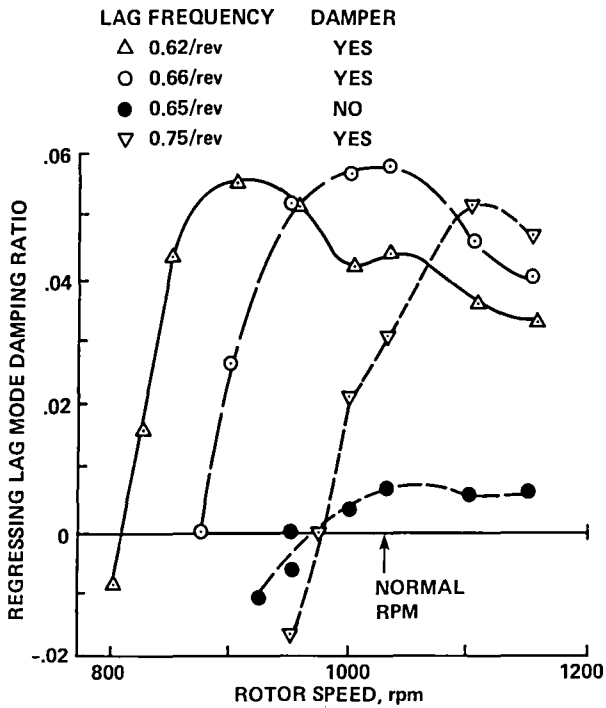


Fig. 112. Measured model bearingless rotor stability (Ref. 116).

MODEL BEARINGLESS ROTOR
HOVER TESTS, 1-g THRUST

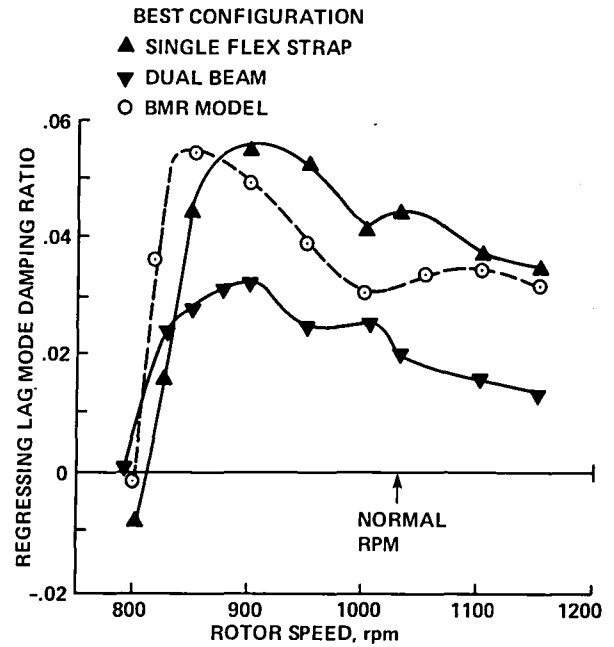


Fig. 113. Measured model bearingless rotor stability (Ref. 116).

MODEL BEARINGLESS ROTOR
ISOLATED ROTOR, HOVER, 1-g THRUST

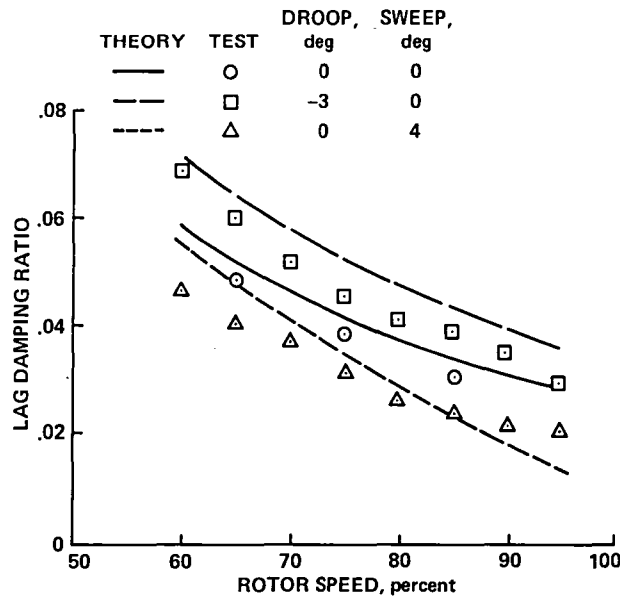


Fig. 114. Small scale Model 680 bearingless rotor stability (Ref. 119).

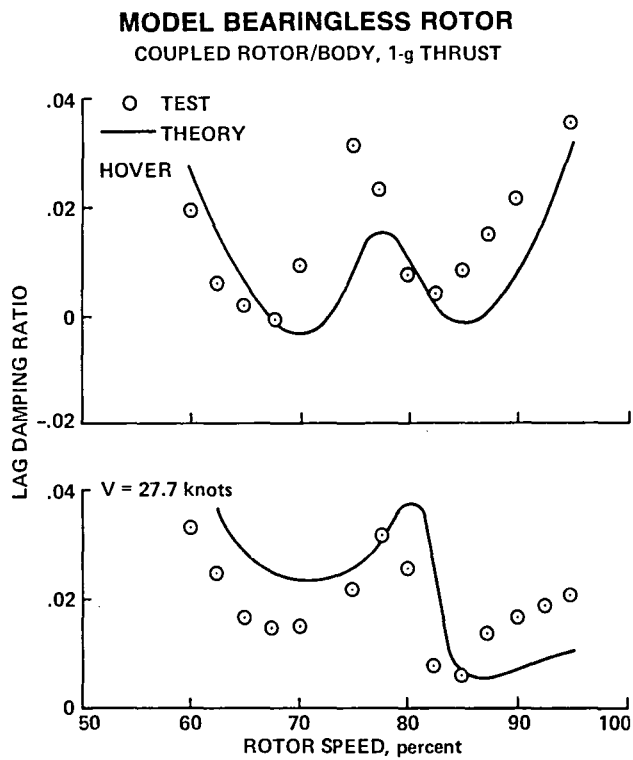


Fig. 115. Small scale Model 680 bearingless rotor stability (Ref. 119).

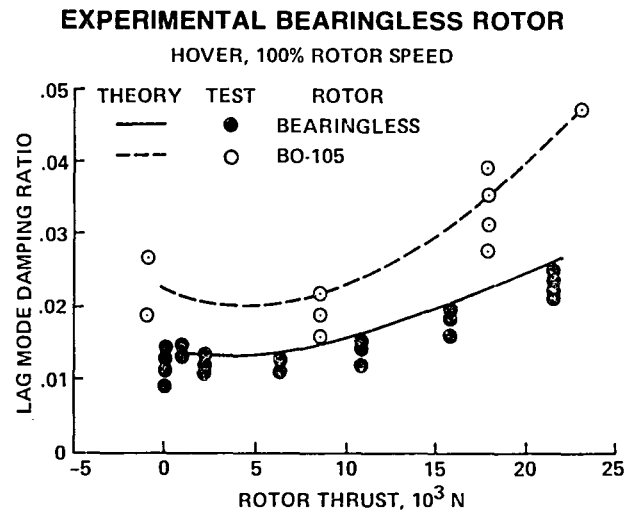


Fig. 116. Experimental bearingless rotor stability (Ref. 102).

**YUH-61A BEARINGLESS TAIL ROTOR
HOVER TEST**

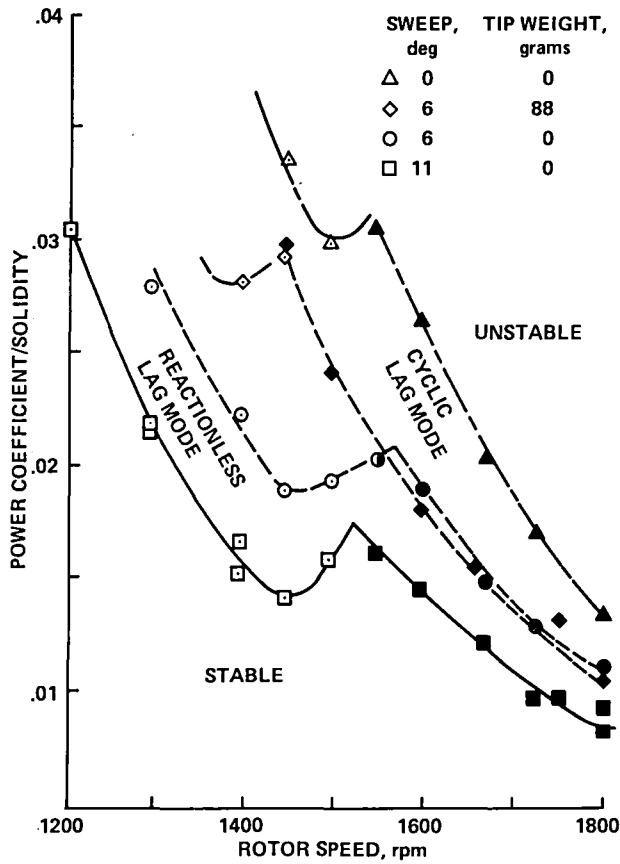


Fig. 117. Measured YUH-61A bearingless tail rotor stability boundaries (Ref. 123).

**YUH-61A BEARINGLESS TAIL ROTOR
HOVER TEST**

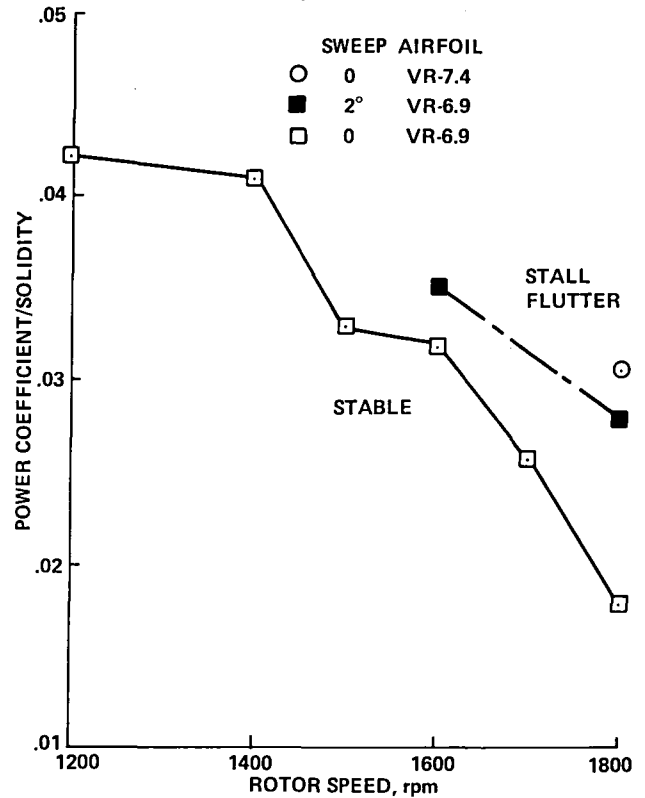


Fig. 118. Measured YUH-61A bearingless tail rotor stability boundaries (Ref. 123).

HINGELESS ROTOR WITH CIRCULATION CONTROL

HOVER, $\nu_\beta = 1.1$, $R = 0$, $K_{P_\zeta} = 0$

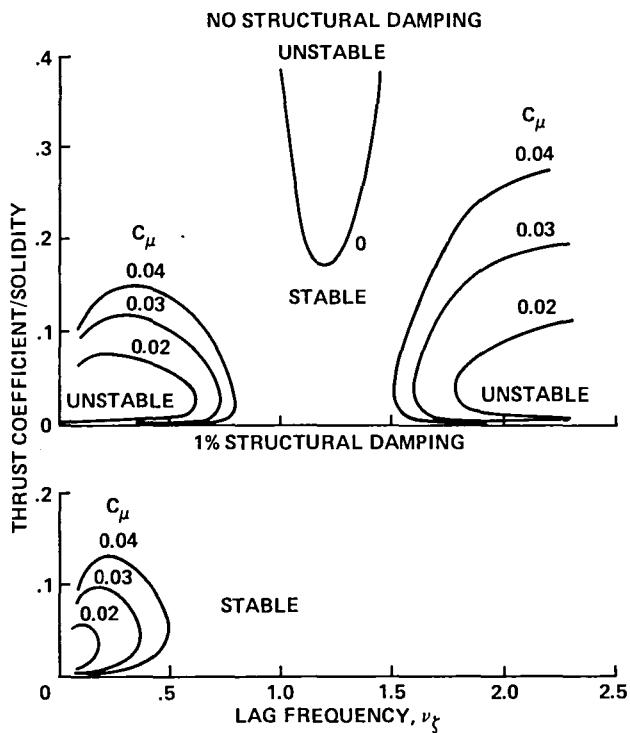


Fig. 119. Calculated flap-lag stability boundaries with circulation control (Ref. 127).

HINGELESS ROTOR WITH CIRCULATION CONTROL

HOVER, $\nu_\beta = 1.1$, $R = 0$, 1% STRUCTURAL DAMPING

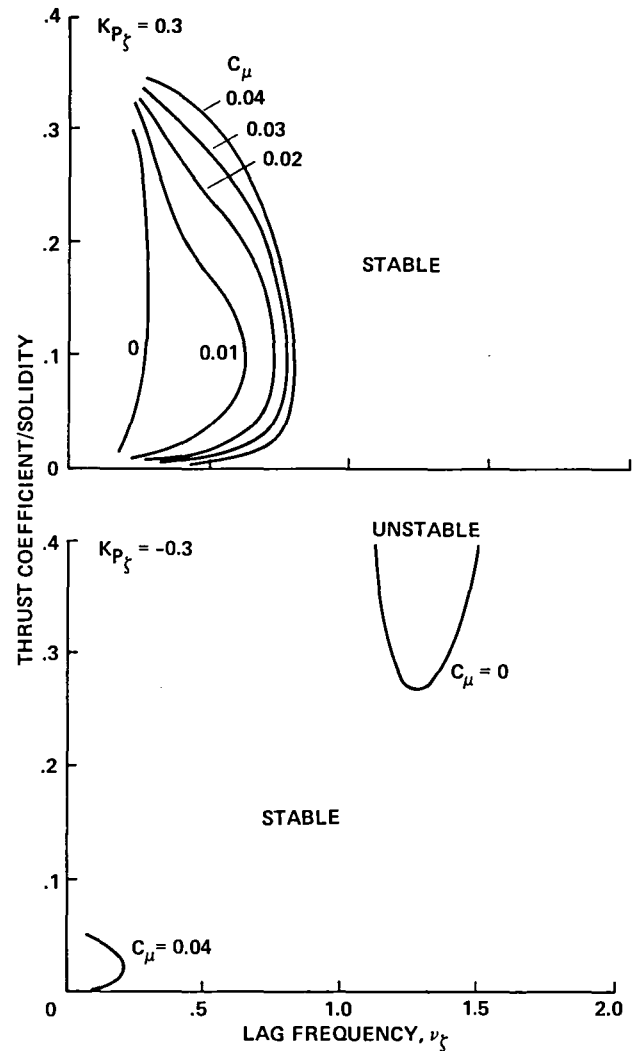


Fig. 120. Calculated flap-lag stability boundaries with circulation control (Ref. 127).

HINGELESS ROTOR WITH CIRCULATION CONTROL

HOVER, $\nu_\beta = 1.8$, $R = 1$, 1% STRUCTURAL DAMPING

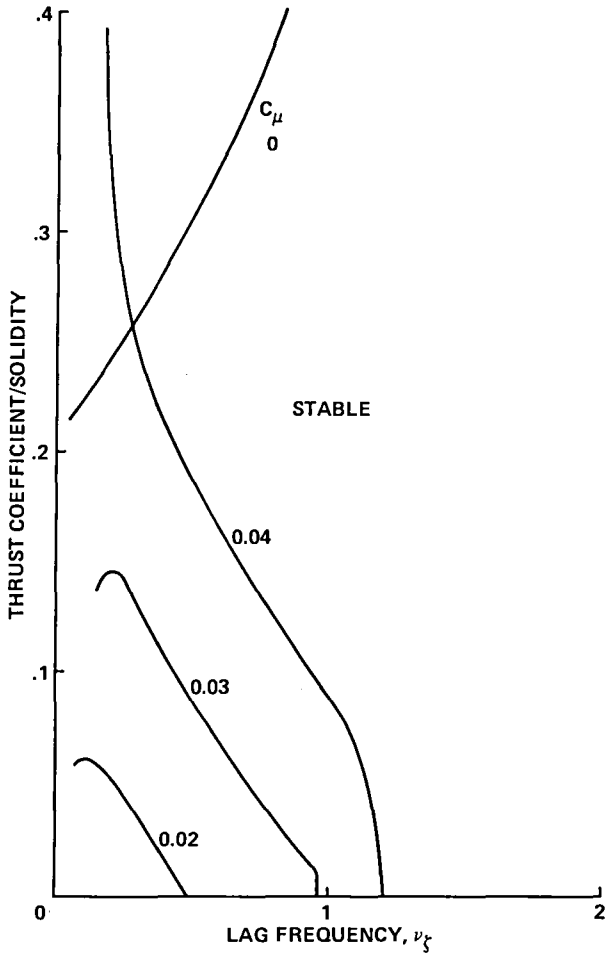


Fig. 121. Calculated flap-lag stability boundaries with circulation control (Ref. 127).

BEARINGLESS ROTOR WITH CIRCULATION CONTROL

LEADING AND TRAILING EDGE PITCH LINKS,
NO STRUCTURAL DAMPING,
HOVER THEORY, $\nu_\beta = 2.3$, $\nu_\zeta = 2.5$, $\omega_\phi = 17.4$

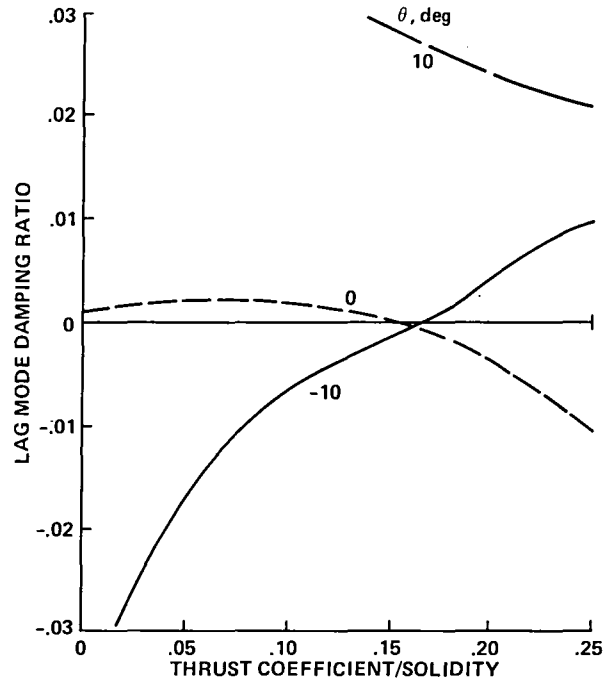


Fig. 122. Calculated bearingless rotor stability with circulation control (Ref. 45).

T55-L-11/CH-47C FUEL CONTROLLER

GAIN, percent	TIME LAG, sec
— 100	0.03
- - - 30	0.03
- - - 100	0.10
- - - 30	0.10

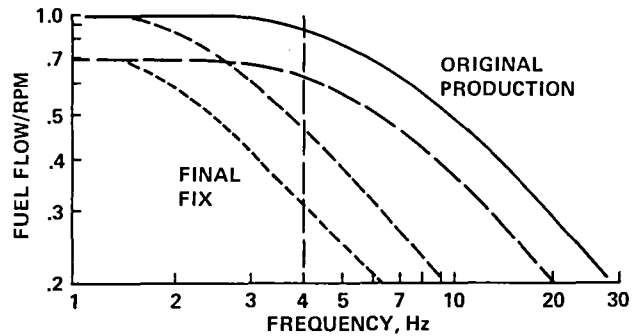


Fig. 123. Fuel control frequency response (Ref. 134).

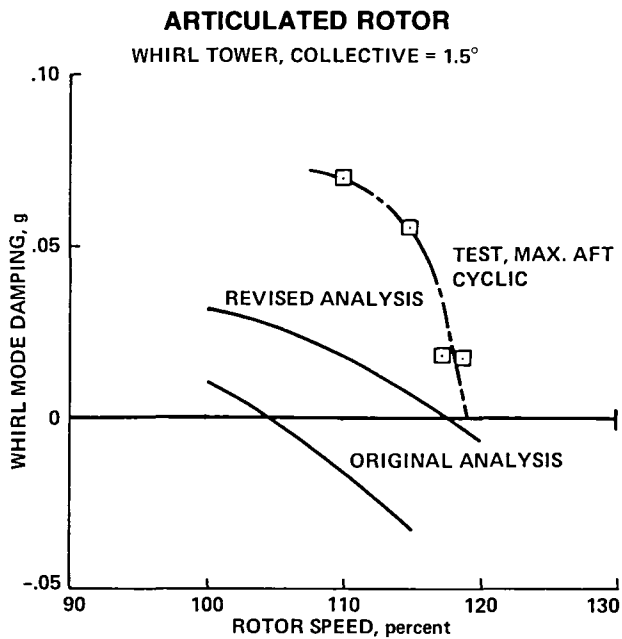


Fig. 124. Articulated rotor whirl mode stability (Ref. 137).

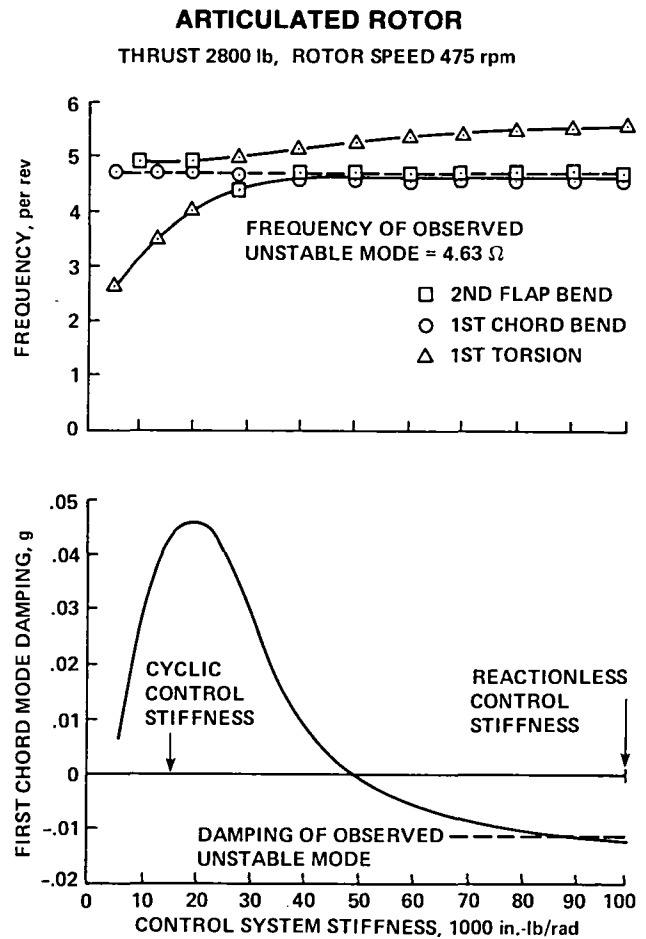


Fig. 125. Articulated rotor blade stability (Ref. 138).

GIMBALLED TILTING PROPROTOR AIRCRAFT

THEORY, AIRPLANE MODE, LEVEL FLIGHT

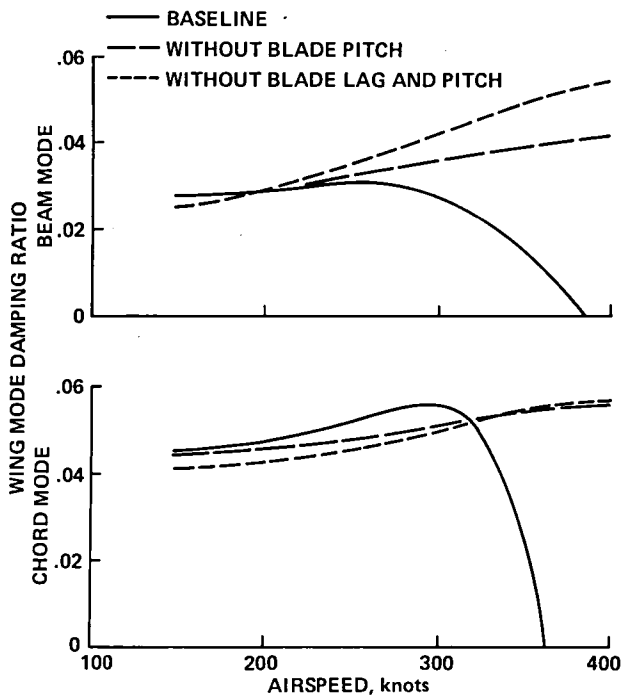


Fig. 126. Calculated tilting prop-rotor aircraft whirl flutter stability.

GIMBALLED TILTING PROPROTOR AIRCRAFT

THEORY, AIRPLANE MODE, LEVEL FLIGHT

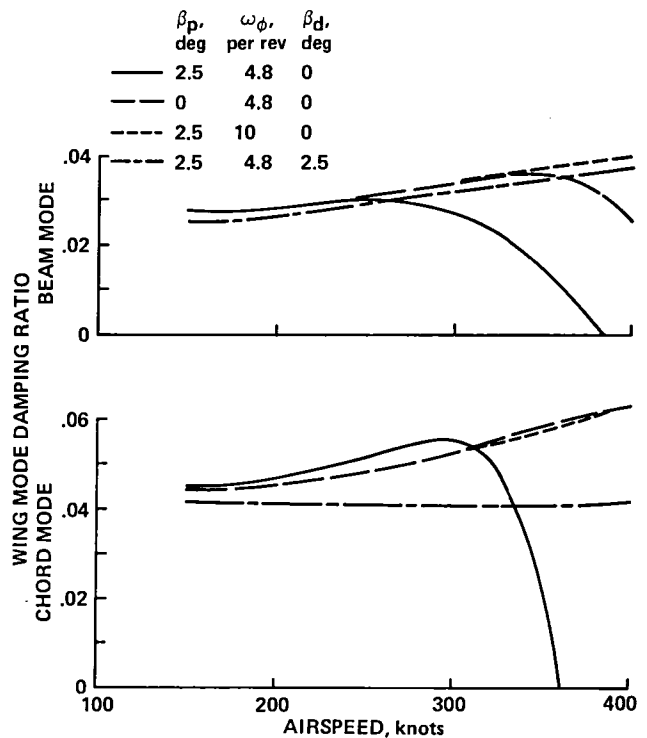


Fig. 127. Calculated tilting prop-rotor aircraft whirl flutter stability.

SOFT-INPLANE HINGELESS TILTING PROPROTOR

THEORY, AXIAL FLOW

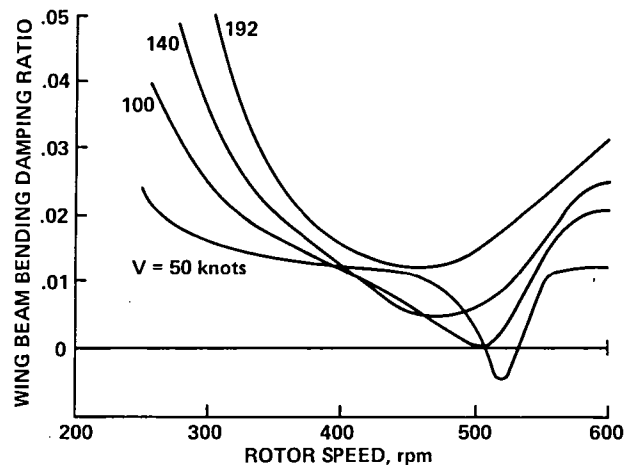


Fig. 128. Calculated tilting prop-rotor aircraft air resonance stability.

GIMBALLED TILTING PROPROTOR AIRCRAFT

THEORY, AIRPLANE MODE, LEVEL FLIGHT

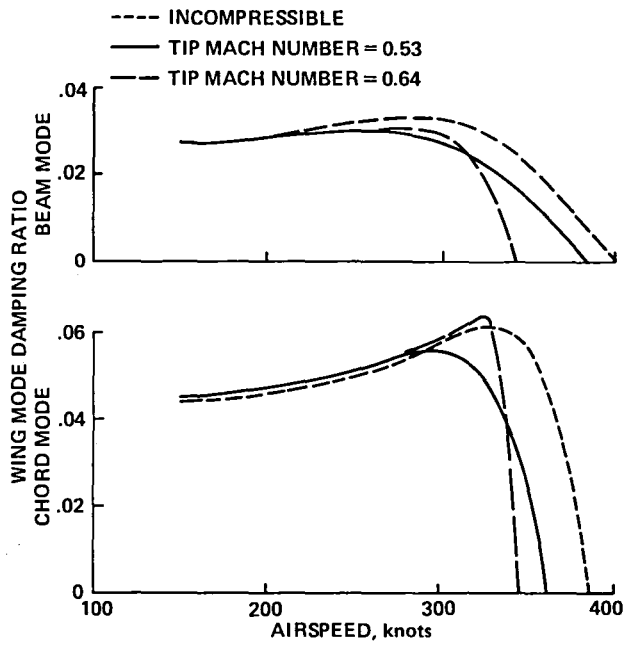


Fig. 129. Calculated tilting prop-rotor aircraft whirl flutter stability.

GIMBALLED TILTING PROPROTOR AIRCRAFT

THEORY, AIRPLANE MODE, LEVEL FLIGHT

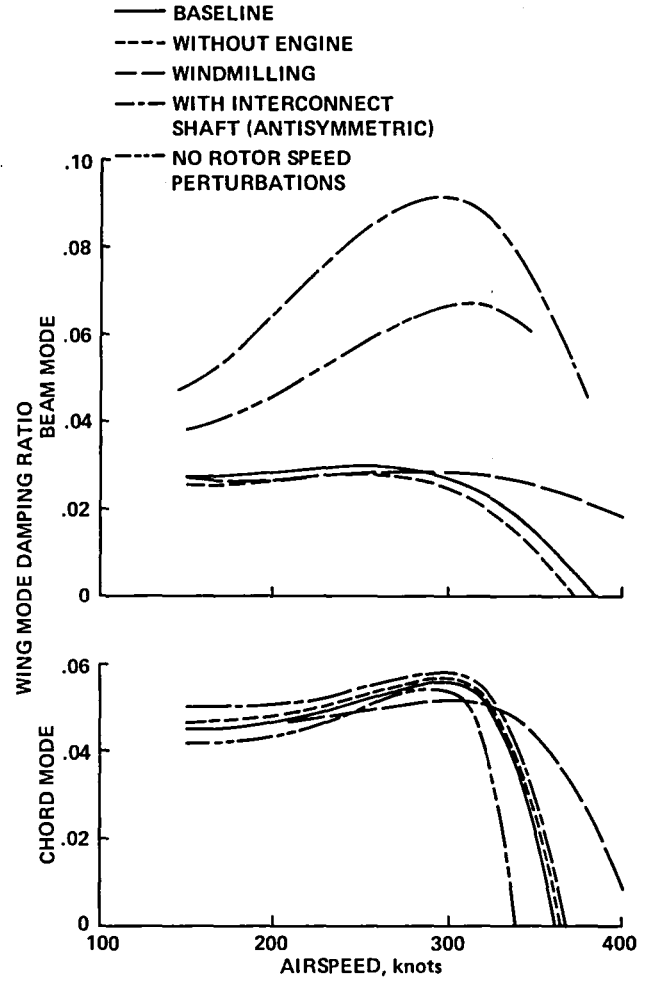


Fig. 130. Calculated tilting prop-rotor aircraft whirl flutter stability.

XV-15 TILT ROTOR RESEARCH AIRCRAFT

FLIGHT TEST, AIRPLANE MODE, V = 190 knots

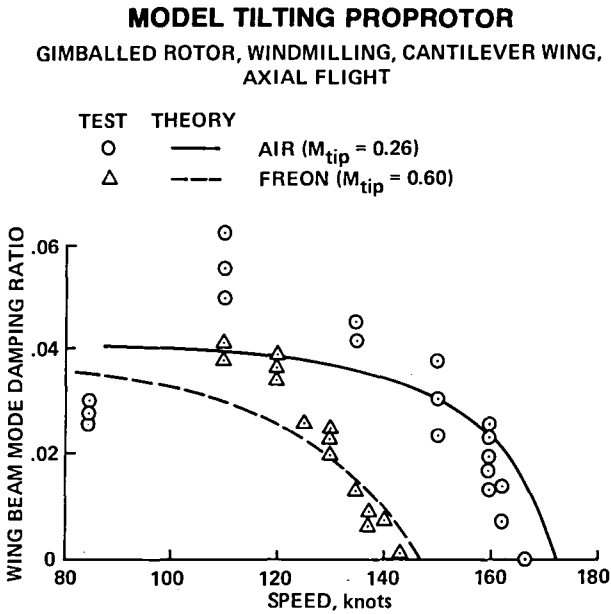


Fig. 131. Model tilting propotor whirl flutter stability (Ref. 144).

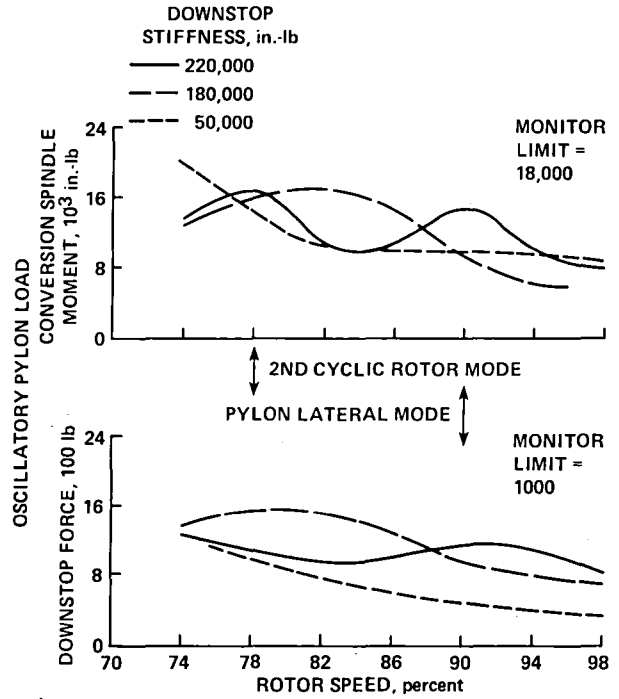


Fig. 132. Measured XV-15 Tilting Proprotor Research Aircraft pylon loads (Ref. 145).

XV-15 TILT ROTOR RESEARCH AIRCRAFT

FLIGHT TEST, AIRPLANE MODE, V = 190 knots

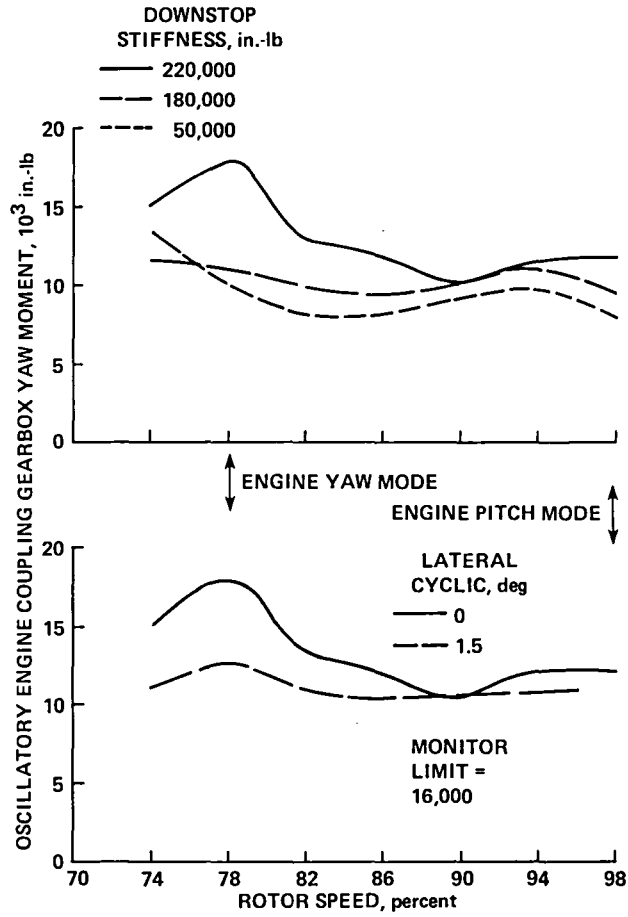


Fig. 133. Measured XV-15 Tilting Proprotor Research Aircraft pylon loads (Ref. 145).

1. Report No. NASA TM-86669		2. Government Accession No.		3. Recipient's Catalog No.	
4. Title and Subtitle RECENT DEVELOPMENTS IN THE DYNAMICS OF ADVANCED ROTOR SYSTEMS				5. Report Date March 1985	
				6. Performing Organization Code	
7. Author(s) Wayne Johnson				8. Performing Organization Report No. 85089	
9. Performing Organization Name and Address NASA Ames Research Center Moffett Field, CA 94035				10. Work Unit No.	
				11. Contract or Grant No.	
12. Sponsoring Agency Name and Address National Aeronautics and Space Administration Washington, DC 20546				13. Type of Report and Period Covered Technical Memorandum	
				14. Sponsoring Agency Code 505-42-11	
15. Supplementary Notes Point of contact: Wayne Johnson, Ames Research Center, MS 247-1, Moffett Field, CA 94035 (415) 694-5043 or FTS 464-5043					
16. Abstract The problems that have been encountered in the dynamics of advanced rotor systems are described. The methods for analyzing these problems are discussed, as are past solutions of the problems. To begin, the basic dynamic problems of rotors are discussed: aeroelastic stability, rotor and airframe loads, and aircraft vibration. Next, advanced topics that are the subject of current research are described: vibration control, dynamic inflow, finite element analyses, and composite materials. Finally, the dynamics of various rotorcraft configurations are considered: hingeless rotors, bearingless rotors, rotors with circulation control, coupled rotor/engine dynamics, articulated rotors, and tilting proprotor aircraft.					
17. Key Words (Suggested by Author(s)) Rotorcraft dynamics Rotorcraft design				18. Distribution Statement Unlimited Subject category - 39	
19. Security Classif. (of this report) Unclassified		20. Security Classif. (of this page) Unclassified		21. No. of Pages 116	22. Price* A06

End of Document